Politecnico di Milano

SCHOOL OF INDUSTRIAL AND INFORMATION ENGINEERING

Master of Science – Nuclear Engineering

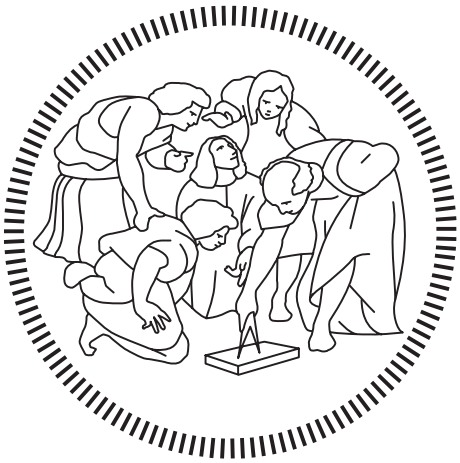

A subchannel thermal-hydraulic analysis of the 250 kW TRIGA nuclear reactor

Supervisor

Cammi Antonio

Co-Supervisor

Carolina Introini

Candidate

Castelli Davide – 913411

Academic Year 2019 – 2020

Acknowledgements

Voglio ringraziare tutti quelli che mi sono stati vicino, in particolare i miei genitori, che mi hanno sostenuto sia moralemente che economicamente e mia sorella.

Ringrazio particolarmente tutti quelle persone interne e esterne all'università che ci sono state nei momenti difficili, in particolare Stefano F., che mi ha sempre supportato, Giovanni P. e Andrea G., che mi hanno sempre fatto da guida negli ultimi anni.

Oltre a questi voglio ringraziare i docenti e studenti che hanno avuto la pazienza e la saggezza di formarmi e guidarmi in questo percorso universitario, che ho sempre voluto fare sin da piccolo.

Sommario

Il principale obiettivo di questo lavoro di tesi consiste nell'elaborare i possibili regimi di scambio termico che si possono verificare durante le diverse condizioni operative del reattore TRIGA MkII della General Atomics.

Più precisamente, condizioni differenti portano a sostanziali diversità nei meccanismi di scambio termico che saranno investigati.

Diverse correlazioni e ipotesi saranno applicate e comparate le une con le altre in base alla loro capacità di riprodurre dati sperimentali e calcoli CFD.

Dopo una breve introduzione e validazione delle singole, sarà presa in considerazione la migliore che predica al meglio le diverse situazioni possibili. Una particolare attenzione sarà data alla scelta di correlazioni di in grado di predire e quindi prevenire possibili situazioni critiche come la crisi termica, per aggiornare le procedure di esercizio in termini di sicurezza.

Inizialmente verrà fatta una descrizione generale del reattore TRIGA, al fine di presentare al lettore il tipo di macchina in esame. Verranno presentate tutte le funzioni e le scelte tecnologiche per spiegare come funziona questa macchina e perché sorgono diversi meccanismi di scambio termico durante il suo funzionamento.

Successivamente, verranno utilizzate diverse correlazioni empiriche e semi-empiriche per interpretare i dati sperimentali e anche per prevedere situazioni particolari con i loro valori caratteristici, come quello della crisi termica. Questa può risultar essere una situazione catastrofica che può danneggiare gravemente il reattore o, nel peggiore dei casi, generare una situazione critica per quanto riguarda la salute delle persone limitrofe.

Poi si procede con i commenti di sicurezza sul funzionamento di questo reattore. Verranno poi confrontati i dati ottenuti con questo approccio con Relap, software per la simulazione di comportamenti termoidraulici nei reattori nucleari.

Abstract

The main objective of this thesis work is to elaborate on the possible heat exchange regimes that can be created under different operating conditions for the General Atomics TRIGA Reactor Mark II.

More precisely, different operating conditions, that can bring to different behaviors of heat exchange mechanisms for this type of reactor, will be investigated.

Several correlations and hypothesis will be applied and compared to each other, based on their capability to reproduce experimental and CFD results.

Following the introduction and validation of different correlations, the best one for the considered operating condition will be chosen, also according to its validity to predict all possible situations that can arise in the reactor. Particular attention is given to the ability of the chosen correlation to prevent and predict dangerous situations such as thermal crisis, in order to update the safety procedures.

At first, a general description of the TRIGA reactor will be done, in order to present to the reader, the type of machine under consideration. All functions and technology choices will be presented to explain how this machine works, and why different heat exchange mechanism arise during its functioning.

After that, different empirical and semi-empirical correlations, will be used to interpret the experimental data and also to predict particular situations and their characteristic values, such as the thermal crisis one. This can be a catastrophic situation that can seriously damage the reactor or, in the worst case, generate a critical situation regarding the health of neighboring people.

After thatit will be exposed safety comments about how well this reactor works, and a comparison with Relap results, that is a software to license and simulate thermo-hydraulic nuclear systems.

Extended Abstract

Il presente lavoro viene effettuato come analisi termoidraulica e con accenno di sicurezza sui principali problemi che si hanno nei reattori nucleari raffreddati ad acqua, in particolare il reattore TRIGA, reattore nucleare che non ha come scopo la produzione di energia elettrica, venendo appunto impiegato come sito sperimentale per i più svariati scopi.

Inizialmente verrà presentato una breve panoramica sullo scambio termico che avviene nei reattori nucleari, per poi soffermarsi, sempre a livello di introduzione sull'ebollizione sottoraffreddata, che permette di innalzare anche di un ordine di grandezza il coefficiente di scambio termico, rendendo efficiente lo scambio termico in certe condizioni.

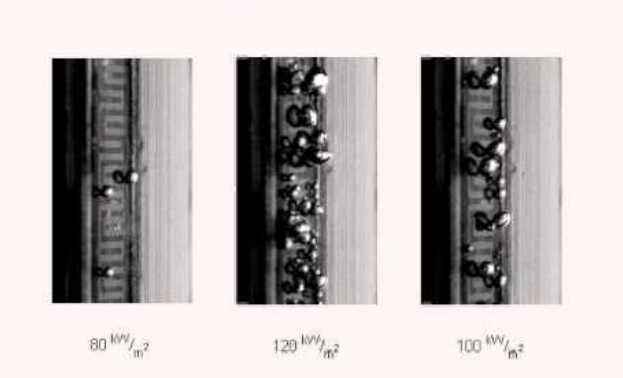

Figura 1: diversi comportamenti di ebollizione a diversi flussi termici

Questo fenomeno è molto studiato, sia perché facilita lo scambio di calore in scambiatori di calore, diminuendo l'area richiesta a parità di calore da scambiare e quindi dimensioni e costi, sia perché, come più evidente nel nostro caso, può portare ad una specie di effetto tampone per le temperature coinvolte, permettendo di scambiare grosse quantità di potenza calorica senza l'ausilio di differenze di temperatura troppo elevate, che in alcuni casi non risulterebbero idonee o peggio risulterebbero pericolose.

Da qui lo studio e la quantificazione di questo fenomeno, che risulta di grande importanza per tutte le categorie di impianti che hanno a che fare con scambio termico ad acqua.

Il caso esaminato poi va a rispecchiarsi in un'analisi 1D del fenomeno appena descritto nel reattore TRIGA in cui, come molti impianti nucleari, le barre di combustibile sono raffreddate da acqua; questa si trova ad una pressione leggermente superiore a quella atmosferica, e grazie ad un sistema di circolazione naturale e ebollizione sottoraffreddata che si viene a creare autonomamante, il reattore viene correttamente refrigerato.

Prima di addentrarsi nello studio dei fenomenti coinvolti è presentata la tecnologia, con tutte le dimensioni di maggiore interesse.

Dall'impiantistica di base e uno schema di funzionamento si passa poi ad un maggiore dettaglio di descrizione per quanto riguarda il core, che è il cuore del reattore e soggetto principale del lavoro. Descrivendo la natura del combustibile e poi delle barre di controllo si può già intuire la grande sicurezza intrinseca di questa macchina, che viene spiegata maggiormente nella sottosezione dedicata.

Altre sezioni sono dedicate alla desrizione dell'impianto di raffreddamento della piscina in cui il reattore è immerso e alla strumentazione necessari al controllo e verifica dei parametri fondamentali della macchina.

Una volta fatta questa presentazione discorsiva del TRIGA si passa poi alla fase di descrizione di geometria e dimensioni caratteristiche che risultano fondamentali per la caratterizzazione del fenomeno.

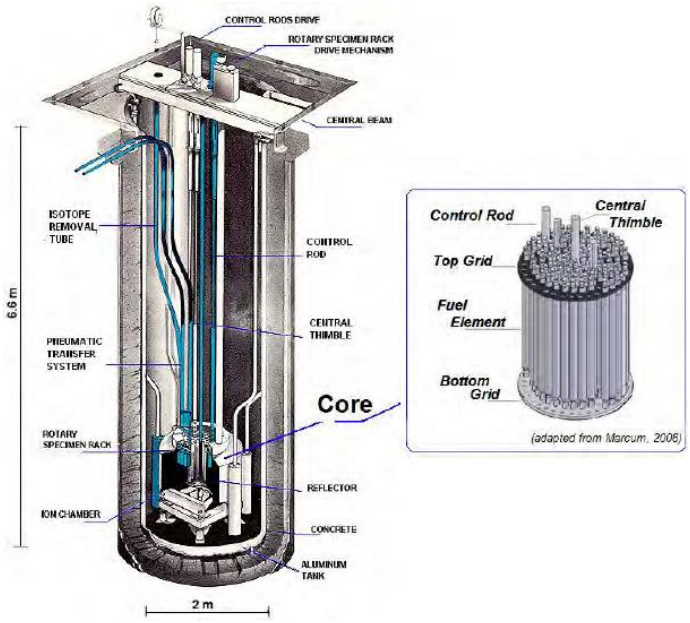

Figura 2: schema del reattore TRIGA (IPR)

Si presenteranno le dimensioni caratteristiche fondamentali, oltre che a i canali del reattore presi in esame, per poi passare ad una descrizione della potenza in gioco.

A riguardo di ques'ultima è importante introdurre il fatto che essa deve essere valutata sia in termini di media globale che livello locale partendo da una distribuzione calcolata da simulazioni Monte-Carlo, poichè vi sono parametri critici che necessitano analisi in specifici punti del reattore.

Da questo una suddivizione della potenza del reattore prima in funzione degli anelli da cui è composto, ovvero la distanza dal centro che è funzione del flusso neutronico, sia a livello

assiale per lo stesso motivo, con uno sguardo anche alla potenza assorbita dal singolo canale, parametro fondamentale per determinare le portate di refrigerante.

Una volta introdotti tutti gli ingredienti necessari per effettuare l'analisi, si inizia con la quantificazione delle portate, parametro fondamentale per la costruzione delle successive analisi.

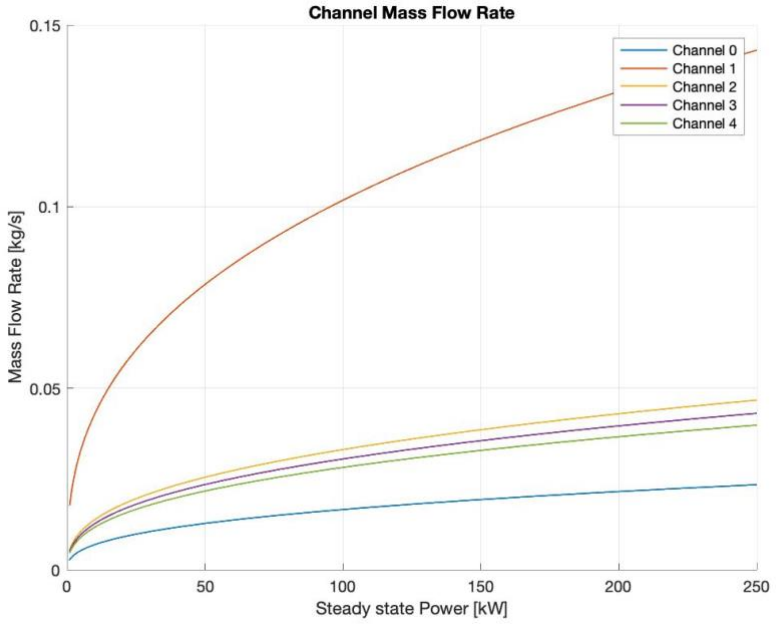

Figura 3: portate massiche per convezione naturale in funzione della potenza

Mediante l'uso di un'equazione di bilancio di pressioni, è possibile ricavare la portata massica presente nel reattore in ogni canale. Per fare questo verranno usate 2 strade, che verranno poi confrontate tra loro: la prima è di considerare un fattore di attrito medio, mentre la seconda quella di utilizzare una correlazione solida, come quella di Colebrook-White.

Una volta messa in evidenza la rilevante differenza tra l'uso dei due approcci, si sceglie il secondo per effettuare i tutti i calcoli che seguono, poiché risulta più solido dal punto di vista sperimentale e teorico.

Si passa poi al calcolo del coefficiente di scambio termico h mediante l'uso di una correlazione per il calcolo dello scambio termico in convezione naturale, mostrandone i risultati.

Successivamente si descrive il comportamento a fase singola, ovvero la parte che riguarda lo scambio termico con l'utilizzo di correlazioni che prevedono la convezione forzata, che noi consideriamo tale usando invece le portate ricavate dalla convezione naturale.

L'analisi viene condotta con due correlazioni principali, che sono la Dittus-Boelter e la Gnielinski venenedo poi messe a confronto, per capire qualle delle due risulta la migliore.

Le differenze sostanziali vengono messe in risalto con grafici sovrapposti, facendo notare che la seconda non funziona particolarmente bene per le condizioni di interesse.

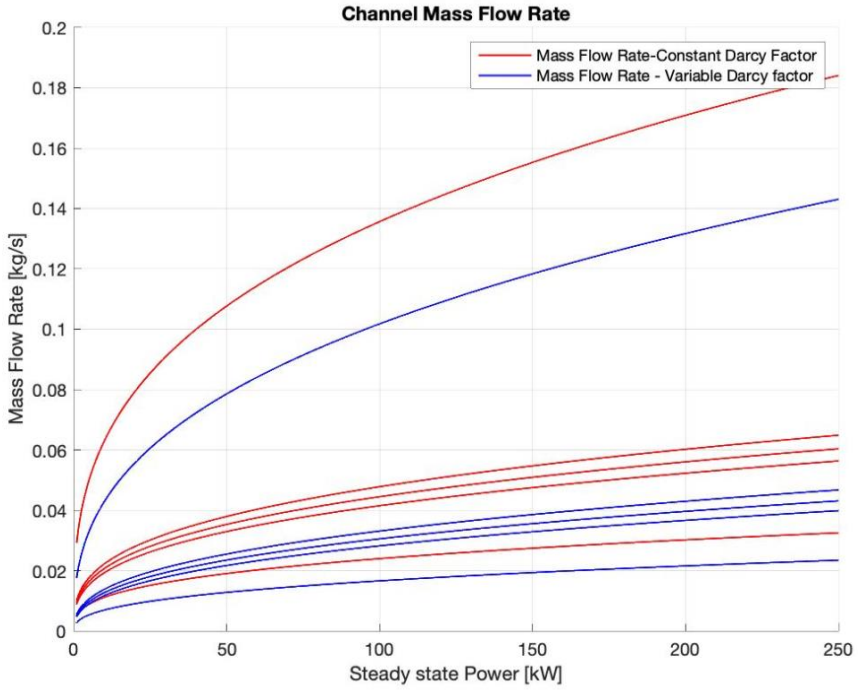

Figura 4: differenze di portata usando i due approcci

Una volta terminata l'analisi a fase singola si procede ad una descrizione delle resistenze termiche coinvolte nell'intero meccanismo di scambio termico, dalla fase convettiva al cladding, per poi passare al gap e infine al fuel.

Viene anche illustrato il peso relativo della fase convettiva sul coefficiente globale di scambio termico in funzione della potenza esercita, che va a diminuire perché aumentando la potenza si incentiva lo scambio termico, seppur rimanendo nelle ipotesi di fluido non bollente. Questo viene mostrato per vedere effettivamente come l'aumento della potenza favorisce lo scambio termico.

A questo punto viene poi condotta un'analisi approfondita tra le correlazioni più indicate allo studio del fenomeno dell'ebollizione sottoraffreddata. Inoltre viene svolto correlazione per correlazione un confronto dei risultati ottenuti con quelli ottenuti dalla prima correlazione usata: la Rohsenow

Dopo una descrizione dettagliata del fenomeno dell'ebollizione sottoraffreddata per quanto riguarda il reattore, si passa alla descrizione e definizione della temperatura di onset, che è in sostanza la temperatura, leggermente superiore a quella di saturazione, che la parete calda

deve raggiungere per generare ebollizione sottoraffreddata. Una correlazione apposita per il nostro caso, che è quella di Bergles-Rohsenow, viene usata per predirre correttamente questa temperatura per acqua a bassa pressione. Il profilo di temperatura viene plottato per i primi tre canali dell'analisi radiale, essendo che, come poi sarà reso noto, l'ebollizione raffreddata viene vista solamente in questi tre canali, mentre gli altri non hanno sufficiente flusso termico per generare il fenomeno, poiché non viene raggiunta la temperatura di onset.

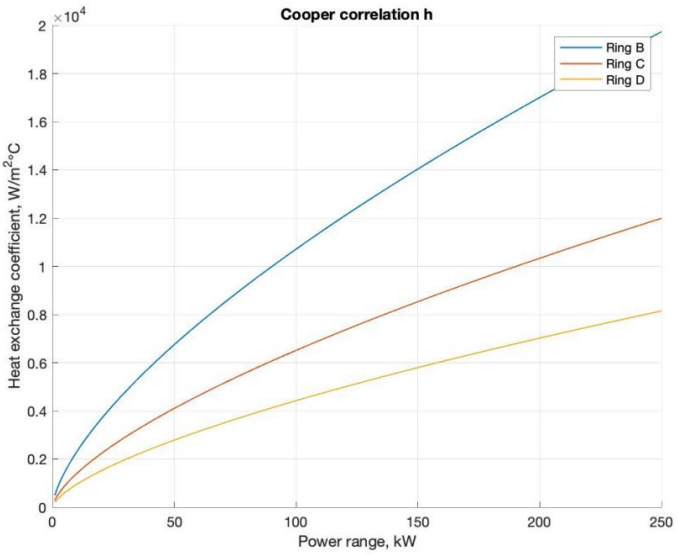

Figura 5: esempio di risultati ottenuti da correlazioni double phase

Dopodichè viene condotta un'analisi schematica delle correlazioni più o meno plausibili per la valutazione del coefficiente di scambio termico nei canali sopra descritti, ove possiamo osservare il fenomeno.

Per ogni correlazione viene fatta una breve introduzione, vengono esposte le espressioni necessarie, le condizioni di validità e infine un grafico che mostra la variazione del coefficiente di scambio termico in funzione della potenza.

Si sono usate le correlazioni più famose, anche se non ricalcano perfettamente le condizioni del TRIGA, anche per vedere la loro capacità di prevedere situazioni leggermente diverse da quelle per cui sono state scritte. Le prime usate infatti sono per il fenomeno del pool-boiling, il fenomeno di ebollizione che avviene a liquido sostanzialmente fermo, mentre solo le ultime sono rigorose per il subcooled flow boiling, che è appunto il nostro caso.

Alcuni grafici mostrano l'andamento di tutte le correlationi in funzione della potenza, oltre alla curiosità di considerare le relazioni di tipo locale e non globale e un grafico di tipo puramente illustrativo di un possibile andamento del coefficiente di scambio convettivo lungo l'asse del canale.

Una volta illustrati i valori dei possibili regimi di scambio, è tempo di vedere la loro influenza sulle temperature, fase necessaria per valutare la sicurezza o il corretto funzionamento dell'impianto.

Il primo profilo di temperatura ad essere esposto è quello della temperatura di bulk, che è fondamentale per capire se le masse calcolate siano corrette o meno, per poi effettuare un confronto con i dati del TRIGA di Pavia dell'anno acccademico corrente e passare ad una piccola dimostrazione di come sarebbe il profilo di temperatura non tenendo in considerazione il fenomeno di ebollizione, ovvero considerando esclusivamente i coefficienti di scambio termico a fase singola, mostrando come le temperature raggiunte sarebbero troppo elevate per operare in sicurezza.

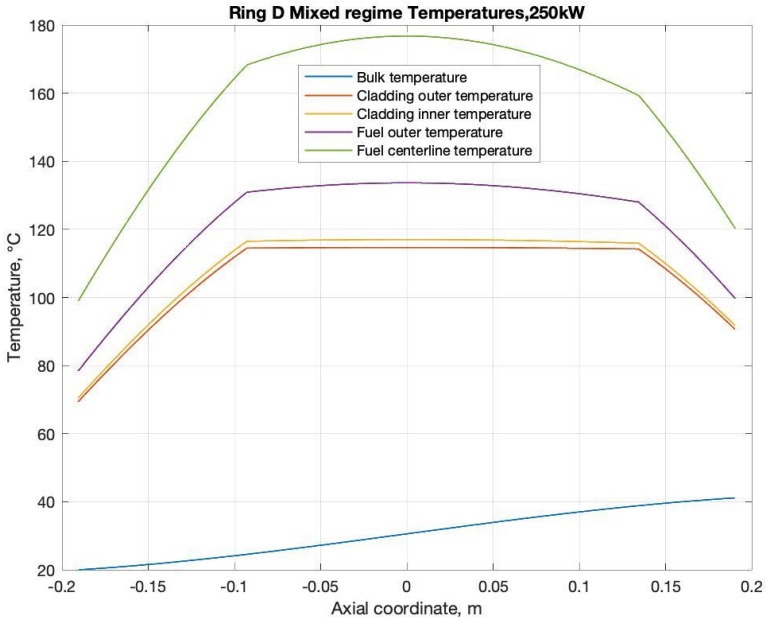

Figura 6: esempio di profilo di temperatura

La fase successiva consiste in una analisi delle temperature calcolate tenendo conto di un'opportuna selezione tra dove si ha e ove non si ha ebollizione sottoraffreddata, tenendo in considerazione il cambio dei coefficienti. Si notano infatti una grossa diversità rispetto ai profili precendenti. Si espongono quindi i grafici dei profili di temperatura per tutti i canali.

Un'altra cosa mostrata è il calcolo dei profili di temperatura con i coefficienti di scambio calcolati dalla convezione naturale, che sono leggermente più bassi; da qui il confronto con alcuni precedenti e la non conformità con quanto succede, poiché si trova ebollizione in un canale in cui non avviene, in disaccordo anche i con i dati CFD.

Oltre a questo, vengono riportate tabelle che riassumono le potenze del reattore necessarie per osservare l'ebollizione sottoraffreddata per ogni canale, sia nel caso di utilizzo di coefficienti provenienti da convezione naturale che fase singola.

Una volta compiuta l'analisi sulla temperatura si passa ad un'analisi di un parametro fondamentale per la sicurezza, il DNBr, che rappresenza la "distanza" delle nostre condizioni operative dal raggiungimento del flusso critico.

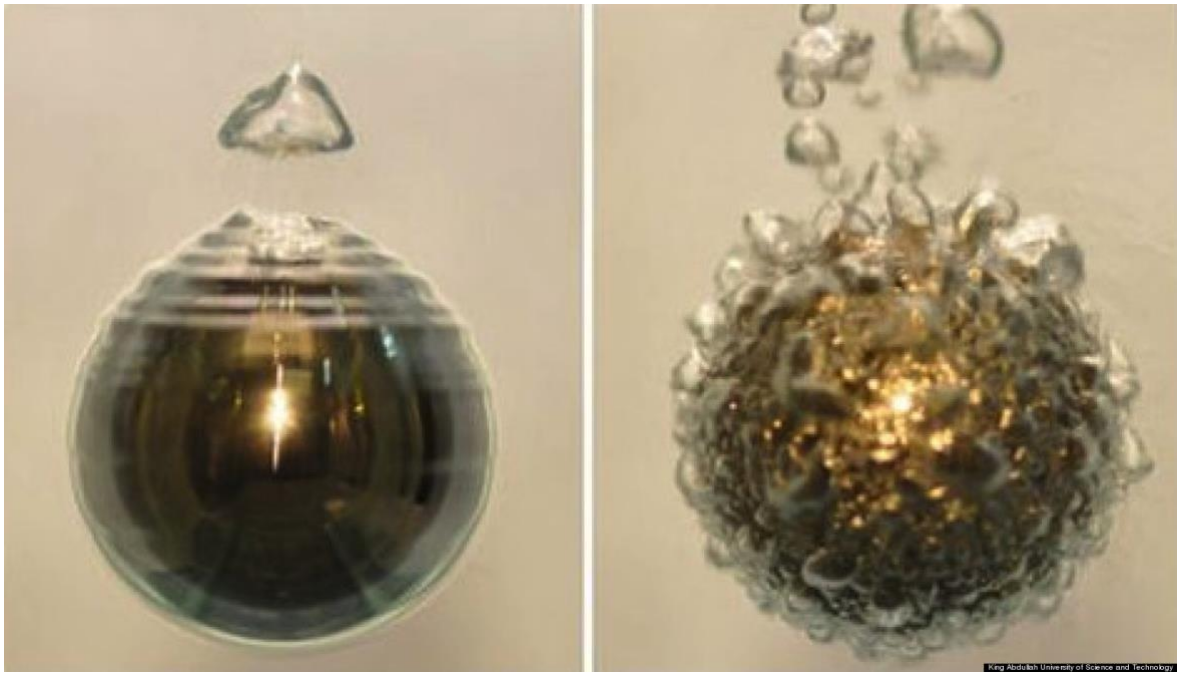

Figura 7: A sinistra: effetto del raggiungimento del flusso critico su di una sfera di metallo ad alta temperatura: DNB; a destra, il nucleate boiling, prima del raggiungimento del flusso critico (huffingtonpost.com)

Una spiegazione sul raggiungimento del punto critico di ebollizione in funzione del flusso termico viene mostrata, dando particolare attenzione a tutte le fasi di sviluppo di questo fenomeno, dalla semplice convezione al minimo flusso raggiunto.

Tre correlazioni per il calcolo del flusso critico, e quindi del DNBr sono implementate, con i relativi commenti e validità, in modo analogo all'analisi delle correlazioni sulla fase doppia.

Vengono mostrate le differenze nell'uso di queste correlazioni e si argomenta sulla sicurezza del reattore TRIGA, che risulta ottima dagli alti valori di DNBr ottenuti, a dispetto dei minimi valori accettabili per un reattore nucleare, oltre che ad un confronto con i più comuni DNBr dei reattori LWR.

L'analisi è incentrata principalmente sul canale 0, che risulta quello di maggiore interesse in quanto ha il più alto flusso termico.

Oltre al semplice modello 1D si replica anche ogni singolo canale con RELAP5, programma americano che ha lo specifico scopo di simulare e validare tutte le strutture presenti in un impianto nucleare. I risultati ottenuti verranno poi commentati e confrontati con quelli ottenuti in precedenza.

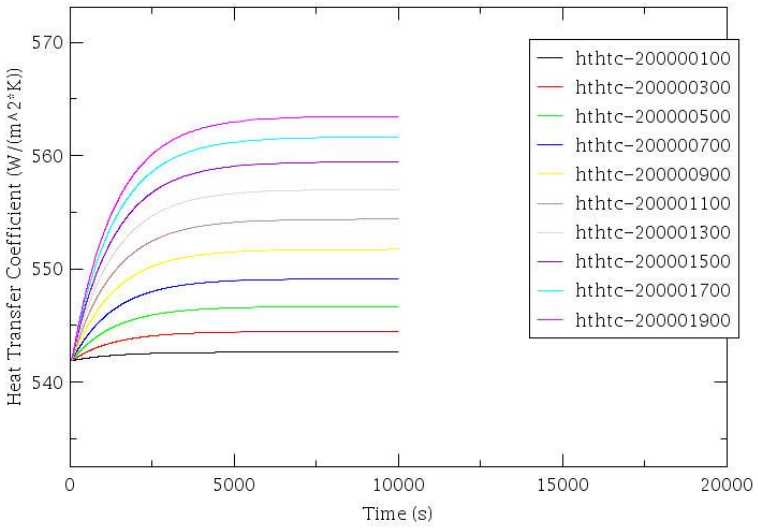

Figura 8: esempio di coefficiente di scambio termico per il canale 3 con Relap

Un confronto molto diretto viene mostrato nelle conclusioni per il canale 0, che risulta essere il più critico dal punto di vista delle condizioni operative.

Table of contents

Acknowledgements ..... ***III***

Sommario ..... ***VII***

Abstract ..... ***XI***

Extended Abstract ..... ***XIII***

Chapter 1 Introduction ***1***

1.1 Thermal exchange in water-cooled nuclear reactors *1*

1.2 Subcooled boiling problem *3*

1.3 Heat exchange regimes and boiling in TRIGA reactor *4*

Chapter 2 TRIGA reactor ***7***

2.1 Technology *7*

2.2 Plant scheme *9*

2.3 Core *10*

2.3.1 Nuclear fuel 10

2.3.2 Control rods 12

2.4 Cooling system *13*

2.5 Instrumentation *14*

2.6 Intrinsic security *15*

Chapter 3 Geometry and power distribution ***16***

3.1 Geometry and characteristic dimensions *16*

3.2 Power production *20*

Chapter 4 Natural circulation analysis ***26***

4.1 Mass flow evaluation *26*

4.1.1 Constant Darcy factor 29

4.1.2 Variable Darcy factor 31

4.2 Natural heat exchange coefficient 36

Chapter 5 Single phase correlations 41

5.1 Dittus-Boelter 42

5.2 Gnielinski correlation 44

5.3 Differences between correlations 46

5.4 Single phase thermal resistances 48

Chapter 6 Double phase correlations 51

6.1 Onset temperature for nucleate boiling 53

6.2 Rohsenow correlation 55

6.3 Stephan-Abdelsalam correlation 57

6.4 Cooper correlation 59

6.5 Gorenflo correlation 60

6.6 McAdams correlation 62

6.7 Jens-Lottes correlation 63

6.8 Chen correlation 64

6.9 Differences between correlations 66

Chapter 7 Temperature profiles 70

7.1 Bulk temperature profile 71

7.2 Single phase temperatures 72

7.3 Double phase temperature profiles 74

7.3.1 Double phase temperature profiles with natural convection coefficients 81

7.4 Other channel analysis 83

Chapter 8 DNB ratio and critical heat flux 86

8.1 Departure from nucleate boiling 86

8.2 Bernath correlation 88

8.3 Bowring correlation 89

8.4 Tong correlation 91

8.5 Results and comment 92

Chapter 9 Relap results 94

9.1 Relap model 94

9.2 Pipe simulation results 96

Chapter 10 Conclusions 109

10.1 Channel 0 comparison 109

10.2 Extended work 114

Acronyms 115

Variables 116

Bibliography 119

Chapter 1 Introduction

In this introductory chapter the problem of heat exchange in water-cooled nuclear reactors is introduced, since it's the most common technology in nuclear energy plants. It brings with it some peculiarities and problems that must be investigated.

1.1 Thermal exchange in water-cooled nuclear reactors

All nuclear plants produce a big quantity of energy from fission reactions, and all this energy is only available in heat form.

A big problem for any nuclear plant is how to efficiently and safely extract this heat and produce energy with a thermo-dynamical cycle. Obviously, there are many technologies based on different types of heat exchange, that are used in nuclear reactors. The most common fluid used for the cooling of the reactor core is obviously water, since it is the safest, cheapest and less toxic one. However, there are many others cooling technologies, such as molten metal or gas, each one with its own peculiarities and problems.

Water cooling is also used in conventional plants, for the reasons said before, but differently from those, for nuclear reactors peculiar and unique scenarios may arise, with catastrophic effects.

Normally, water enters the reactor core, in order to control its temperature, remove heat and, in some reactor technologies, moderate the neutrons. In the most common industrial nuclear plants like PWR (Pressurized Water Reactor) or BWR (Boiling Water Reactor), the cooling mechanism is forced, since there are many pumps that moves water thought reactor. Some Generation IV reactor types aim to use natural convection instead, to improve safety and to ensure the cooling even without the aid of pumps, as could happen in an accident that leads to a blackout.

In water-cooled reactors, the water is directly in contact with the hot fuel elements, exchanging power in steady state conditions, once reached. Re-heated water can boil, like in BWRs producing steam that is conducted directly in turbines, or in a heat-exchanger to give off heat to the cooling fluid of the secondary cycle, that boils and goes in the turbine, like PWRs.

Once steam reaches the turbine is possible to produce energy.

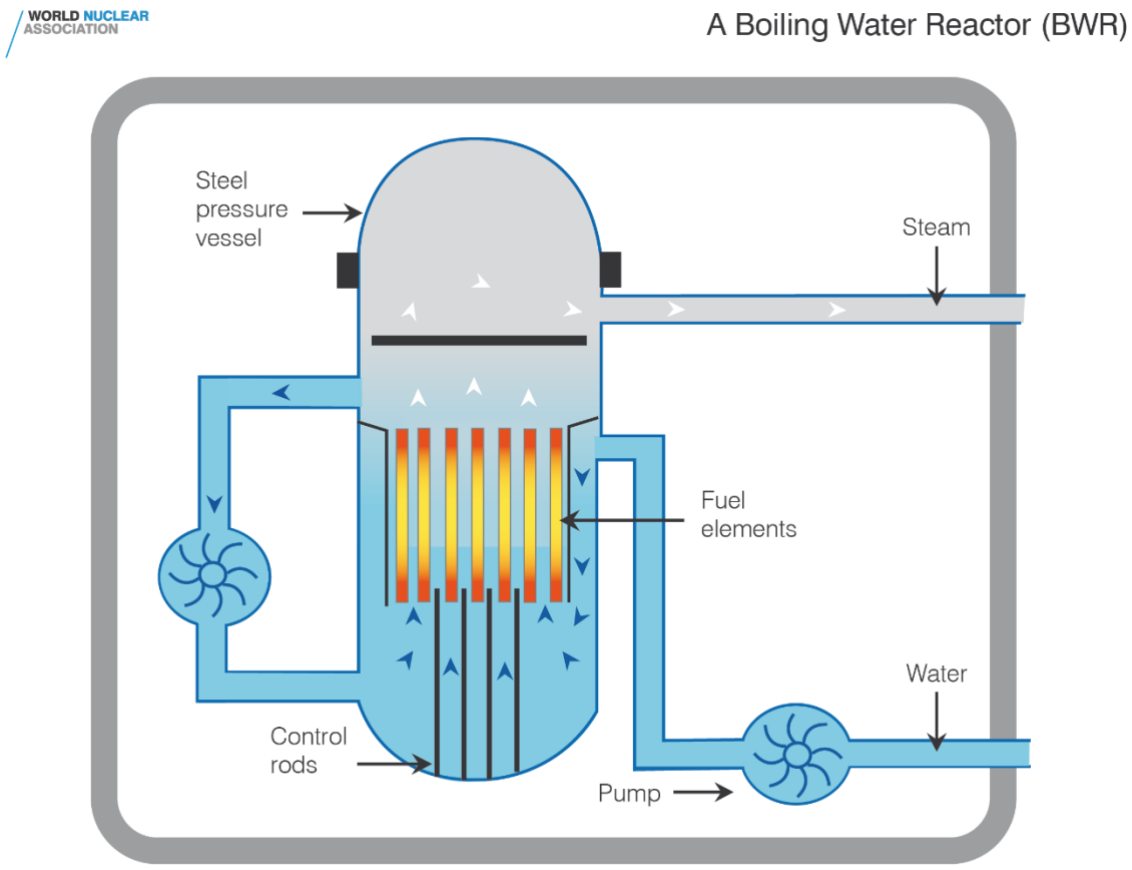

Figure 4.1: BWR scheme, (World Nuclear Association)

In every case, high heat fluxes must be exchanged between the components in order to contain the machine dimensions and so costs, needing higher power densities exchanged in less surface.

Water is an excellent coolant, but both BWRs and PWRs may suffer a phenomenon, called thermal crisis, that represents a very dangerous condition for water-cooled reactors.

In BWRs, water normally boils, so this phenomenon is not so dangerous (the main concern in BWRs is film dryout). In PWRs, the water is normally pressurized to avoid boiling in the primary circuit. In both cases, a threshold value for the heat flux can be determined as a function of many parameters. This value is called critical heat flux: once this value is reached, thermal crisis occurs. In water cooled reactors, thermal crisis occurs when the small bubbles formed during the nucleate boiling phase, which occurs in both reactors, coalesce to form a vapor film covering the fuel element's surface. This causes a dramatic decrease of the heat transfer coefficient and therefore of the efficiency of the heat exchange, causing a sudden rise in the temperature. In PWRs, this condition is called Departure from Nucleate Boiling, whereas in BWRs is called Film Dryout. Although different, they have some similar characteristics. The focus of this work is on the first condition, Departure from Nucleate Boiling.

This condition must be completely avoided, to prevent fuel degeneration in high temperature accidents, like cladding failure that could cause fission gases and products release or melting in most dangerous cases.

Therefore, it's extremely important to study the thermo-hydraulic aspects of the system both to improve the technology in terms of heat exchange and to keep under control the operating temperatures to improve the reactor safety.

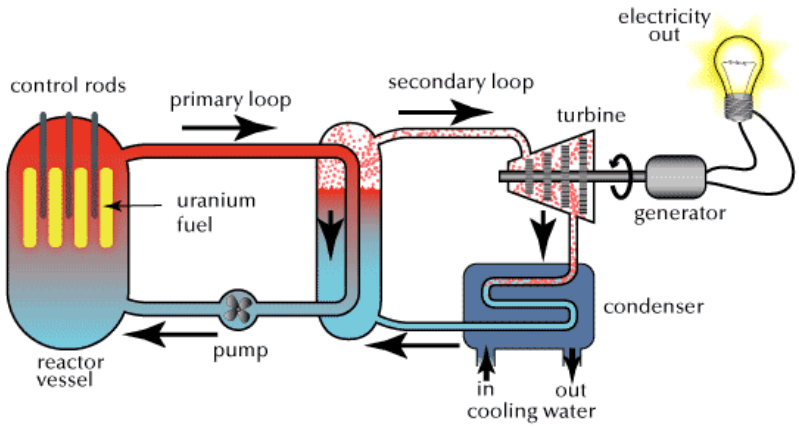

Figure 1.2: PWR scheme (Uaf.edu)

1.2 Subcooled boiling problem

Subcooled boiling is a phenomenon that is highly studied because it's very complex, but it can be very useful in terms of reducing the heat exchange surface and for safety applications. Its mechanism will be described in a more detailed way in a later chapter; to briefly introduce it, if the heat flux is so high to induce close-wall temperature to reach saturation temperature, we can observe bubbles formation near the walls, even when the bulk temperature is significantly lower than the saturation one. It differs from saturated boiling in which all the fluid is on saturated conditions.

The classification of subcooled boiling is pool or flow boiling. In the first case the fluid is prevalently stationary, while in the second one the fluid is moving in a preferential direction.

This phenomenon is used in many heat exchangers; due to the turbulence generated by bubbles, the heat exchange coefficient can be improved several times with respect to the one without considering boiling (fig 1.3 a).

In conventional geometry exchangers with single-phase liquid fluid, maximum values for the heat transfer coefficient is around 20000 $W/m^2°C$; however, with two-phase fluid, like in steam generators, values ten times higher can be reached. This can help keeping under control the temperatures, in case of nuclear reactors. For example, in PWRs, if an accident occurs, both the water temperature and power produced increase result in water boiling,

increasing the heat transfer coefficient and thus “locking” the temperatures, acting as a tampon, and giving time to act in order to bring the reactor back to normal conditions.

However, if the severity of the accident is such that the heat flux increases above the critical heat flux (figure 1.3 b), a film of steam along the cladding outer wall will prevent the correct heat exchange, compromising operational safety.

For this reason, it’s important to study this phenomenon, in order to determine if the reactor operates in safe conditions, and whether the magnitude of the accidents is such that it compromises the reactor integrity.

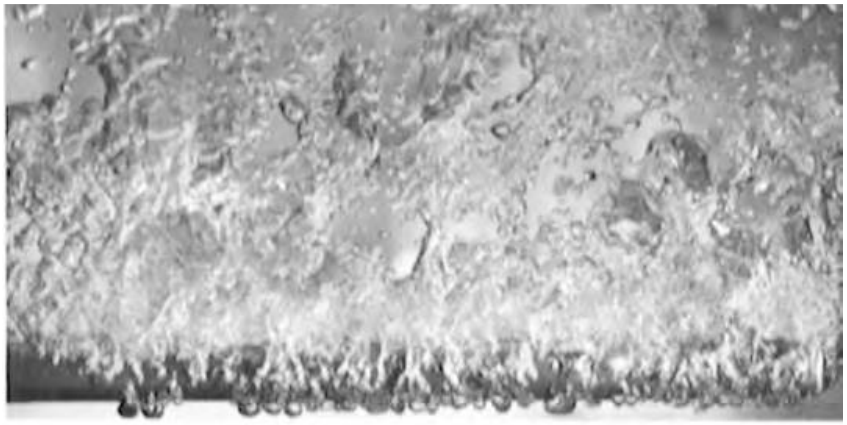

(*a*)

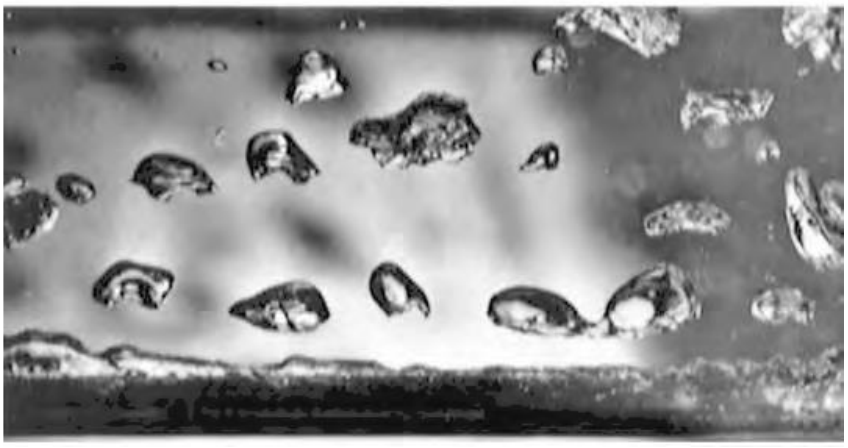

(*b*)

Figure 1.3: a) horizontal subcooled boiling. b) film boiling [8]

1.3 Heat exchange regimes and boiling in TRIGA reactor

The TRIGA Mark II reactor in Pavia was chosen for the analysis of the heat exchange regimes, because in this reactor either single-phase heat exchange or subcooled boiling regime can be observed. This reactor was designed mainly for research and is very flexible; it can be configured for measurements or for testing new technologies.

This thesis work has the objective of analyzing all the possible regimes and values of the parameters of the thermal exchange between water and reactor's fuel elements, focusing on the TRIGA reactor, a pool-type reactor with natural convection-type cooling. Although having dimensions and powers significantly lower than those of commercial reactors, even in this reactor subcooled boiling occurs, and hence the motive for this work, to verify and estimate the quantity of DNB in the highest power conditions.

Although some work has already been done on heat exchange analysis for this reactor model, no in-depth analysis has been performed up to now for the TRIGA reactor in Pavia. Aim of this thesis work is indeed to perform an in-depth analysis of the heat exchange regimes and parameters for the Pavia TRIGA reactor, without the use of 3D model. Starting from the available experimental data and CFD models, several 1D empirical correlations will be analyzed. With respect to the main study on this reactor model, done by Mesquita on the Brazilian IPR-R1 TRIGA reactor and focused on forced convection, this thesis work will consider also natural circulation analysis and a rigorous evaluation of the performance of different and widely used empirical correlations to select the best one in terms of reproducing the experimental data, also taking into account subcooled boiling.

Chapter 2 TRIGA reactor

The acronym TRIGA stands for “Training, Research, Isotopes, General Atomics”. In fact, this reactor model was developed and built by General Atomics Energy department, mainly to improve nuclear research and for the neutron irradiation of various samples.

The TRIGA Mark II operating at the University of Pavia is a testbed for joint research activities by Politecnico and INFN (National Institute of Nuclear Physics), providing experimental information for the study of the reactor dynamics, for neutronics and thermal-hydraulic characterization of the reactor operating regime and for the validation of modeling tools and strategies for the control-oriented simulation.

Many studies have been performed on the characterization of the neutron flux, the burnup analysis, the development of control-oriented models for the core spatial kinetics and the core dynamics simulation. Only recently studies on the reactor thermal-hydraulics and on the heat exchange regime within the core have been started, such as this thesis work.

It is only a few years that thermo-hydraulic analysis have been carried out on this type of reactor and in any case a complete thermo-hydraulic study has never been done.

2.1 Technology

The plant in Pavia is licensed to operate up to 250 kW full-power steady state conditions; it is a pool-type reactor, with the core immersed in 18 m_3 of demineralized water, whose principal purpose is core cooling and radiation shielding. Differently from most other thermal reactors, water is not the principal moderator: the most moderating effect is caused by the fuel itself, as explained better later.

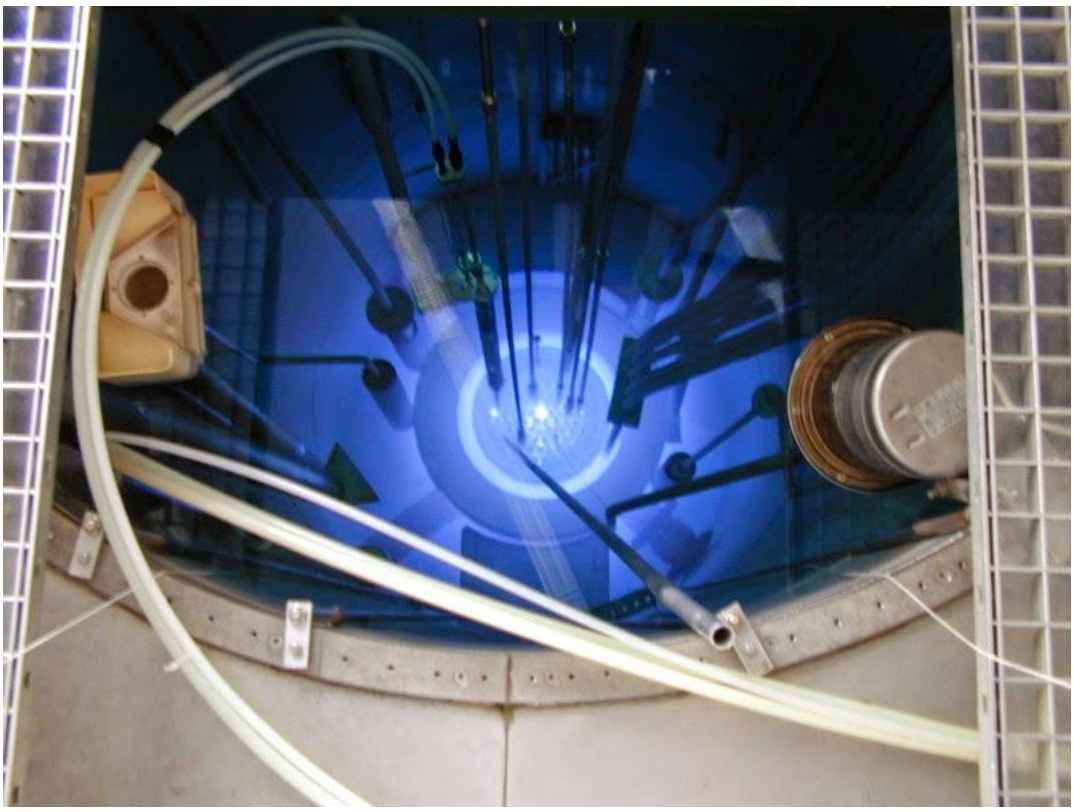

Figure 2.1: running TRIGA

Fig. 2.1 shows the pool in which the reactor is immersed, and the pipes that are needed to cool the reactor. The blue light is the Cerenkov effect caused by the high neutron density.

The core shape is an upright cylinder with diameter 44.6 cm. The fuel elements are distributed along five concentric rings. A layer of graphite surrounds the core radially to further reduce the neutrons leakages, acting as a reflector. The core is placed at 60 cm from the bottom of a 6.26 m cylindrical water pool; a buoyancy force is set up by the density difference among the colder water at the top of the tank and the hotter water at the bottom, where the nuclear thermal power is released. This establishes a natural circulation regime that automatically cools the core.

The central and lateral irradiation channel can be filled by cylindrical samples that will be irradiated by the neutron flux. There are several horizontal irradiation tunnels exiting from the pool, such as the thermal channel in which can be inserted other samples that doesn't need direct irradiation, but flux diminished by water of the pool.

The pool walls are made by boron-enriched concrete and surrounded externally with mobile blocks of a neutron absorbing material, in order to absorb all radiation leaks coming from the reactor core, to minimize the radiation exposure of the operators and the release in the

environment, thus minimizing the biological risk and increasing the overall safety of the plant.

2.2 Plant scheme

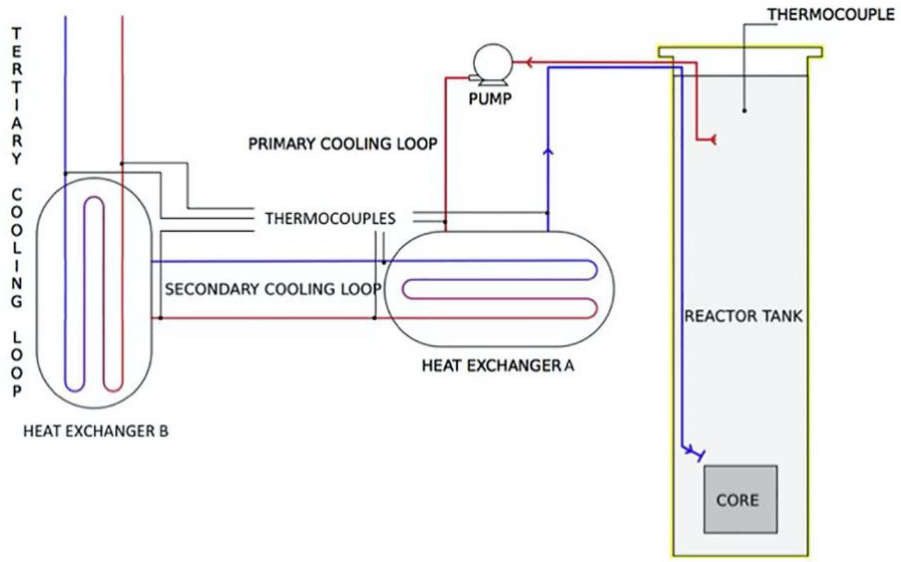

Figure 2.2: plant simplified scheme [5]

Figure 2.2 shows the functioning scheme of the reactor. The primary circuit pulls out hot water from the top of the core, that flows upwards due to the higher temperature. The so called “hot leg” is driven in a U-tube heat exchanger in order to be cooled by a secondary circuit, that is closed and exchanges heat with aqueduct water. The system is hence composed by three different cooling circuits that act in series to adequately cool the reactor. All systems are controlled by a PID system and pneumatic valves to ensure acceptable temperatures of the machine.

2.3 Core

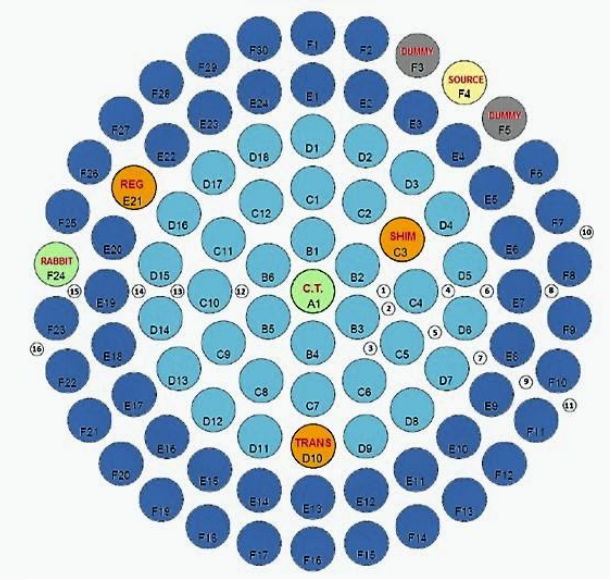

Figure 2.3: core configuration [1].

The configuration of the core is shown in fig 2.3. The aluminum-cladding fuel elements are represented in dark blue, the steel-cladding ones in light blue, the control rods, the sample irradiation channel in green, the dummy graphite elements in grey and the neutron source. The latter can be used for the reactor startup with fresh fuel or to perform experiments on reactor.

This configuration is such that it improves both safety and durability of plant. The use of steel-cladding fuel elements in the inner part of core is justified because near the center of the core higher temperatures and thermal stresses are expected; steel-cladding provides better mechanic properties and thermal resistance, despite the worse thermal conductivity and neutron transparence. The aluminum-cladding elements are positioned in the outer part of the core, where the neutron flux is lower and therefore a lower absorption rate is needed. In addition, due to the lower power generated, also the temperatures are lower.

2.3.1 Nuclear fuel

This type of nuclear reactor is characterized in most part by a particular type of nuclear fuel, composed by solid mixed fuel and moderator.

The fuel is composed by uranium dispersed in a zirconium-hydride matrix (8.5% wt. uranium in fuel and 20% wt. enriched in ^{235}U). This specific composition, with the presence of hydrogen in the ZrH lattice, gives the fuel a moderating effect, even higher than that of water. Indeed, this fuel composition has a large, prompt negative thermal coefficient of

reactivity, meaning that as the temperature of the core increases, the reactivity rapidly decreases.

The fuel matrix appears as a ceramic, hard material, with a good thermal conductivity and chemical compatibility. In fact, the fuel itself represents an important safety aspect, since its moderating effect, and hence its reactivity feedback effect, is prompt, being fuel and moderator in the same solid matrix. The moderation is done by the hydrogen in ZrH_x, which very efficiently moderates the neutrons coming from the uranium fission. The water around the core takes care of the residual part of the moderation, on neutrons that are scattered out of the fuel. In fig 2.4 the fuel is represented by letter A; the top and bottom parts of the rods are made of nuclear graphite (B) and play the role of axial neutron reflectors. In the core there are 90 slots in which the fuel elements, control rods, neutron source and irradiation channels are located, kept in position with the supporting pins (E). There are also 2 samarium burnable poisons between fuel and graphite (C). The cladding is represented by the letter D.

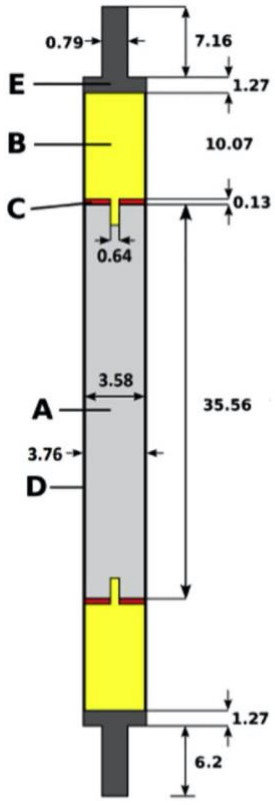

Figure 5.4: fuel element composition

2.3.2 Control rods

The control rods are three and are positioned in different, asymmetrical positions. Each one manages different quantities of reactivity insertion.

The three rods have three different names:

- TRANS: the transient control rod is in the third ring (D) and can either be fully inserted or fully extracted. During reactor operation is always kept extracted to be able to quickly scram the reactor via a pneumatic system, if necessary. It drops about 2$ of reactivity. The insert height can be modified in order to little increase or decrease the reactivity inserted.

- REG: the regulating control rod is placed in the fourth ring (E) and it is used for fine reactivity regulation. It manages about 1$ of reactivity.

- SHIM: it is the inner and most worth control rod, located in the second ring (C) and used for big reactivity regulation and poison compensation (3$ moving).

This configuration is such that it respects the high safety requirement of the reactor, giving it a shutdown margin of 3.5$ in order to keep the reactor subcritical also in the worst

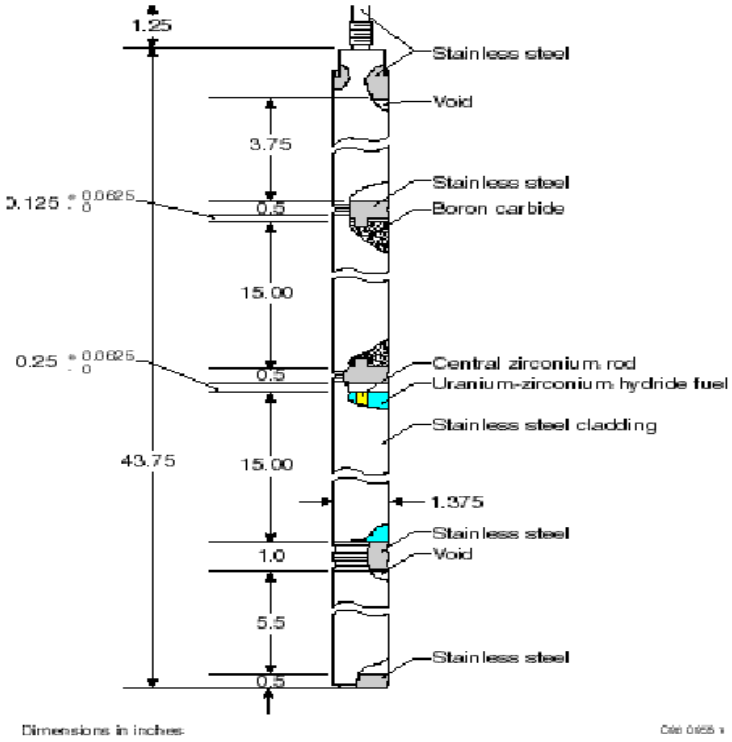

Figure 2.5: Transient control rod axial section (IPR image)

possible condition, with the most influential control rod (SHIM) completely extracted; in fact, to reach criticality at least two control rods must be completely extracted. Another

safety criterion is that the reactor must have excess reactivity less than a half of the total reactivity worth by all 3 control rods.

Fig 2.5 shows a representation of the transient control rods in which the presence of boron carbide, which acts as poison for neutrons, is highlighted. Since it is a pneumatic rod, the lower part of it is still fuel, needed to ensure the correct functioning during pulse operations. In fact, for this reactor it is possible to instantaneously insert reactivity, with the thermal reactivity feedback able to stop the reactor without needing the scram of the control rods.

2.4 Cooling system

The plant has a hydraulic cooling system made of three different circuits (fig. 2.6). The primary circuit draws water from the top of the reactor pool and sends it to a shell-and-tube heat exchanger with exchange surface of 30.7 m^2. The water is then re-injected above the core upper plate, in the bottom of the pool. This causes an interference with the natural circulation flow rising out of the core but helps to control the release of some volatile activated elements from the pool.

This loop allows the natural decay of ^{16}N and other radioactive nuclides that are formed in water prevalently by neutron absorption. In particular, ^{16}N has a mean lifetime of 7/8 seconds and represents the major contribute of radioactivity brought by the coolant. The primary circuit generates a recirculation of the coolant that doesn't permit to these nuclides to go up before being decayed.

An intermediate closed loop removes the heat through a second, plate-type heat exchanger with 45 plates and total exchange surface area of 10.3 m^2. The latter exchanges with a tertiary water line, that draws coolant from the water aqueduct at about 15 °C.

A pH and saline water control system is needed to avoid the formation of incrustations on the surface area of the exchangers, that may lead to lower heat exchange factor and hence higher temperatures of the coolant re-entering in the pool.

All the circuits are controlled by pneumatic valves and thermocouples, and water is moved by electric pumps; they are also armed by an auxiliary pool that serves as storage and emergency buffer stock of coolant.

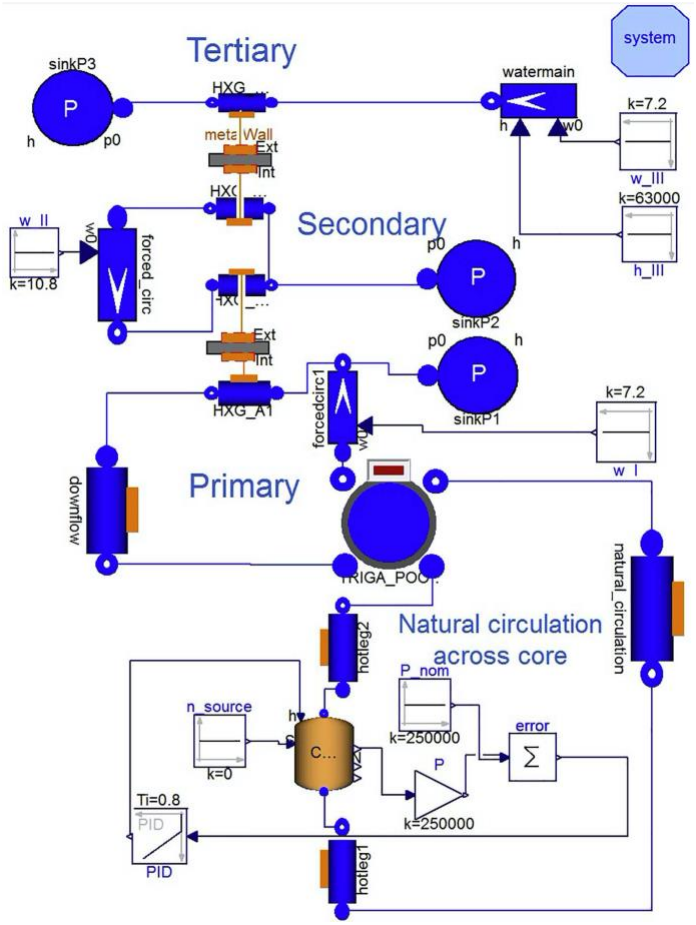

Figure 2.6: more detailed plant scheme

This type of configuration is an example of perfectly safe cooling system.

2.5 Instrumentation

There are many instrumentations that permit the control and management of the plant. As seen in fig 2.6, there are many manometers, thermocouples, flow measure and control tools inside all the cooling loops, but the most significant ones are in the reactor in order to directly monitor the “heart” of the system.

There are a series of fission chambers inside and outside the reactor, which permits the measurement of the neutron flux in critical locations, thus having a measure of the power produced by the reactor core during operation.

There are also some thermocouples in various locations of the reactor core, that give precise information about the temperature reached by the fuel, the coolant and other components of the core.

Some emergency devices and systems are activated if one of these instruments gives a measure that can mean a critical situation, in order to avoid disasters.

An example of devices could be the scram procedure or the lock of outside ventilation by depressurization of the environment, to prevent the diffusion of radioactive contaminants outside the reactor.

2.6 Intrinsic security

The TRIGA reactor was built to be very safe, in order to perform research and development tasks without worrying about running into dangerous accidents. In fact, this reactor was designed primarily for research purposes, giving less importance to energy purposes; such a reactor model would not be suitable for industrial energy production.

The most important safety factor is the high prompt reactivity feedback described before that only this type of technology has. In addition, the three heat exchangers in series together with the auxiliary tank ensure the removal of large quantities of heat.

Finally, natural convection allows to cool down the reactor even in the event of a loss of power accident. This feature, combined with the enormous capacity of the pool, ensures long intervention times in case of accidents.

There are many other features that ensure the correct operating conditions of the reactor, guaranteeing the enormous safety of the TRIGA Mark II reactor.

Chapter 3 Geometry and power distribution

In this chapter the geometry of the reactor will be analyzed detailer, along with all concepts and tools needed to characterize the power distribution of the reactor and the cooling channel dimensions that allow to dissipate it.

3.1 Geometry and characteristic dimensions

The reactor is cooled by itself thanks to natural circulation. This regime is established by the buoyancy force established by the generated heat in the core, which is transferred from the fuel elements to the water of the pool. This buoyancy force implies an upward movement of the coolant, cooling the system. In order to describe this phenomenon and other heat exchange phenomena, the geometry of the cooling channels must be accurately described.

In order to evaluate the geometry features of the system, the main dimensions of the core must be introduced. The radius of the fuel element is 1.88 cm, while the pitch between the fuel elements is a half of ring B diameter:

$$X = \frac{D_{ring}}{2} = 4.11\ cm \tag{3.1}$$

Each ring of elements is arranged at a radius equal to the pitch from the previous one, which means that the space between two radially adjacent elements is:

$$\Delta X = X - 2R = 0.35\ cm \tag{3.2}$$

where R is the radius of the fuel element. The total height of the core is 72.06 cm, of which the so-called active height, where fissions take place, is 38.1 cm. Water is heated in this region and then channeled to the exit of the core. In the upper and lower part of the core respectively grid spacers and supporting holes are present to guarantee the correct spacing of the elements and prevent excessive vibrations during operation. They represent concentrated pressure losses, not considered in this work.

The first step of the analysis is the calculation of the hydraulic area of each channel, taken radially from center to outer core. The considered radial channels are shown in figure 3.1. This radial slice of the reactor was chosen for the analysis because it is the farthest one from discontinuities generated by the control rods and the empty channels.

Each of the 5 channels between two rings has different area and geometry. From center to outer core, the channels are labelled from 0 to 4.

Intuitively, the power generated is higher in the inner channel, called channel zero, and decreases going into the outer channels.

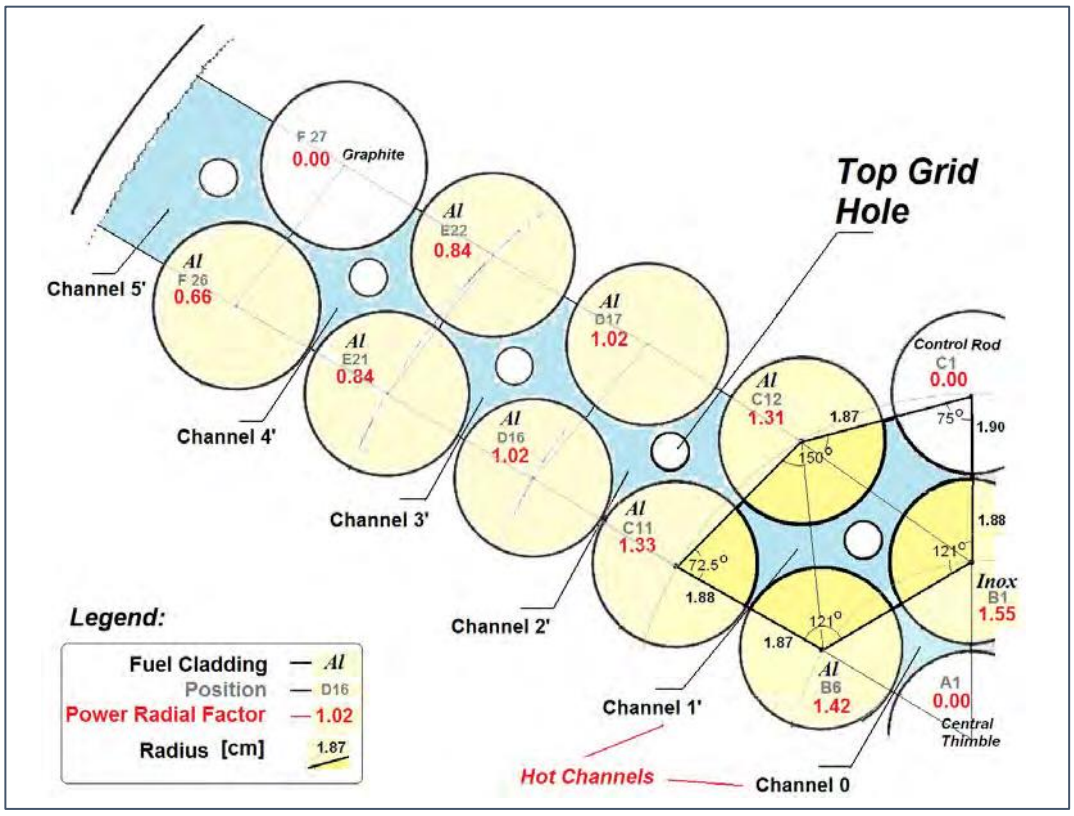

Figure 3.1: detailed representation of aluminum configuration Radial TRIGA channels [6]

The fundamental parameter for thermal-hydraulics analysis is the characteristic dimension of the conduct in which the fluid flows, represented by hydraulic diameter:

$$D_h = 4A_h/p_w \tag{3.3}$$

where A_h is the hydraulic area, that is, the cross section in which flows the fluid, and p_{wet}, is the perimeter that is wetted by the fluid in the channel. These two parameters must be computed for each channel.

Channel 0 is between ring A and B, and it has a triangular pitch. It is visible in fig 3.2.

$$A_{h1} = X^2 \frac{\sqrt{3}}{4} - \frac{\pi R^2}{2} \tag{3.4}$$

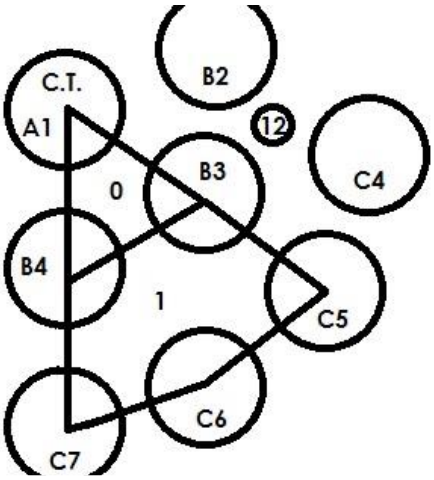

Figure 3.2: zoom on first two channel geometry (upper view)

The wetted perimeter is easily calculated by:

$$p_{w1} = \pi R \tag{3.5}$$

For this channel, also the heated perimeter is important. This quantity differs from the wetted perimeter only for this channel because the central element (A1in fig 3.2), being the irradiation channel doesn't provide heat to the water. Therefore, this quantity is defined as:

$$p_{heat1} = \frac{2}{3} p_{w1} \tag{3.6}$$

Channel 1 has a more complicated geometry, since it is a pentagonal-like channel (fig 3.2). The hydraulic area can be obtained summing the area of all sub-triangles and subtracting the fuel element occupied area:

$$A_{h2} = \left(2 - \frac{\sqrt{3}}{4}\right) X^2 - \frac{3}{2}\pi R^2 \tag{3.7}$$

The wetted perimeter is easily obtained, like before:

$$p_{w2} = \frac{3}{2}\pi R \tag{3.8}$$

The other three radial channels (2,3 and 4) have roughly the same shape, that can be approximated as a parallelogram minus the area occupied by the 4 fuel elements:

$$A_h = X^2 \sin(\theta) - \pi R^2 \tag{3.9}$$

where θ is the angle between the core radius and the junction of two adjacent elements of the ring (75°,80° and 84° respectively for channel 2,3 and 4).

The wetted perimeter for these channels is computed as:

$$p_w = 2\pi R \tag{3.10}$$

The geometry parameters are summarized in table 3.1:

Table 3.1: Geometry data found

Channel	Hydraulic diameter (cm)	Hydraulic Area (cm^2)	Wetted perimeter (cm)
0	1.21	1.78	5.91
1	2.23	9.87	17.7
2	1.46	4.32	11.8
3	1.63	4.82	11.8
4	1.77	5.22	11.8

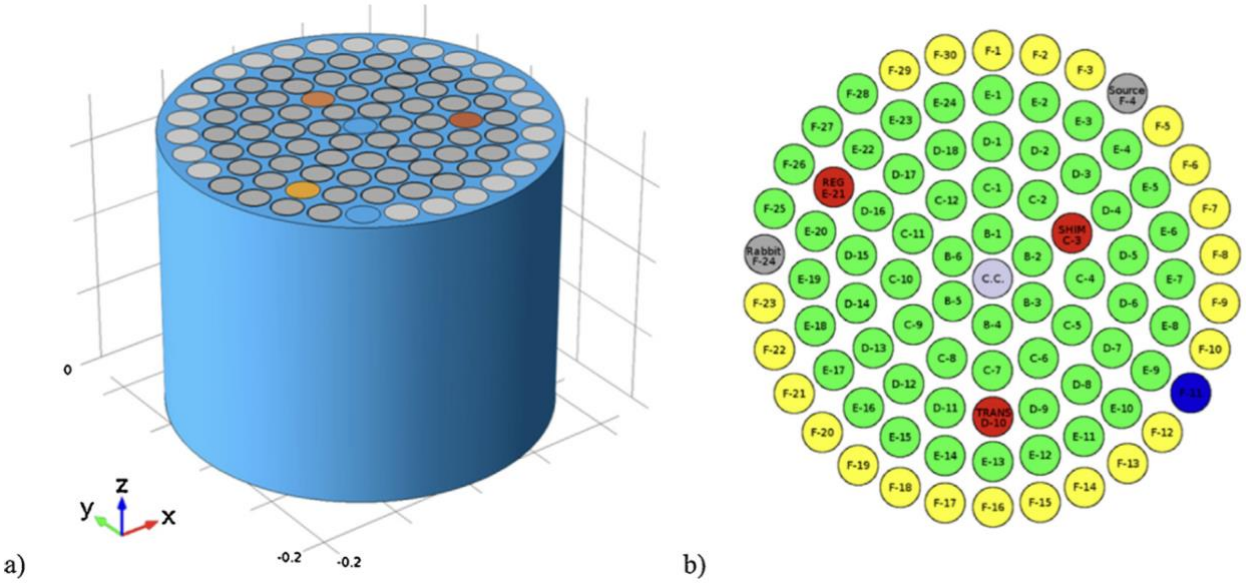

Figure 3.3: 3D and upper representation of the core configuration [4]

3.2 Power production

The fuel elements in the TRIGA reactor are located in five concentric rings (six, considering also the empty central channel), equidistant from the center and labelled with the letters A to F from inner to outer part of the core. Each ring produces a different percentage of power, as the neutron flux has a maximum in the center of the reactor. The produced power can be approximated as a zero order Bessel function of the radius; however, this isn't completely true, because the core configuration is asymmetric. Still, the asymmetry is not so marked as to completely exclude this approximation. In this work the Bessel function approximation is not used, but rather a Monte-Carlo simulation [4] of the entire reactor is taken as reference to statistically determine how much power is produced per ring.Table 3.2 reports the power per ring produced.

Table 3.2: power distribution according with Monte-Carlo simulations

Ring power percentage	Ring B	Ring C	Ring D	Ring E	Ring F
Power percentage	26.8%	23.3%	20.2%	16.9%	12.8%
Number of active fuel elements	6	11	17	23	26
Power percentage per element	4.46%	2.12%	1.19%	0.734%	0.427%

These numbers are calculated with respect to the configuration of the core shown in fig 3.3, considering that some elements of the rings are control rods or empty channels.

These quantities are sufficient to describe global parameters, such as the natural convection heat exchange factor, and to reconstruct the power distribution within each fuel element.

This work will reproduce the entire power regime that can be exercised by the reactor, rescaling the power of the component by means of the factors described in table 3.2.

At first, after having chosen the desired power regime of the reactor, the power per ring can be defined as:

$$\dot{Q}_{ring} = \dot{Q}\chi_{ring} \tag{3.11}$$

where $\dot{Q}$ is the overall power of the reactor and χ_{ring} is the power fraction produced per ring as listed in table 3.2. Dividing it by the number of elements the power per element of the ring can be determined:

$$\dot{Q}_{el} = \frac{\dot{Q}_{ring}}{N_{el}} \tag{3.12}$$

Finally, the power transferred from the elements to the corresponding cooling channels can be found, considering the portion of the element that heats the channel and the corresponding power production, as a function of the element of the ring. For example, channel 0 is heated by 2 elements of ring B, but only one sixth of the power per each element is given to channel 0, resulting in 1/3 of the power produced by the elements of ring B. All relations for each channel are:

$$\dot{Q}_{ch} = \begin{pmatrix} \frac{1}{3}\dot{Q}_B \\ \frac{2}{3}\dot{Q}_B + \frac{5}{6}\dot{Q}_C \\ \frac{1}{2}\dot{Q}_C + \frac{1}{2}\dot{Q}_D \\ \frac{1}{2}\dot{Q}_D + \frac{1}{2}\dot{Q}_E \\ \frac{1}{2}\dot{Q}_E + \frac{1}{2}\dot{Q}_F \end{pmatrix} \tag{3.13}$$

The above represents the quantity of power absorbed by a single channel due to its geometrical parameters.

Table 3.3: Power given to single channel at total reactor power of 250 kW

Power per channel absorbed	Ch 0	Ch 1	Ch 2	Ch 3	Ch 4
Power (kW)	3.722	11.857	4.133	2.403	1.5339

In order to evaluate the other quantities, also some additional local parameters, coming from local correlations for heat exchange, are needed.

The evaluation of parameters like the DNBr or the ΔT_{wall}, quantities explained better in the DNBr chapter, require the local distribution of power and local heat flux; therefore, additional data are required.

All the calculated parameters do not depend only on the reactor power, but also on axial coordinate, since the power produced in the midplane of the reactor, like the radius coordinate, is higher than in the outer part of the reactor.

The present analysis refers to linear power production and its axial dependence; it is measured in kW/m and has the big advantage of not depending on the area of heat exchange, that is, it doesn't depend on the radius of fuel elements, that may change during operation due to thermal expansions.

Unlike the power distribution first approximation with respect to the radial coordinate, which is a zero order Bessel function, the linear power production is well approximated as a cosine function, whose reference system has its origin in the midplane coordinate:

$$q'(z) = q'_0 \cos\left(\frac{\pi z}{H_e}\right) \tag{3.14}$$

where z is the axial coordinate from the center and H_e is the so-called extrapolated length; this quantity is a representation of the neutronic leakages and represents the height where the neutronic flux, and consequently the power produced, would be zero.

This analysis must be performed for each ring element, because in the outer parts of the core the leakages tend to be higher than in the inner part, thus reducing the produced power. To do this, some Monte-Carlo simulation parameters are considered, based on the

work done by Cammi et al. [6], in which each fuel element has been simulated in average conditions and subdivided in 8 parts from top to bottom, each one with its power production (Table 3.4):

Table 3.4: power production data from Monte-Carlo simulations in average conditions

Fuel Section	**Power production (W)**				
	Ring B	Ring C	Ring D	Ring E	Ring F
1	561	485	427	362	298
2	703	608	526	432	338
3	826	712	614	496	376
4	879	760	657	528	404
5	830	720	626	515	394
6	722	632	548	463	347
7	589	514	443	386	280
8	443	391	341	308	229
Total	5553	4824	4183	3491	2666

These calculations refer to an average situation, that means that reactor is simulated at medium power (100-120 kW), and since the main goal is to reproduce all the possible power ranges of the reactor, these data are only be used to build the model starting from the extrapolated height. That is, the data are interpolated only to obtain the H_e, that determines the shape of the neutron flux.

In the Monte-Carlo simulation, active height H_a has been divided in 8 parts, each one with its power produced.

To obtain local power function these data have been fitted with MATLAB, considering the generic function:

$$y = a\cos\left(\frac{\pi}{b}x\right) \tag{3.15}$$

From the interpolation two parameters are obtained, a and b; only the second is useful since it represents the extrapolated height.

$$H_e = \begin{pmatrix} 54.9 \\ 55.2 \\ 55.7 \\ 59.3 \\ 60.1 \end{pmatrix}$$

All values are expressed in cm. In agreement with the theorical expectation, the extrapolated length for the outer channel is higher, since the neutron leakages are higher.

In order to get a complete evaluation of the linear power, the cosine function must be correlated with the power range. The integral of this function must be equal to the power produced:

$$\dot{Q}_{el} = \int_{-\frac{H_a}{2}}^{+\frac{H_a}{2}} q_0' \cos\left(\frac{\pi z}{H_e}\right) dz \tag{3.16}$$

The constant term q_0' can be extracted from the integral, and obtained from the evaluation of the integral and power range:

$$\int_{-\frac{H_a}{2}}^{+\frac{H_a}{2}} q_0' \cos\left(\frac{\pi z}{H_e}\right) dz = q_0' \frac{2H_e}{\pi} \sin\left(\frac{\pi H_a}{2H_e}\right) \tag{3.17}$$

$$q_0' = \frac{\dot{Q}_{el}}{\frac{2H_e}{\pi} \sin\left(\frac{\pi H_a}{2H_e}\right)} \tag{3.18}$$

Now all the terms needed to evaluate the local linear power as a function of the axial coordinate and the power range are defined:

$$q' = q_0' \cos\left(\frac{\pi z}{H_e}\right) \quad kW/m \tag{3.19}$$

In the present work it has been decided to employ 3000 interpolation points for the power range (from 1 to 250 kW), and 1000 for axial coordinate.

In the actual, three-dimensional system there are some asymmetrical features that make the linear power profile asymmetrical. Since this work is focused on a 1D analysis, these features are not considered.

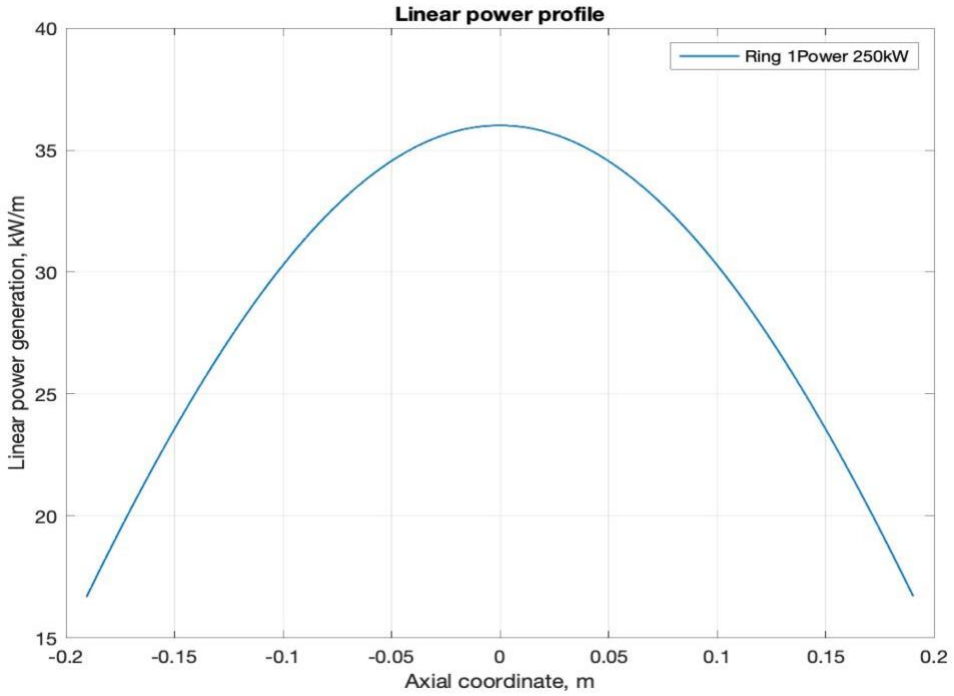

Figure 3.4: ring B linear power profile

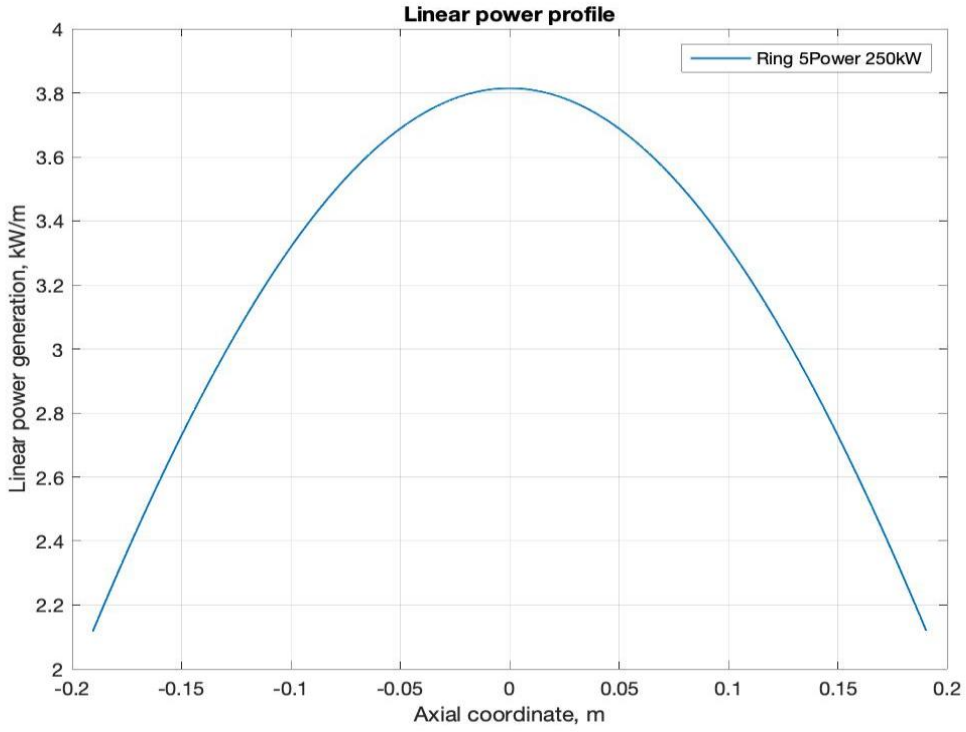

Figure 3.5: ring F linear power profile

Chapter 4 Natural circulation analysis

In this chapter, all the features and quantities related to natural circulation will be analyzed, in order to understand the parameters of the reactor and their order of magnitude.

4.1 Mass flow evaluation

First, the mass of water that flows inside each channel, due to the buoyancy effect, must be quantified.

This effect derives from the Archimede's principle, which states that an object in a fluid receives a thrust proportional to the weight of the volume of liquid moved. In this case the object is not a solid one, but is the fluid itself, that it is heated by the reactor fuel elements, decreasing its density and thus generating an upward thrust force that generates an upward flow.

This is the so-called buoyancy effect, which causes the natural cooling of the reactor, without the need of pumps. Natural circulation is a critical aspect for reactor safety because it happens without external inputs, even in case of loss of power accidents or other emergency situations.

Being in a steady state condition, the equations to determine the mass flow derive from a balance of pressure between the upper and the lower part of the reactor. This implies that in the whole reactor the pressure losses generated due to the flow must be equal to the density decrease caused by the temperature increase of water:

$$\Delta P_\rho = P_{down} - P_{up} = \Delta \rho g H \tag{4.1}$$

where g is the value of the gravity acceleration field, ρ is the density of water and H the total height of the reactor. This expression must be balanced with the pressure losses generated due to the flow, considering a pipe-like conduct:

$$\Delta P_l = f_d \frac{H}{D_h} \rho_{in} \frac{v^2}{2g} \tag{4.2}$$

The quantity v is the velocity in m/s of the coolant in the conduct, and ρ_{in} is the inlet density. Density variations due to changes in the fluid temperature are not considered in this estimation, because the density variation within the conduct does not exceed 0.7% in the worst case. With this formula only the distributed pressure losses are estimated, since grids and spacers, which represents concentrated pressure losses, are not considered in this work.

Another justified approximation is to completely neglect the pressure losses due to the thermal expansion of the channel. This because the channel is not closed, and the thermal dilatation factor has an order of magnitude of about 10^{-5}-10^{-6}. Hence, this phenomenon has not be considered in this work.

The f_d term is called the Darcy friction factor, and is a factor depending on geometry, velocity of the coolant and roughness of conduct. This factor correlates the pressure losses to the velocity, and it will be treated more accurately later.

The final balance equation is:

$$f_d \frac{H}{D_h} \rho_{in} \frac{v^2}{2g} = \Delta \rho g H \tag{4.3}$$

Now, to calculate the mass flow, the above equation must be rewritten. At first, the left-hand side will be analyzed. The mass flow is correlated with velocity, density and the hydraulic area as:

$$\dot{m} = \rho_{in} A_h v \tag{4.4}$$

The velocity squared rewritten in terms of mass flow has the form:

$$v^2 = \left(\frac{\dot{m}}{\rho_{in} A_h}\right)^2 \tag{4.5}$$

The left-hand side thus becomes:

$$f_d \frac{H}{D_h} \frac{1}{2g\rho_{in}} \frac{\dot{m}^2}{{A_h}^2} \tag{4.6}$$

The right-hand side is written considering the density variation Δρ:

$$\Delta\rho = \rho_{in} \beta \Delta T \tag{4.7}$$

where β is the thermal density variation coefficient factor (1/°C), having supposed a linear variation of density with temperature. This approximation is true for low pressures and low temperature changes, as is the case of the TRIGA reactor.

The term ΔT, that is, the water temperature difference between inlet and outlet, can be rewritten considering the transferred power:

$$\Delta T = \frac{\dot{Q}_{ch}}{\dot{m} Cp} \tag{4.8}$$

where Cp is the isobaric specific heat constant of the water (J/kg°C), taken as constant with respect to the water temperature. The balance equation becomes:

$$f_d(\dot{m}) \frac{H}{D_h} \frac{1}{2g\rho_{in}} \frac{\dot{m}^2}{{A_h}^2} = \frac{\dot{Q}_{ch}}{\dot{m} Cp} \beta \rho_{in} g H \tag{4.9}$$

where the Darcy factor is written as function of the mass flow, since it is defined using specific correlations.

4.1.1 Constant Darcy factor

A first approximation is to consider a constant Darcy factor, that is a function of neither the mass flow nor dimensions.

$$fd = 0.04$$

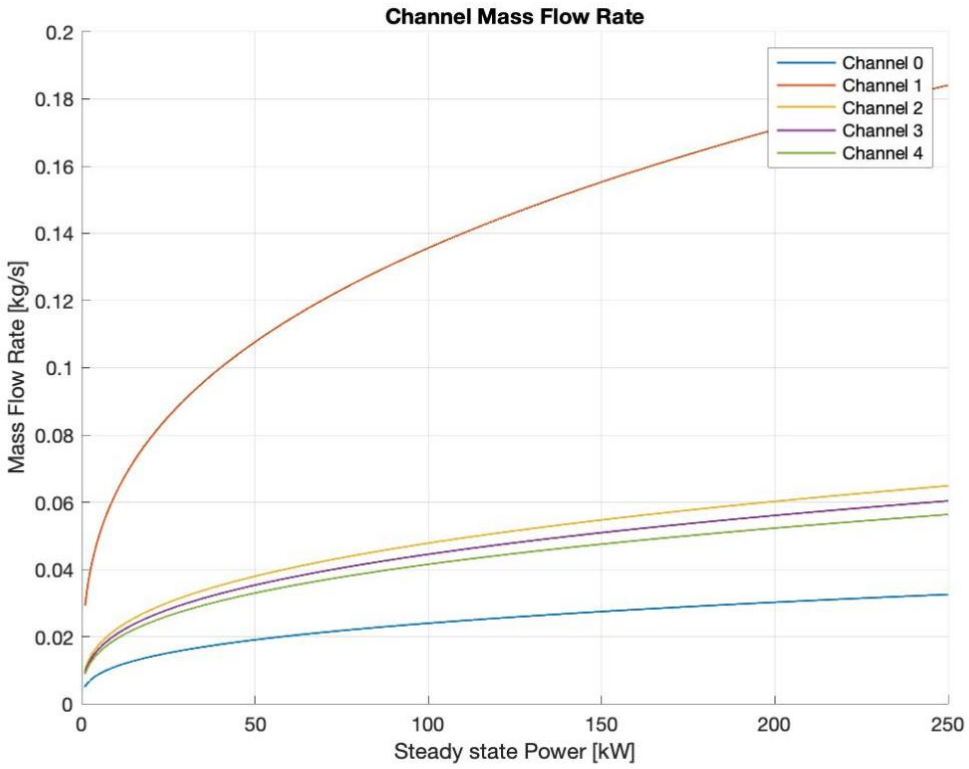

Figure 4.1: constant darcy friction factor mass flows

This first tentative value refers to tubes of similar dimensions and water flow regime. Under this strong first order approximation, the magnitude of the mass flow in each channel can be estimated.

From eq 4.9, an explicit expression of the mass flow rate can be written:

$$\dot{m} = \sqrt[3]{\frac{2\dot{Q}_{ch}\beta g D_h {A_h}^2 {\rho_{in}}^2}{Cpf_d}} \tag{4.10}$$

This is a simple, explicit function that describes the mass flow rate as a function of the power entering the water channel and the geometry. Fig 4.1 shows the magnitude of mass flow with constant Darcy factor. The mass flow rate of channel 1 is the highest, due to the highest power per channel and hydraulic area, while is lowest for channel 0, the narrowest.

Another quantity useful to analyze is the Reynolds number, a dimensionless quantity which represents the ratio between the inertial forces (related to the flow velocity) and the viscous ones of the system. It is usually used for forced convection system, still it is interesting to describe its behavior. It is defined as:

$$Re = \frac{\rho v D_h}{\mu} \tag{4.11}$$

where μ is the viscosity of fluid, considered constant and equal to the one at the inlet temperature (20°C) and pressure of the bottom of pool (1.5 bar). It can also be expressed as a function of mass flow:

$$Re = \frac{4\dot{m}}{p_w \mu} \tag{4.12}$$

Fig 4.2 shows the Reynolds number of each channel as a function of the power.

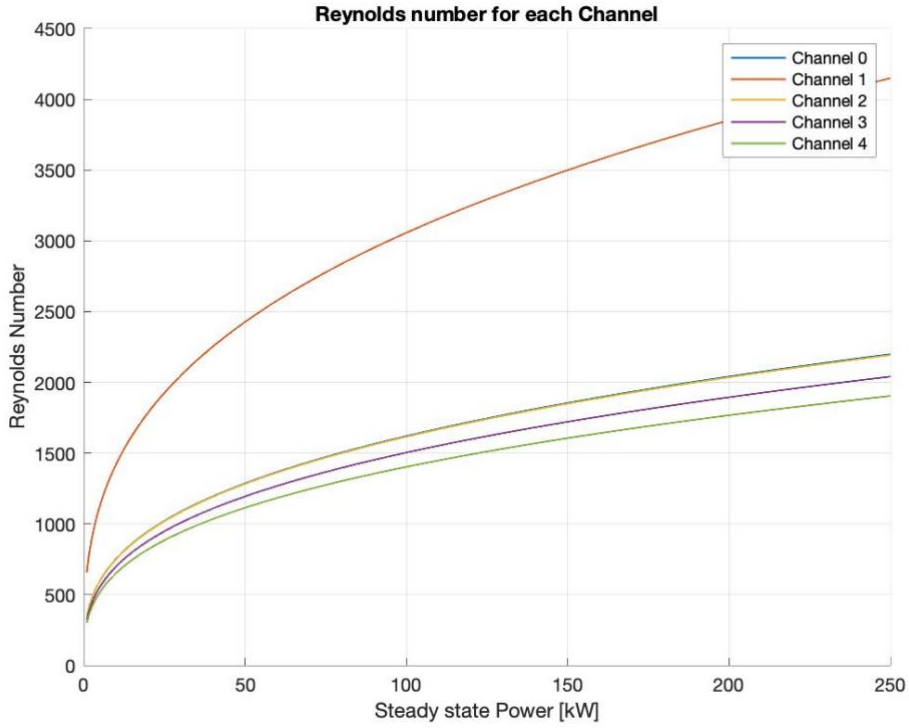

Figure 4.2: Reynolds per channel function of power

From Fig. 4.2 it can be seen how, according to the Reynolds number and considering a pipe-like geometry, the flow regime is expected to be laminar for all power and all channels excluding the channel 1, whose flow regime enters the transition region above 50 kW, considering that the transition starts around Re>2300.

4.1.2 Variable Darcy factor

In order to have a more precise estimation for the mass flow, a more accurate definition of the friction factor can be considered, taking the Darcy factor as a function of velocity, geometry and roughness factor:

$$f_d = f_d(Re(v, D_h), Rgh) \tag{4.13}$$

where Rgh is the average roughness dimensions, which, considering steel-cladded elements, is about 1μm for the present case. The correlation chosen for the evaluation factor is the implicit Colebrook-White correlation:

$$\frac{1}{\sqrt{f_d}} = -2\log_{10}\left(\frac{Rgh}{3.71D_h} + \frac{2.51}{Re\sqrt{f_d}}\right) \tag{4.14}$$

This equation must be solved in terms of fd. This is a complicated but very accurate correlation, since it predicts very well all flow regimes for the TRIGA reactor, barring the transition regime for which there are no valid correlation. Even though this correlation is commonly used for pipes, it can be also adopted for the considered channels, which are all circular-like.

This correlation can be expressed in explicit form, which has been implemented in MATLAB:

$$f_d = \frac{1}{\left[\frac{2W\left(\frac{\ln(10)}{5.02/Re}10^{\frac{Rgh*Re}{18.574D_h}}\right)}{\ln(10)} - \frac{Rgh*Re}{9.312D_h}\right]^2} \tag{4.15}$$

where W is the Lambert W function of order zero.

To solve with respect to the mass flow, three equations in the three unknowns $\dot{m}, Re, f_d$ are needed. Thus, the solving system is shown in eq 4.16, the definition of Reynolds and the mass flow expression.

$$\left\{\begin{array}{c} \frac{1}{\sqrt{f_d}} = -2\log_{10}\left(\frac{Rgh}{3.71D_h} + \frac{2.51}{Re\sqrt{f_d}}\right) \\ Re = \frac{4\dot{m}}{p_w\mu} \\ \dot{m} = \sqrt[3]{\frac{2\dot{Q}_{ch}\beta g D_h {A_h}^2 {\rho_{in}}^2}{Cpf_d(Re, Rgh)}} \end{array}\right\} \tag{4.16}$$

Once solved, from this system the mass flow rate, the Reynolds number and the Darcy friction factor are obtained:

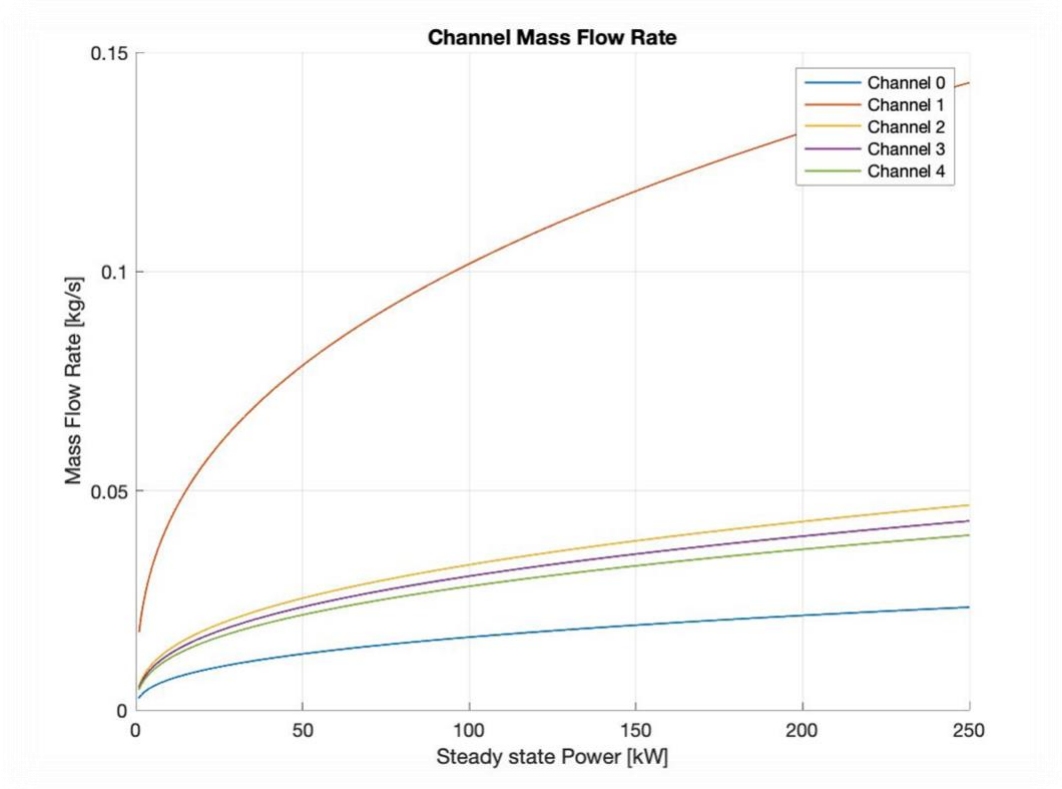

Figure 4.3: mass flow rate with Colebrook-White correlation

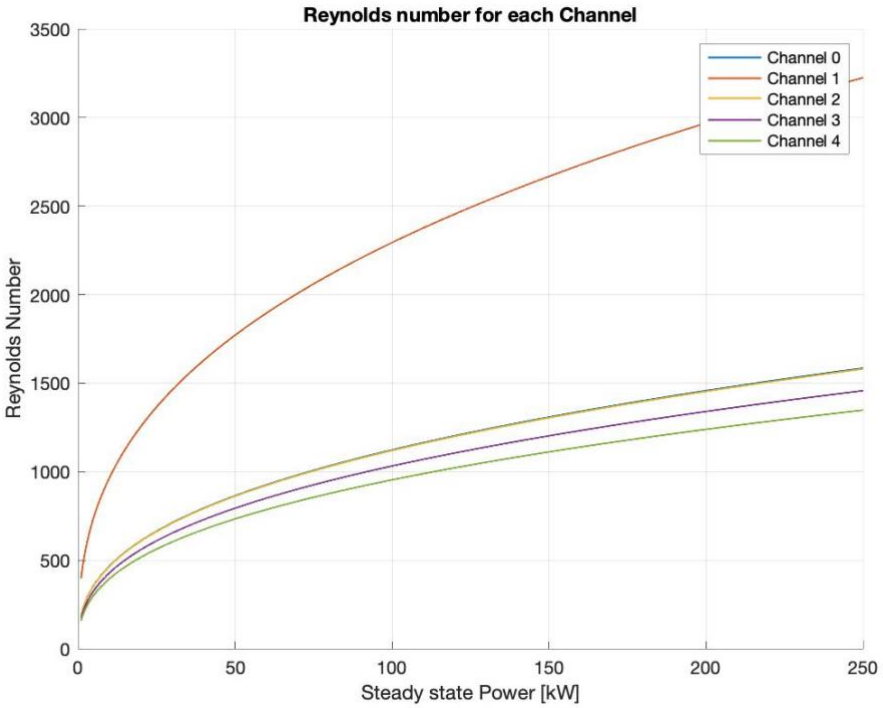

Figure 4.4: Reynolds number with Colebrook-White correlation

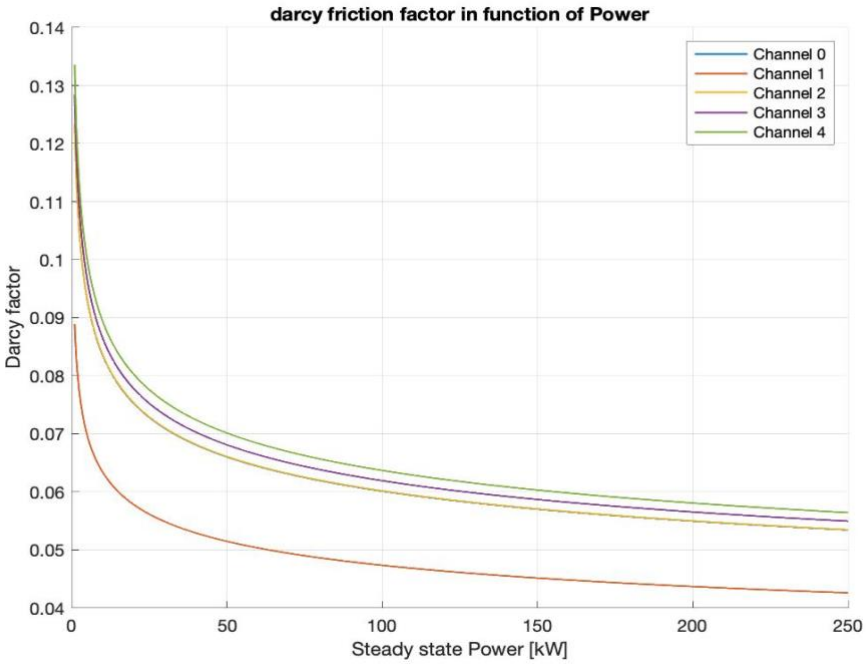

Figure 4.5: Darcy friction factor variation with reactor power

Both mass flow rate and Reynolds number are lower than the ones calculated with a constant friction factor. This means that the approximation of constant fd is an underestimation of the Colebrook-White obtained Darcy factor.

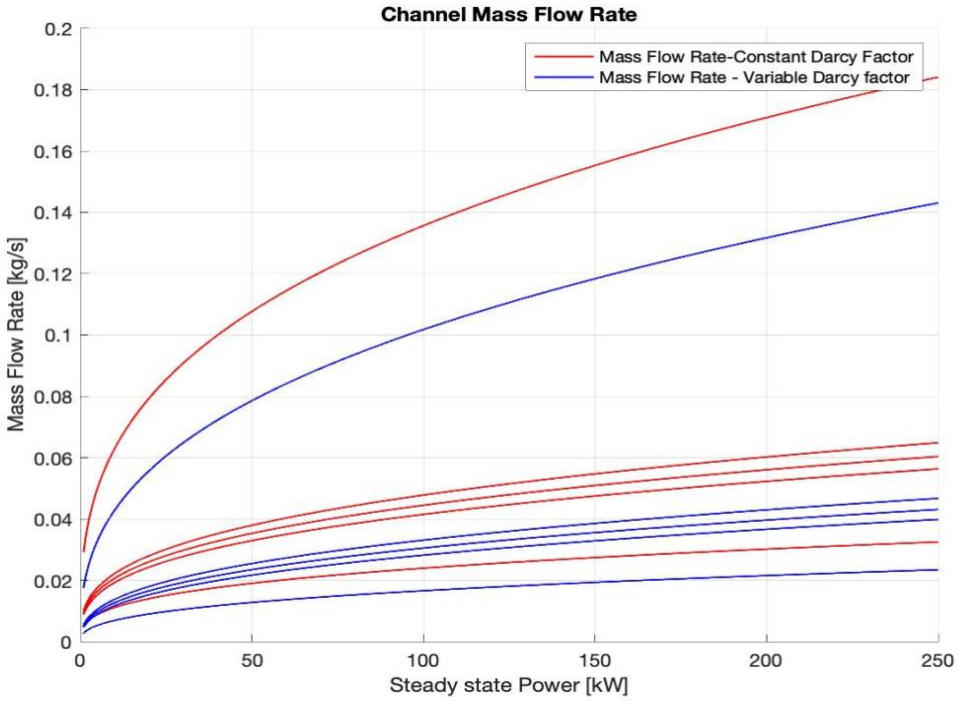

Figure 4.6: mass flow differences

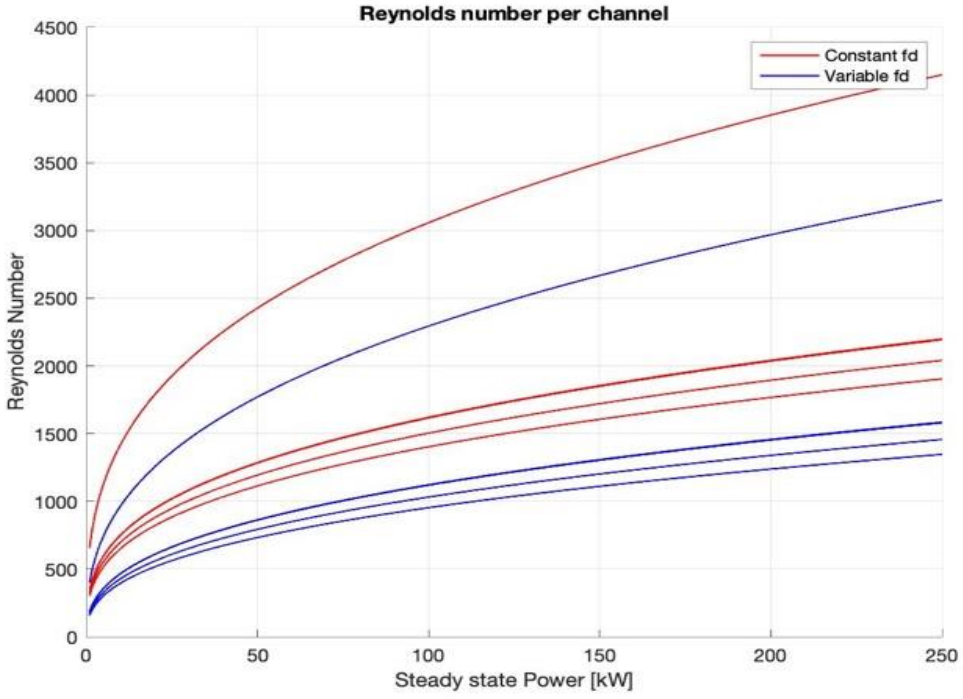

Figure 4.7: Reynold differences

For the rest of this work, the values calculated with the Colebrook-White correlations will be considered, coming from a more accurate approach.

4.2 Natural heat exchange coefficient

Once the mass flow rate has been determined, the next step is to determine the natural convection heat exchange factor, in order to evaluate how much heat is transferred per second due to natural circulation.

A dimensionless number that is specific for the natural convection regime is the Grashof number, defined as:

$$Gr = \frac{g\beta {D_c}^3 (T_s - T_b)}{\nu^2} \tag{4.17}$$

where D_c is the characteristic dimension of system, which for the considered case corresponds to the hydraulic diameter, $T_s - T_b$ is the difference between the temperature at the wall and the temperature of the coolant bulk and ν is the kinematic viscosity.

The Grashof number represents the ratio between buoyancy inertial forces and viscous ones, and thus better describes the natural convection regime with respect to the Reynolds number. This number can be rewritten in order to obtain a more usable form, as a function of the heat flow introduced in the channel, instead of the surface temperature difference.

In fact, this difference can be rewritten as a pure conductive slab, whose characteristic thickness is again the hydraulic diameter:

$$\Delta T_s = \frac{{q_{ch}}'' D_h}{K_w} \tag{4.18}$$

where K_w is the thermal conductivity of water and q_{ch}'' is the channel average heat flux, which is defined as:

$$q_{ch}'' = \frac{\dot{Q}_{ch}}{p_w H_a} \tag{4.19}$$

The expression of the Grashof number thus becomes:

$$Gr = \frac{g\beta {D_h}^4 {q_{ch}}''}{K_w \nu^2} \tag{4.20}$$

Another dimensionless quantity of fundamental importance is the Prandtl number, defined as:

$$Pr = \frac{\nu}{\alpha} = \frac{Cp\mu}{K_w} \tag{4.21}$$

where α is the thermal diffusivity. This number represents the ratio between the momentum and thermal diffusivity of the material, and thus depends on the material considered. For water, it's about 6.99.

The majority of the correlations used to calculate the heat exchange factor uses the Nusselt number, that is the ratio between convective and conductive heat transfer of the system:

$$Nu = \frac{h}{K_w D_h} \tag{4.22}$$

where K_w is the thermal conductivity of fluid, h the convective heat coefficient (W/m^2 °C). The most common general form for this correlation is:

$$Nu = ARe^a Pr^b \tag{4.23}$$

where Re can be substituted by Gr in case of natural convection, keeping the same value for a and b. Using the Grashof and Prandtl numbers a fourth dimensionless quantity, the Rayleigh number, can be defined:

$$Ra = GrPr \tag{4.24}$$

This number represents the ratio between the buoyancy forces and viscous forces, and explicitly it is defined as:

$$Ra = \frac{g\beta {D_h}^4 q''}{K_w \nu \alpha} \tag{4.25}$$

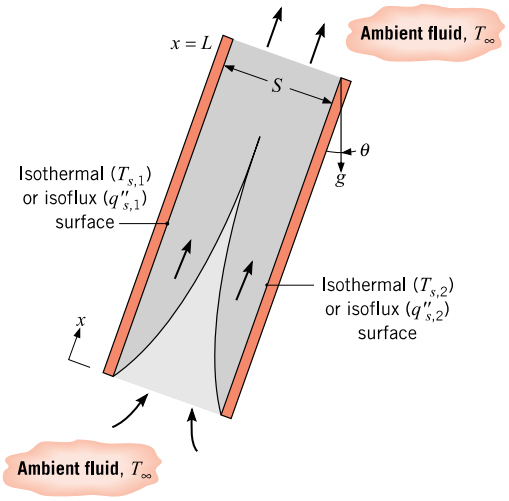

Figure 4.8: bilateral channel natural heat exchange representation [8]

The Nusselt number for all channels under consideration and for all power regimes of the reactor must now be evaluated. From dedicated chapter in Incropera book [8], the best correlation is found to be the Bar-Cohen and Rohsenow one, that describes parallel-plate vertical channels geometries. This correlation has the form:

$$Nu = \left[\frac{C_1}{\left(Ra \frac{D_h}{H_a} \right)} + \frac{C_1}{\left(Ra \frac{D_h}{H_a} \right)^{2/5}} \right]^{-0.5} \tag{4.26}$$

$$h = \frac{NuK_w}{D_h} \tag{4.27s}$$

where the constants C1 and C2 depends on the geometry and flow conditions, and they assume values of 48 and 2.51 respectively, considering an iso-flux condition.

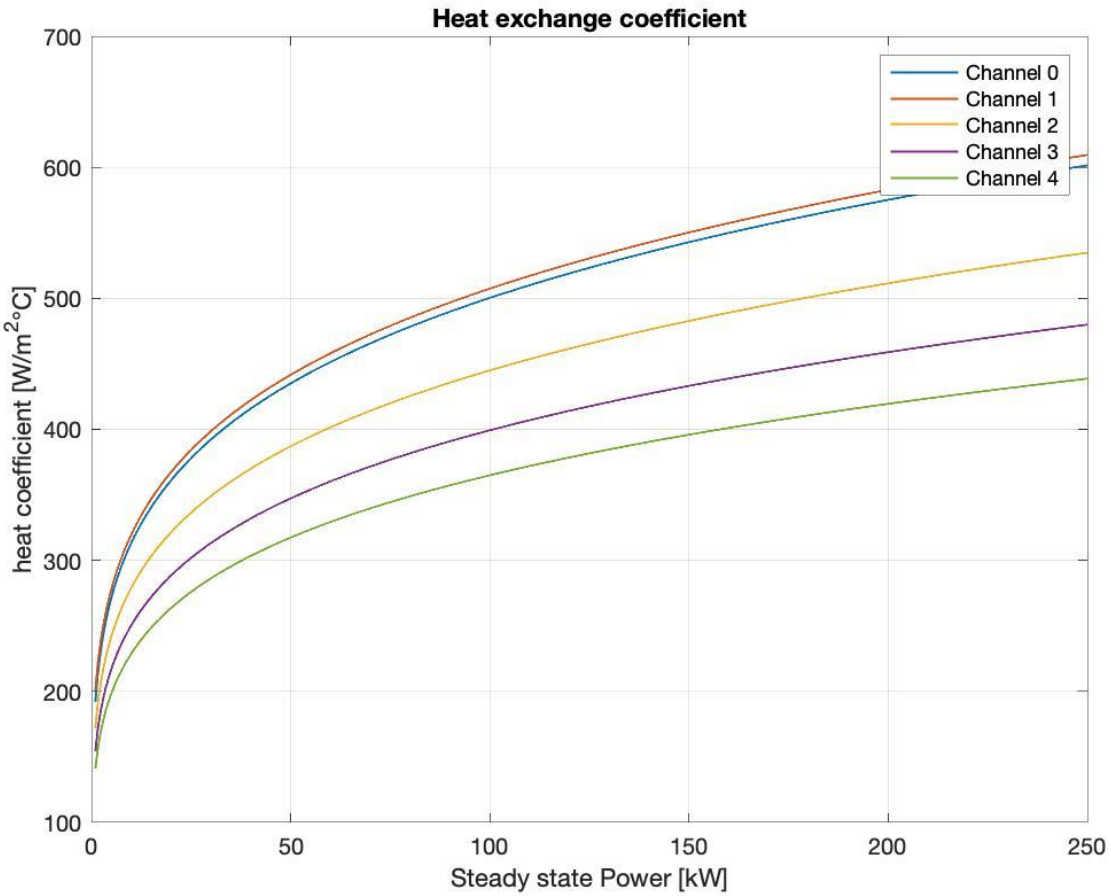

Figure 6.9: heat exchange coefficient function of power reactor

Fig 4.9 shows how increasing power causes an increase of also h. These values, which were found considering only natural circulation, are expected to be more accurate for the more external channels and lower powers, since at a certain power value forced convection of the system or subcooled nucleate boiling are expected to severely improve the heat exchange coefficient.

Chapter 5 Single phase correlations

In this chapter the most suitable correlations that can better describe the behavior of single-phase heat exchange, starting from the flow rate calculated using the Colebrook-White correlations, will be shown and compared. Most of these correlations are used for turbulent forced convection. Still, it is possible to use them also for the TRIGA reactor, because of the presence of spacers and grid plates that causes flow mixing alongside the channel. To support this consideration, it will be seen that laminar correlations severely underestimate the heat exchange coefficient; however, the fluid dynamics of the reactor remains unconfirmed. The graph plotted in fig 4.4 predicts Reynolds number in laminar/turbulent flow, but only distributed charge losses are taken into account; being the presence of these grids it can be said that Re calculated is probably an underestimation of real one, concluding that the regime is prone to be turbulent. We have natural convection, but for high power regimes forced convection cooling is turned on, in order to easily cool the machine. For evaluate which one is prevalent a simple ratio can be taken into account [8]:

$$\frac{Gr}{Re^2} \ll 1 \tag{5.1}$$

Since it tends to zero, natural convection is negligible in comparison with the forced one. This relation is verified in each channel and in each power condition, when forced convection is active. To check if the behavior can be considered forced, we take into consideration the previously calculated mass flow rates and use them as if they were forced instead of natural.

Most of these single-phase correlations are adapted for high pressures and fully developed flow; therefore, the most suitable one for the TRIGA reactor must be selected comparing all suitable correlations.

5.1 Dittus-Boelter

This correlation is one of the simplest and has a form similar to one described in eq 4.22:

$$Nu = ARe^{0.8}Pr^{0.4} \tag{5.2}$$

where A is a constant that depends on the channel geometry. For the geometry under consideration, the Weisman correlations for a triangular pitch are considered:

$$A = \varphi C \tag{5.3}$$

$$\varphi = 1.13\frac{X}{2R} - 0.2609 \tag{5.4}$$

$$C = 0.026\frac{X}{2R} - 0.006 \tag{5.5}$$

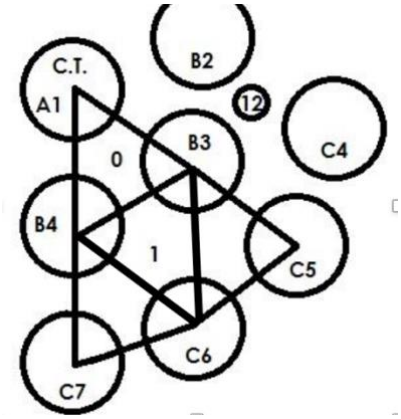

Figure 7.1: first two channel subdivided

Rigorously, this correlation is valid only for channel 0, but it is applied here for all other channels, because they can all be formed by smaller triangular sub-channels.

The validity for the Dittus-Boelter correlation is normally in the range of:

$$Re > 10000$$

$$0.6 < Pr < 160$$

$$\frac{H}{D_h} > 10$$

which are not fully respected (especially for what concerns the Reynolds number). Still, for the reasons mentioned above, it will still be used.

Once Nu is calculated, h can be easily obtained from the Nusselt number definition (eq 4.26).

Another correction that can be used, since the water viscosity at the wall temperature is usually less than the one in the inlet, is the Petrukov one:

$$Nu_c = Nu\left(\frac{\mu_{in}}{\mu_w}\right)^{0.11} \tag{5.6}$$

where the viscosities are referred to inlet temperature and wall temperature, as a first approximation taken as an average between inlet and saturation temperature.

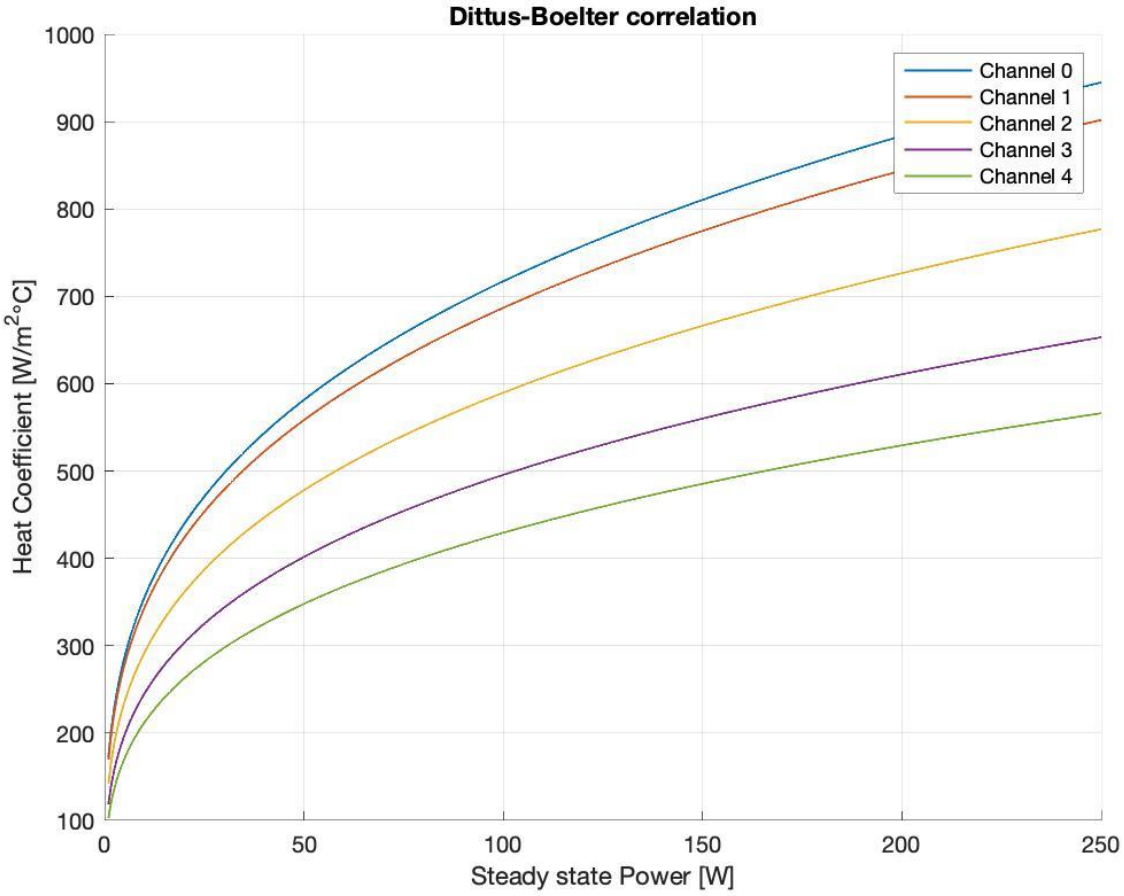

Figure 5.2: Dittus-Boelter correlation coefficients

5.2 Gnielinski correlation

This correlation is valid for conditions that are closer to the ones found in the TRIGA reactor, and therefore it is expected to be the most accurate one. This correlation depends on the Moody friction factor, which for pipes has the following expression:

$$f_m = (0.79 \ln (Re) - 1.64)^{-2} \tag{5.7}$$

The Gnielinski correlation then assumes the form:

$$Nu = \frac{(Re - 1000)\, {f_m}/{8}\ Pr}{\left(1 + 12.7(Pr^{\frac{2}{3}} - 1)\left({f_m}/{8}\right)^{0.5}\right)} \tag{5.8}$$

This correlation has validity in the following ranges:

$$2300 < Re < 10000$$

$$0.5 < Pr < 2000$$

Now, as mentioned before, it is expected that the Gnielinski correlation will provide better results than the Dittus-Boelter one: however, experimental data show that this is not the case when dealing with TRIGA reactors, for which the Gnielinski correlation leads to a huge underestimation of the heat transfer coefficient. It is also worth mentioning that for Re < 2300 the Gnielinski correlation is not defined, and therefore it is not good to predict the heat exchange coefficient value for some channels.

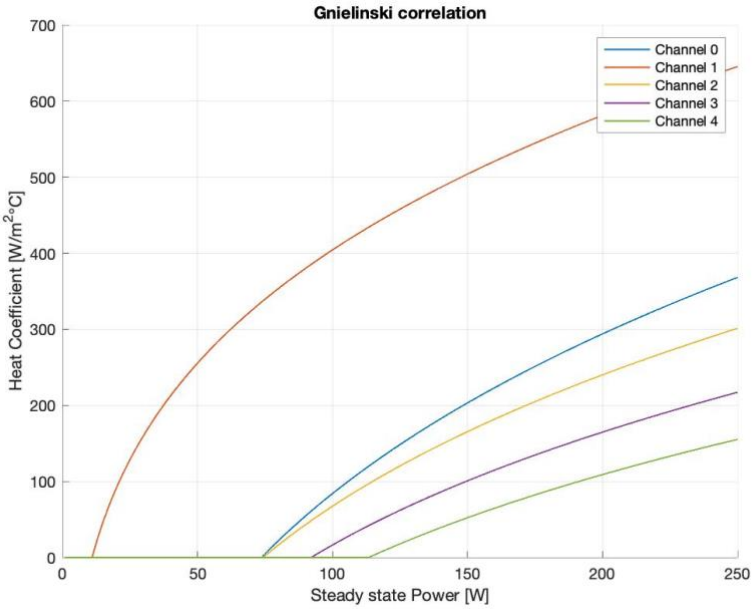

Figure 5.3: Gnielinski coefficients

5.3 Differences between correlations

Following the above analysis, it is useful to see the differences between heat exchange coefficient computed by the two correlations and under the natural circulation regime. The most appreciable differences can be seen at the highest possible power of 250 kW.

For channel 0, it can be seen how the Gnielinski correlation is quite different from the other two cases, since the Reynolds number in this channel is quite low due to the low hydraulic area.

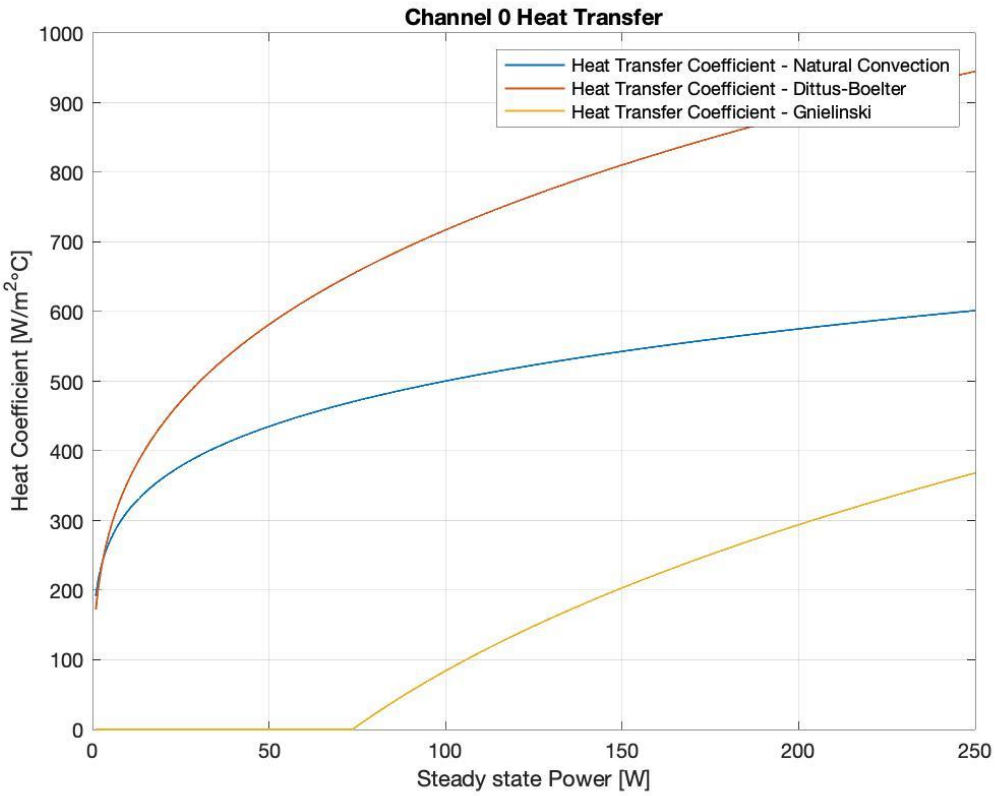

Figure 5.4: Single phase h of channel 0, at 250 kW.

As the channel Reynolds number increases, due to the higher hydraulic area and mass flow, the Gnielinski correlation behaves better than in the previous case, even if it still underestimates the exchange coefficient (as in channel 1). However, the behavior of the Gnielinski is even worse for the external channels, like channel 4 (fig 5.6).

The natural convection and the Dittus-Boelter correlation, instead, work better, as they compute similar values of h. Obviously, the single-phase correlations find a higher heat exchange factor respect to the natural one, since they refer to the turbulent regime. Still, the differences are not so high, and these correlations are expected to well predict the behavior, except when nucleate boiling occurs.

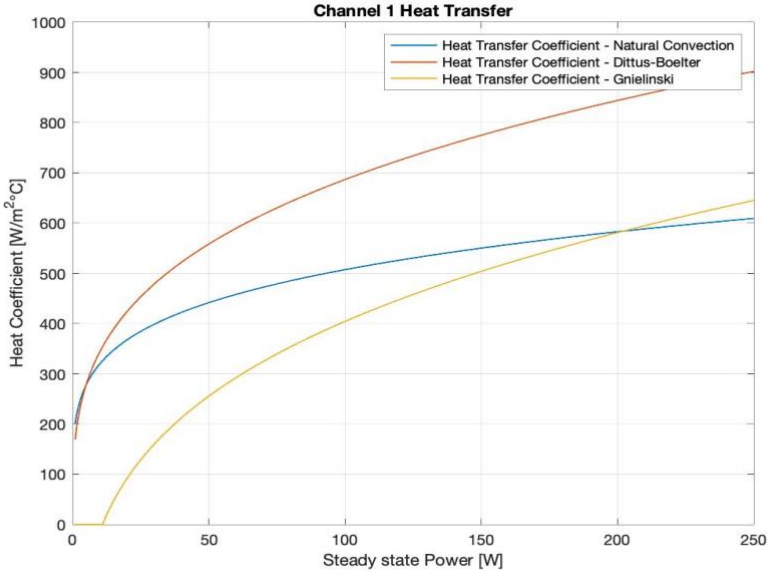

Figure 5.5: Single phase h of channel 1.

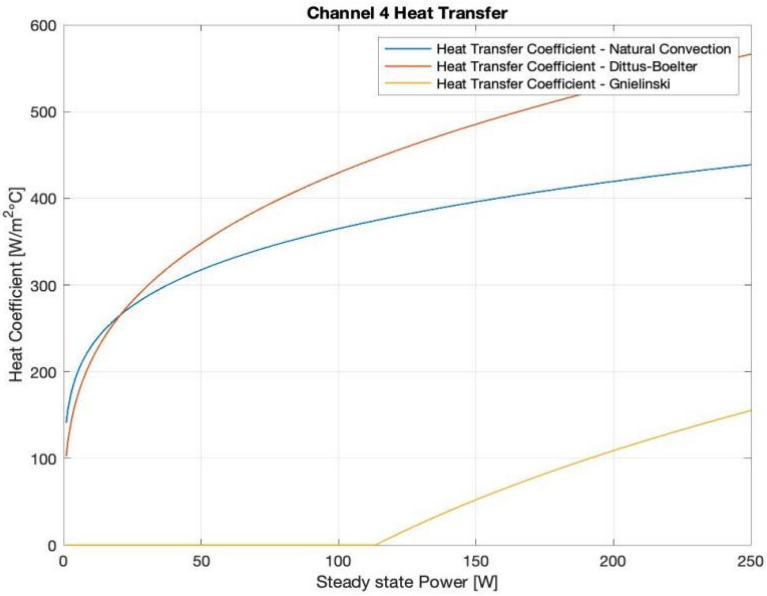

Figure 5.6: Single phase h of channel 4

5.4 Single phase thermal resistances

Finally, it can be useful to observe the variation of the weight of the convection thermal resistance with respect to the total thermal resistances of the core. The thermal resistance is a quantity that, in analogy with the circuit resistances, represents the capacity of a body or material to oppose to a heat flux.

The general thermal resistance is defined as:

$$TR = \frac{\Delta T_{body}}{q_{body}''} \tag{5.9}$$

and is the ratio between the temperature difference between the upstream and downstream of the body and the thermal flux that crosses it.

In analogy with electrical circuits the temperature difference can be compared with the voltage difference ΔV, the flux with the current intensity and the thermal resistance to the electrical one. In fact, for constant flux as the temperature increases so does the resistance.

This quantity is expressed in m^2°C/W, and it's the inverse of thermal exchange coefficient h.

Thermal resistance in series must be added, in analogy with electrical circuits; all these resistances refer to a specified area, that can be chosen arbitrarily. For simplicity, the thermal resistance with respect to the linear power is considered, in order to exclude the dependency from the arbitrary area and the radius. The unit of measure thus becomes the inverse of a linear conductivity, m°C/W.

The first thermal resistance met from the fluid to the fuel centreline is the one related to the convection and is defined as:

$$TR_{conv} = \frac{1}{2\pi R h} \tag{5.10}$$

The second resistance is the one relative to the cladding, and it is the inverse of the conduction coefficient in a cylinder:

$$TR_{cl} = \frac{ln\left(\frac{R}{R_{cli}}\right)}{2\pi K_{cl}} \tag{5.11}$$

where R_{cli} is the inner radius of cladding and K_{cl} is the thermal conductivity of the cladding. For this analysis, the value for steel has been considered.

The third is the gap resistance, between fuel and cladding, that is defined starting by the conductance of the gas inside which acts as a "shock absorber"; a value of h_{gap}=2561 W/m2°C, obtained dividing the gas conductance and gap thickness, is considered, and it is kept constant for all analyzed conditions. The corresponding resistance is:

$$TR_{gap} = \frac{1}{2\pi R_{cli} h_{gap}} \tag{5.12}$$

The last resistance is the one coming from the fuel, approximated as a full cylinder with generation of power inside. For the same reason said before, to simplify the problem only a constant volume power production is considered:

$$TR_{fuel} = \frac{1}{4\pi K_f} \tag{5.13}$$

where K_f is the thermal conductivity of the fuel. To evaluate the overall heat exchange factor U, the inverse of summation of resistances is evaluated:

$$U = \frac{1}{TR_{conv} + TR_{cl} + TR_{gap} + TR_{gap}} \tag{5.14}$$

where at the denominator there is the sum of all thermal resistances in series. The convection weight is evaluated as (fig 5.7):

$$RW_{convection} = \frac{TR_{conv}}{1/U} \tag{5.15}$$

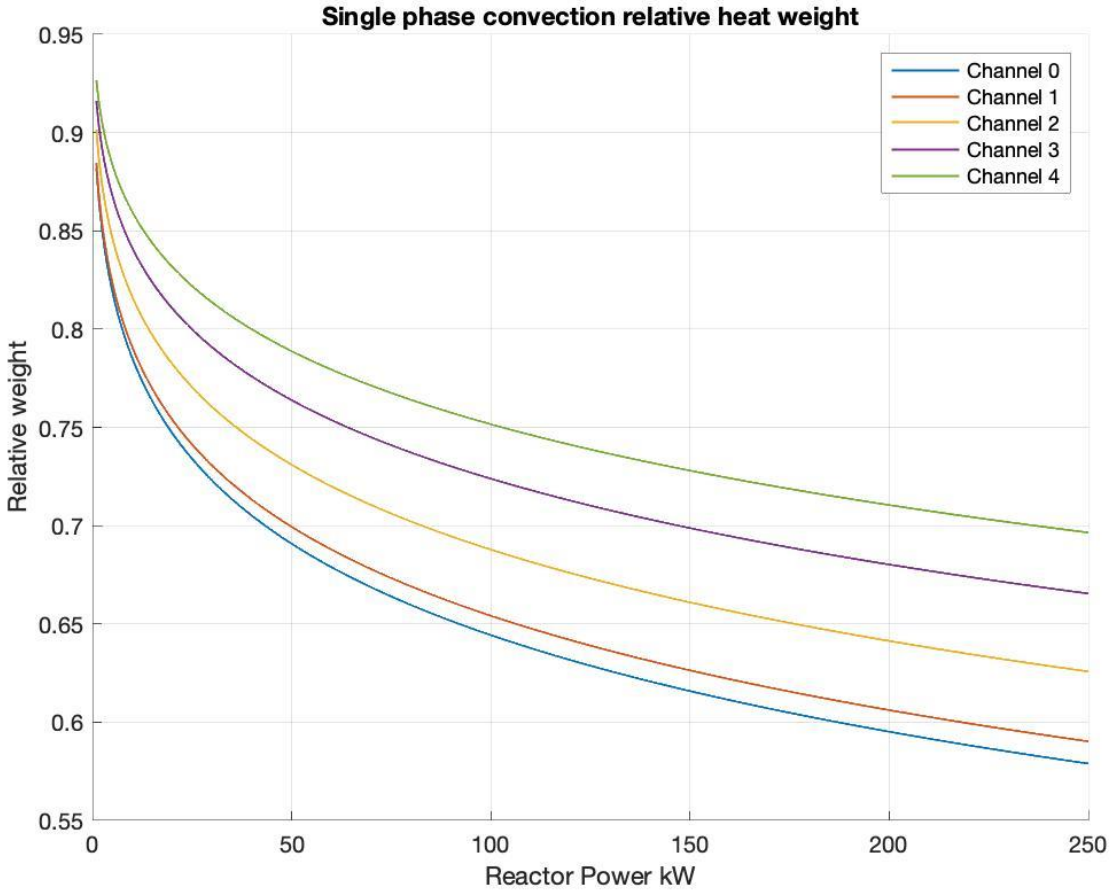

Figure 5.7: relative convection resistance vs overall resistance

The thermal weight decreases, because the convection factor increases with reactor power, since all resistances except the convection one don’t depend on temperature.

Chapter 6 Double phase correlations

The phenomenon of subcooled boiling starts once a certain level of heat flux is reached, that is, once the heat flux is such that the temperature near the wall reaches the saturation one.

Bulk saturation boiling is not observed, since for the heat exchanged and the mass flow considered (even for the maximum power of 250 kW), the coolant bulk never reaches saturation temperature; this is also verified experimentally.

Subcooled boiling can be observed, for example, in a pan with water before boiling. Steam bubbles are formed on the bottom of the pan; however, they cannot rise to the surface, due to the lower water temperature, causing it to condense.

Due to the heat flux, the water layer closest to the wall can reach the saturation temperature, causing the formation of steam bubbles that, at the beginning, stick to the wall surface due to their low dimension and high surface tension, but as their dimension increases with time, generating non negligible buoyancy force, detach from the surface towards more inner layers.

However, since in the coolant the bulk temperature is significantly lower than the saturation one, which for water at pool pressure is 111.5°C, the steam bubbles condense in the surrounding water, disappearing.

This mechanism severely improves the convection heat exchange factor h, since the bubbles movement generates micro-turbulence near the wall, which causes the replacement of the hot water near the wall with colder one. In addition, both in the formation and in the condensation of the bubbles latent heat, which is higher than the sensible one, is exchanged, thus allowing for higher values of h.

This phenomenon is very useful to avoid reaching excessively high temperatures in the inner part of the fuel element, which may cause unwanted degradation phenomena, thus exposing the system to potential risks.

In fact, subcooled boiling can keep the temperature of the cladding close to a threshold value called Onset Temperature (ONB), which is the temperature that the wall must reach to generate the boiling, and it is a function of heat flow and pressure. The dependency on pressure is related to the bubble dimension, and for subcooled boiling the characteristic

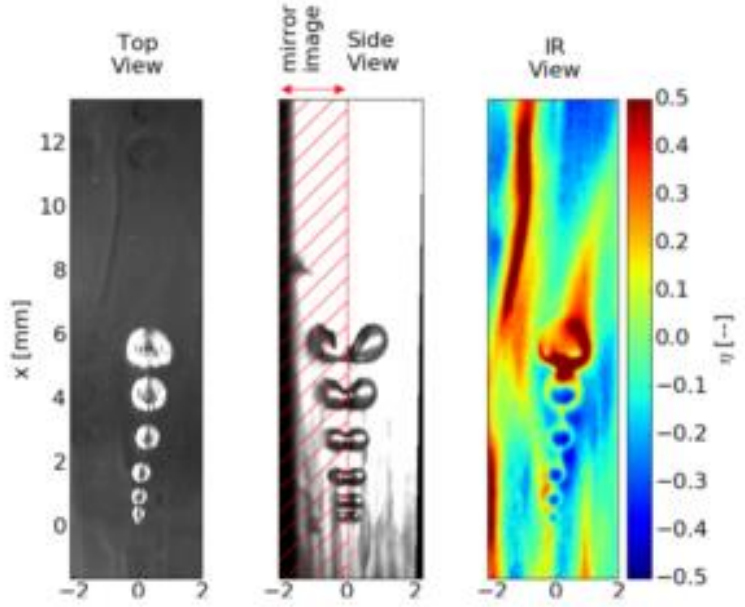

Figure 6.1: nucleate boiling photo (researchgate.net)

dimension of the system changes from the hydraulic diameter to the bubble average dimension, because most of the turbulence and temperature gradient changes occur within this length.

The type of boiling for this reactor is called flow boiling, since there is a preferential direction of flow in which boiling occurs, and along which bubbles are transported.

Since there are now 2 phases inside the channel, double-phase heat transfer mechanism must be considered, and consequently double-phase correlations. All correlations considered are for global-coefficient determination, not local.

Now, before proceeding with the description of all the studied correlations, the onset temperature must be calculated.

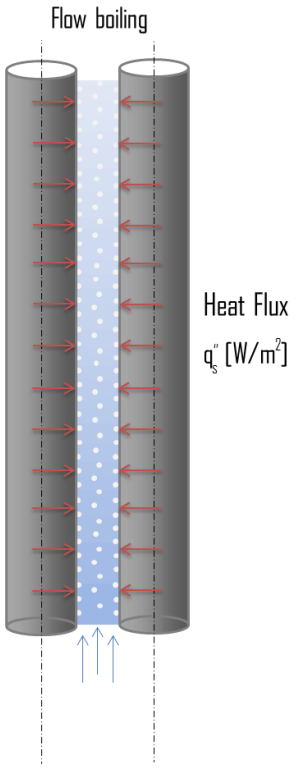

Figure 6.2: subcooled boiling representation [8]

6.1 Onset temperature for nucleate boiling

The most suitable correlation for low pressure and water coupled with metallic surface is the Bergles and Rohsenow correlation, which has the form:

$$T_{ons} = T_{sat}(P) + 0.556\left(\frac{q_{el}''(z)}{1082P^{1.156}}\right)^{0.463P^{0.0234}} \tag{6.1}$$

where all quantities are in the S.I. units except the pool pressure P, that is in bar. The term q_{el}''(z) is the heat flux calculated taking the local linear heat flux produced for each fuel element and multiplied by 2πR. In fact, this analysis must be done not for the cooling channels, but for the single fuel elements, because the transferred heat flux is only related

to them, and as said before the characteristic dimensions are no longer channel dimensions, but bubble one (except Rohsenow and consequently Chen correlations); each element has different onset temperature, which depends on its power production.

For simplicity, the same linear heat flux along the hoop coordinate is considered, mainly to avoid power symmetry distortions due to discontinuities inside the reactor core.

Fig 6.3 shows that the onset temperatures will be a little higher than the saturation one, and they increase as the flux increases, because higher fluxed needs higher temperature difference to be brought.

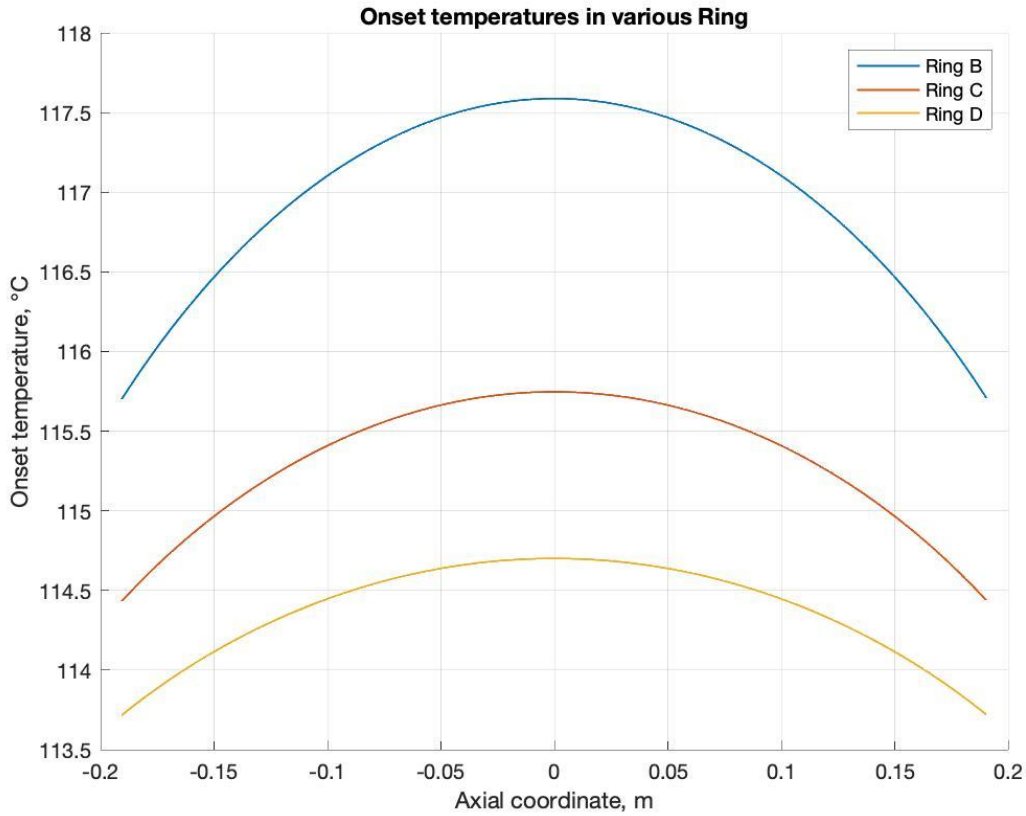

Figure 6.3: onset temeprature at 250 kW

Ring F and E are not considered, since the heat flux is too low to see subcooled nucleate boiling, giving more attention to the elements that produce more power.

Now double-phase correlations are analyzed; a high number is considered, since thermal regime is also unknown in TRIGA.

Therefore, the analysis of a large number of correlations can give a greater range of coefficients to evaluate.

6.2 Rohsenow correlation

The first correlation considered is one mainly used for pool boiling; despite, as mentioned, the type of boiling here considered is flow boiling, it can be interesting to see how well this correlation predicts the h coefficient.

The correlation is the oldest one found by Rohsenow, and despite its simplicity it has a good accuracy in predicting pool boiling, with a maximum error of 25%.

This correlation uses as characteristic dimension the one suggested by Laplace, called Laplace length scale, defined as:

$$D_L = \sqrt{\frac{\sigma}{g\,\Delta\rho_{sat}}} \tag{6.2}$$

This relation derives from the bubble average diameter; σ is the surface tension of steam bubble in the water and $\Delta\rho_{sat}$ is the difference between saturated liquid density and saturated vapor one.

Rohsenow proposed also a definition for the Reynolds number different from the best known one, using different quantities:

$$Re_{Rh} = \frac{\rho_{in} D_L v_a}{\mu_{in}} \tag{6.3}$$

where v_a is the characteristic velocity of agitation of the boiling fluid and can be found by dividing the distance the liquid must travels to fill the space left by a departing bubble (proportional to D_b) by the time between subsequent bubble departures, t_b. The time t_b is equal to the energy it takes to form a vapor bubble (proportional to D_b^3), divided by the rate at which heat is added over the solid–vapor contact area (proportional to D_b^2).

$$v_a = \frac{D_b}{t_b} = \frac{D_b}{\left(\frac{\rho_{in}\Delta h_{sat} {D_b}^3}{{q_{el}}'' {D_b}^2}\right)} = \frac{{q_{el}}''}{\rho_{in}\Delta h_{sat}} \tag{6.4}$$

where Δh_{sat} is the latent boiling heat. The Rohsenow correlation is:

$$Nu = \frac{Re_{Rh}^{(1-n)} Pr^{(1+m)}}{C_{surface}} \tag{6.5}$$

where n and m are characteristic of the coolant, while $C_{surface}$ is a constant that depends on the coolant-wall interface. For water, these constants are n=0.33 and m=0, and for water-steel contact the suggested number is 0.013. As for the single-phase correlations, h can be evaluated as:

$$h = \frac{Nu\ K_w}{D_h} \tag{6.6}$$

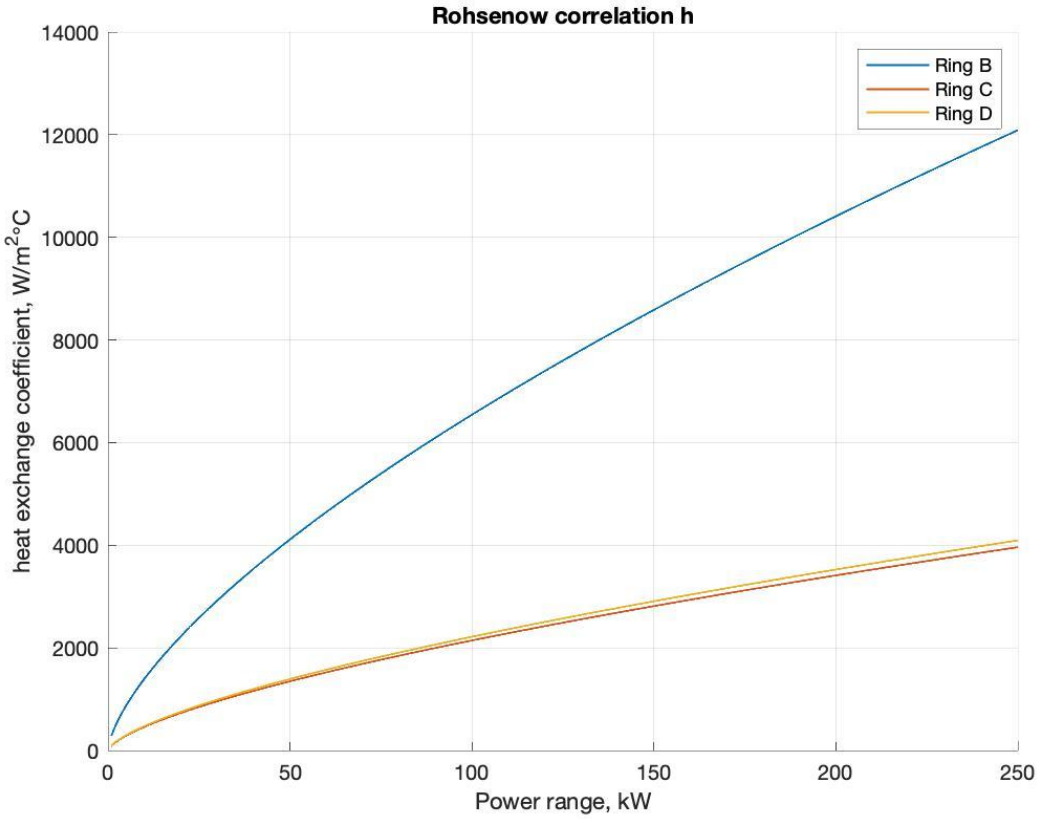

Figure 6.4: h calculated from Rohsenow correlation

Fig 6.4 shows the heat transfer coefficient computed by the Rohsenow correlation. The similarity between the heat exchange values for ring C and D is evident: despite the Dh for these two channels being quite different, the heat flux is higher for the C ring, and these two effects compensate each other. The correlation has been calculated at the average heat flux of the element. These results will be taken into account as reference, since this correlation is the oldest and reproduces very well in all conditions.

6.3 Stephan-Abdelsalam correlation

With respect to the previous one, this correlation is a product of dimensionless quantities, each one with its meaning. Like the previous one, it is based on a characteristic dimension different from the hydraulic diameter, which is the average diameter of the bubble when it departs form wall, evaluated using the Fritz correlation:

$$D_b = 0.0208\,\gamma\sqrt{\frac{\sigma}{g\,\Delta\rho_{sat}}} \tag{6.7}$$

The letter γ is the contect angle for water and metallic steel surface.

The correlation is:

$$Nu = 2.46\cdot 10^{6}\left(\frac{q_{el}''D_b}{K_w T_{sat}}\right)^{0.673}\left(\frac{\Delta h_{sat}{D_b}^2}{\alpha^2}\right)^{-1.58}\left(\frac{Cp T_{sat}{D_b}^2}{\alpha^2}\right)^{1.26}\left(\frac{\Delta\rho_{sat}}{\rho_{in}}\right)^{5.22} \tag{6.8}$$

The range of validity of this correlation depends only on the ratio between critical and current pressure, that is called reduced pressure.

$$10^{-4} < {}^{P}/_{P_{cr}} < 0.886$$

The TRIGA reactor perfectly respects it for all possible operating conditions, since the critical pressure of water is 221 bar, thus having a reduced pressure of 6.7e-3.

As in the previous correlation, h is calculated in the same way, however now the maximum bubble diameter instead of the Laplace length must be used:

$$h = \frac{NuK_w}{D_b} \tag{6.9}$$

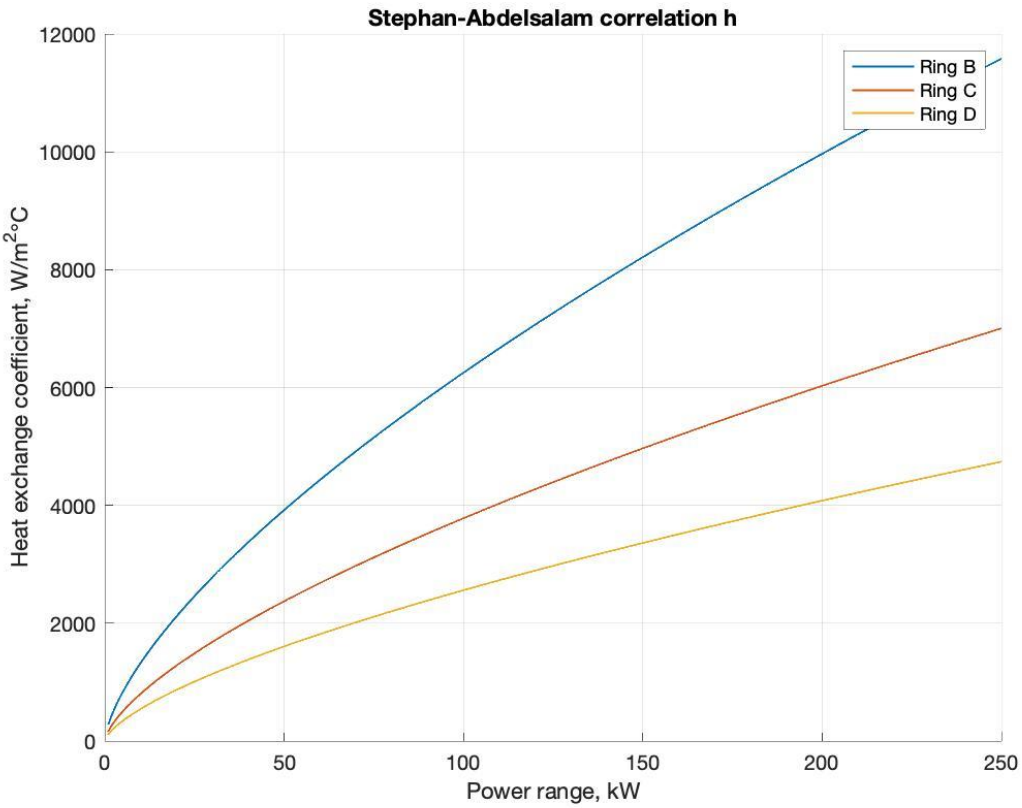

Figure 6.5: Stephan-Abdelsalam results

Fig. 6.5 shows an agreement with the previous values found using the Rohsenow correlation, except for channel 1, which has a different behavior due to the usage of the bubble diameter instead of the hydraulic one.

6.4 Cooper correlation

It is a pressure-based correlation, since it strongly depends on the reduced pressure:

$$Nu = 55\left(\frac{P}{P_{cr}}\right)^{n}\left(-\log_{10}\frac{P}{P_{cr}}\right)^{-0.55}\sqrt{M_w} \tag{6.10}$$

where Mw is the water molecular weight, expressed in g/mol. The parameter n in this case is an exponent that depends on the roughness parameter, expressed in micron.

$$n = 0.12 - 0.434\log_{10}(Rgh) \tag{6.11}$$

The coefficient h is now calculated as:

$$h = Nu\ (q_{el}'')^{2/3} \tag{6.12}$$

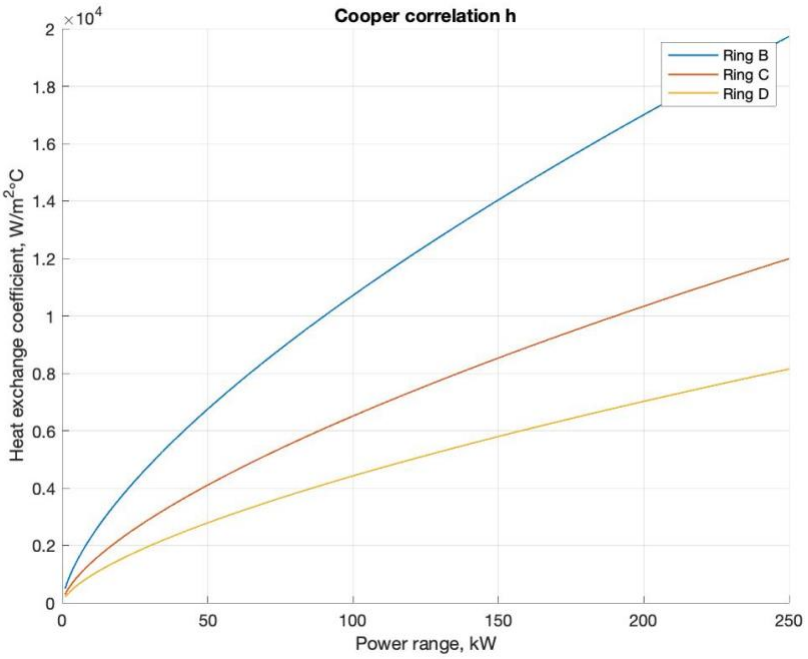

Figure 6.6: Cooper results

where the heat flux is expressed in W.

This correlation is very effective for copper conducts, but in this case severely overestimate the heat exchange respect to Rohsenow correlation. As such, it is not very reliable for the estimation of the boiling heat exchange coefficient for the TRIGA reactor, despite the range of validity being respected:

$$0.002 < {}^{P}/_{P_{cr}} < 0.9$$

$$2 < M_w < 200$$

6.5 Gorenflo correlation

This correlation is based on “standard exchange conditions”, for each combination of fluid and wall. These conditions are the steady exchange conditions for every boiling fluid at referring reduced pressure of 0.1. It has a very large range of validity and it is also based on the reduced pressure:

$$h = h_0 \, F_g \left(\frac{q_{el}''}{q_0''}\right)^n \left(\frac{Rgh}{0.4}\right)^{0.133} \tag{6.13}$$

where h_0 and q_0'' are reference parameter for water and standard condition heat exchange, respectively with values of 5600 W/m2K and 20 kW/m2, while n and F_g are correction factor depending on pressure:

$$n = 0.9 - 0.3\left(\frac{P}{P_{cr}}\right)^{0.15} \tag{6.14}$$

$$F_g = 1.73\left(\frac{P}{P_{cr}}\right)^{0.27} + \left(6.1 + \frac{0.68}{1 - \frac{P}{P_{cr}}}\right)\left(\frac{P}{P_{cr}}\right)^2 \tag{6.15}$$

This correlation is very good in predicting boiling heat exchange for newer type of refrigerants. However, it doesn't work very well with subcooled flow boiling because it overestimates, like the previous correlation, the exchange coefficient. Instead, it predicts very well pool saturated boiling. This despite the ranges of validity being respected:

$$0.0005 < \frac{P}{P_{cr}} < 0.96$$

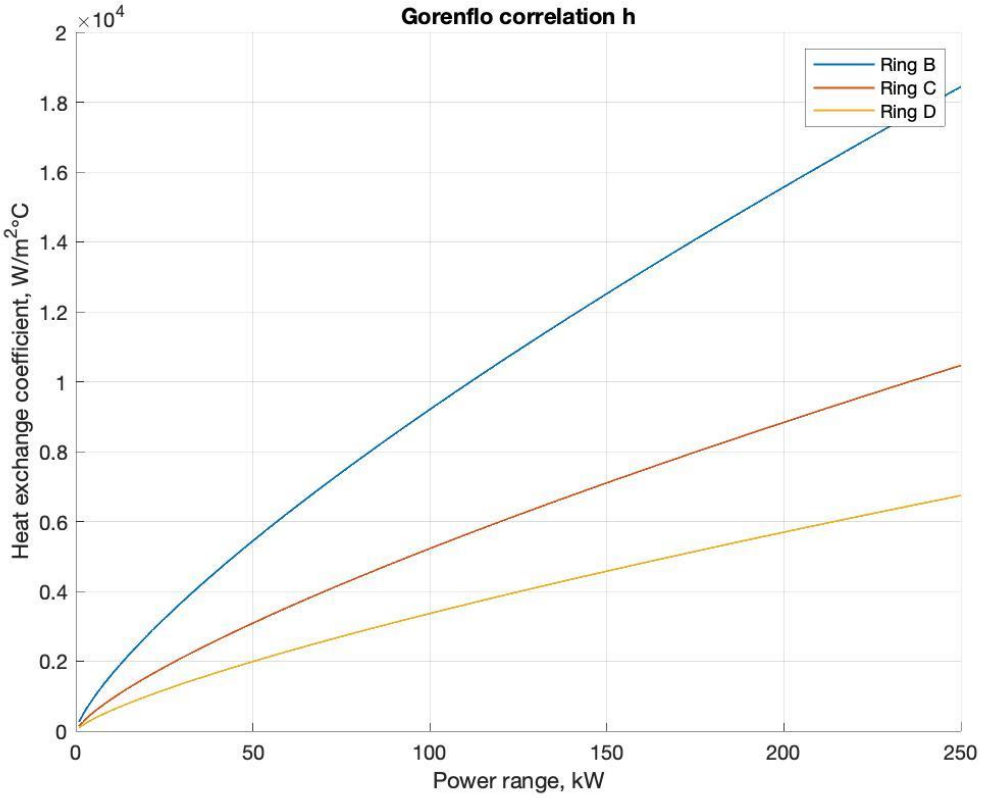

Figure 6.7: Gorenflo correlation results

The fact that some correlations doesn't work well despite the respect of validity ranges means that this condition is not enough to consider adapt the correlation for TRIGA reactor.

For this reason, more correlations are considered, in order to test their accuracy with respect to the results that are obtained.

6.6 McAdams correlation

This correlation is the first used to estimate vertical flow boiling. This type of correlation is purely empirical and is quite different than the other ones in the estimation of the h value. From all thermophysical parameters ΔT_w, that is substantially the difference between the saturation temperature and the wall temperature, is determined as a function of pressure, type of coolant and heat flux. Once obtained, the heat exchange coefficient can be determined from eq 6.16:

$$h = 2.26 \Delta T_w^{\,2.86} \tag{6.16}$$

where ΔT_w is in °C, and comes from the Jens and Lottes boiling correlation:

$$\Delta T_w = 25 (q''_{el})^{0.25} e^{\left(-\frac{P}{62}\right)} \tag{6.17}$$

where the flux must be expressed in MW/m2 and P in bars.

Rigorously, the range of validity of eq 6.16 is not compatible with the TRIGA reactor:

$$2.06 < P < 6.5.$$

where the limits are in bar. However, as the pool pressure for the TRIGA reactor is 1.5 bar, slightly below the lower limit, so this correlation can still be used.

For higher pressures the evaluation of ΔT_w can be done by Thom correlation, used for PWR reactors.

Eq 6.17 has different limits:

$$7 < P < 172$$

This correlation underestimates the heat exchange coefficient, instead. (ever referring to Rohsenow one).

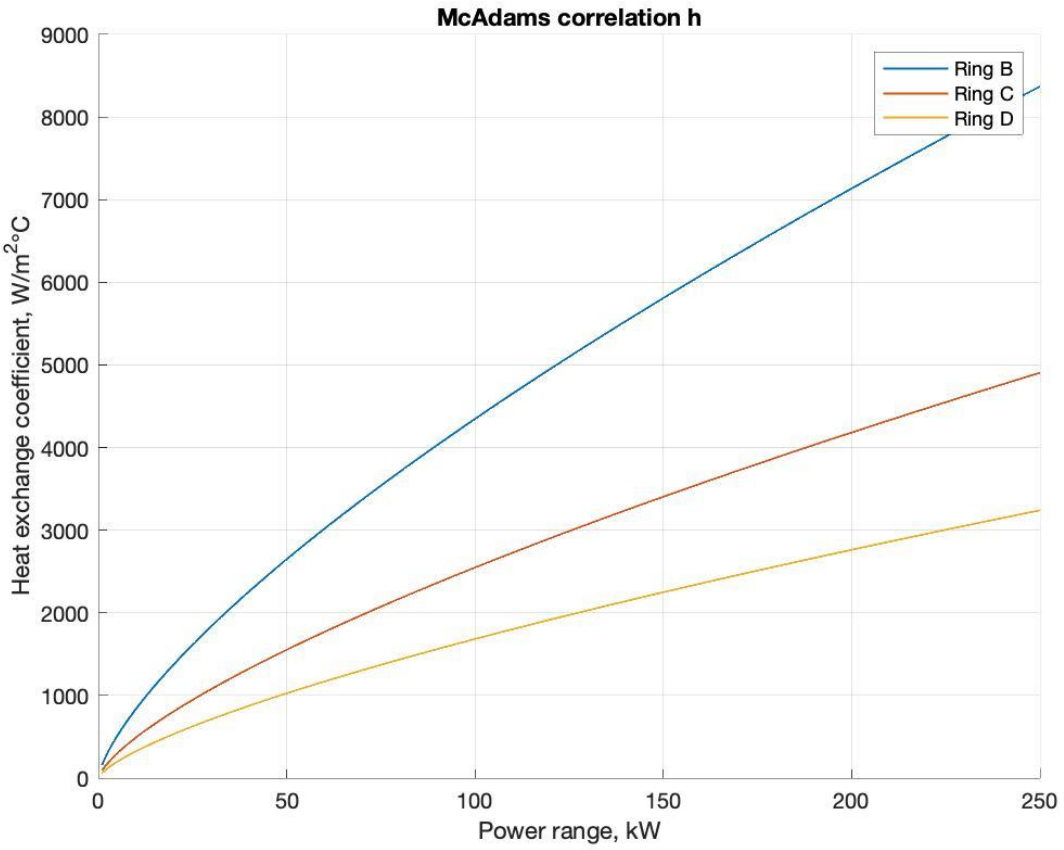

Figure 6.8: McAdams correlations results

6.7 Jens-Lottes correlation

This correlation is like the last one, with the difference that the evaluation of the heat exchange coefficient now is:

$$h = \frac{q''_{el}}{\Delta T_w} \tag{6.18}$$

where the ΔT_w is calculated with the same Jens-Lottes correlation used in the previous correlation (eq 6.17), and it has the same range of validity. The results are shown in fig 6.9.

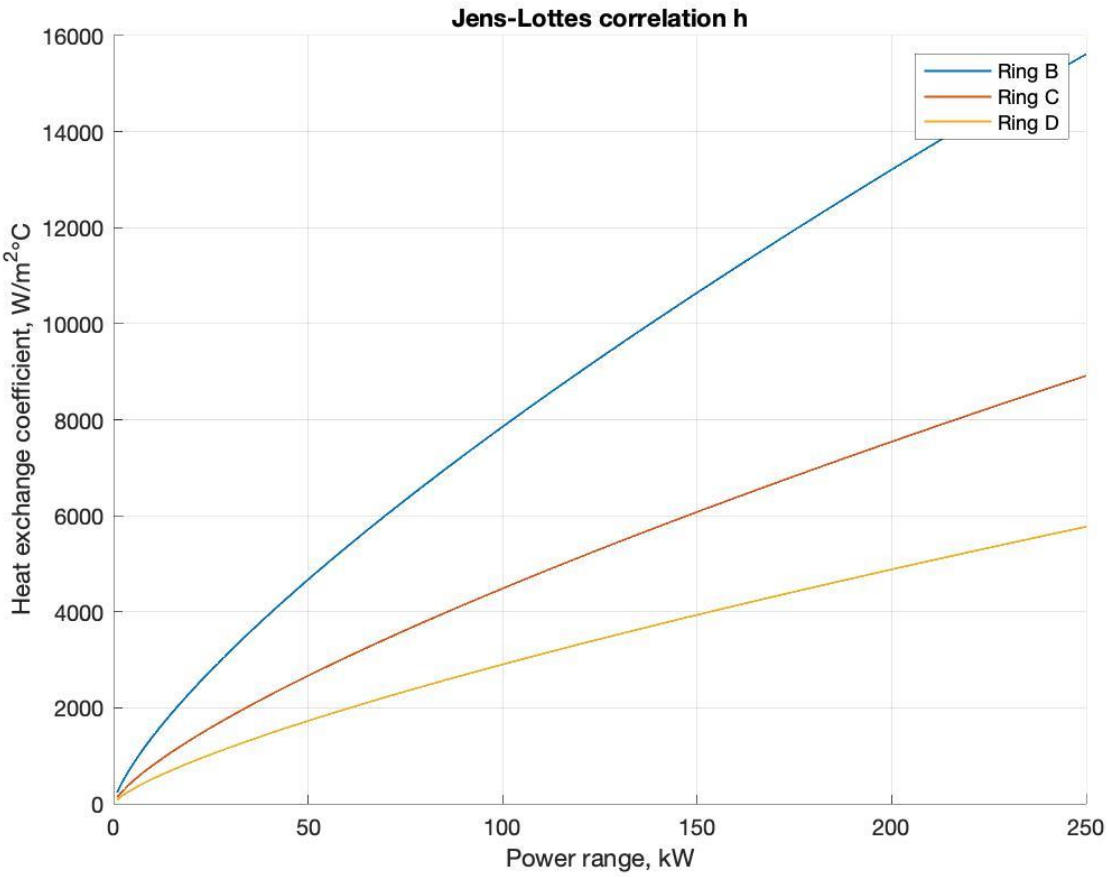

Figure 6.9: Jens Lottes coefficients

6.8 Chen correlation

The last correlation considered is different from the others since it combines the two correlations of Rohsenow (eq 6.5) and Dittus-Boelter (eq 5.2) to describe saturated flow boiling.

In order to do this, two appropriate correction factors must be defined, that act as weights for the values of the two exchange regimes.

The correlation has the form:

$$h = F\, h_{Dittus-Boelter} + S\, h_{Rohsenow} \tag{6.19}$$

where F can be assumed equal to 1 in our condition, since it depends on turbulence and assumes values higher than 1 only if turbulence is significant, while S has the form:

$$S = \frac{1}{1 + 2.53 \cdot 10^{-6}(Re\ F^{1.25})^{1.17}} \tag{6.20}$$

Combining the 2 regimes of single phase and nucleate boiling similar values of h to the ones found with the Rohsenow correlation are found, since the Dittus-Bolter one is an order of magnitude lower and S varies from 0.95 to 0.98.

The ranges of validity are an interval in common with the two correlations, Dittus-Boelter and Rohsenow.

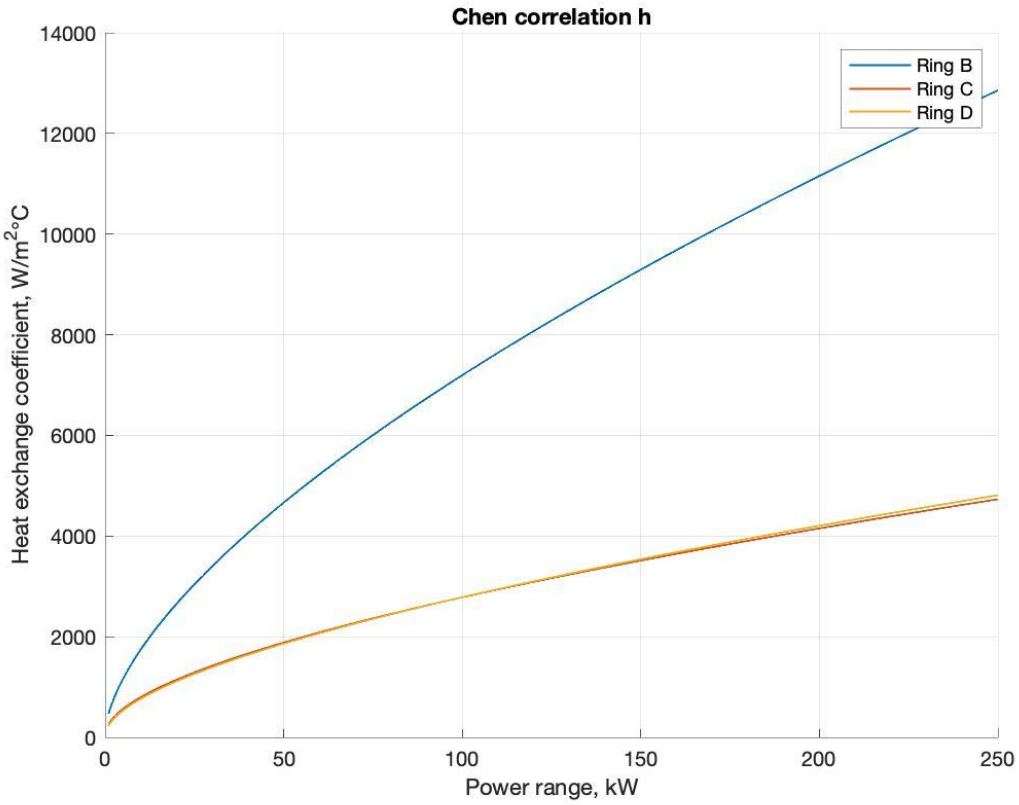

Figure 6.10: Chen correlation results

6.9 Differences between correlations

In this section the results obtained with the different correlations in terms of h are compared. Correlations for both pool and flow boiling are shown.

It can be seen how the Cooper, Gorenflo and Jens-Lottes overestimate the h coefficient respect to Rohsenow, probably because the first is valid for very conductive metal walls like copper, the second doesn't reproduce very well subcooled boiling and the third little exceeds the pressure validity range. The other four correlation, instead, predict a more reasonable result for the heat exchange coefficient, although some of them slightly exceed

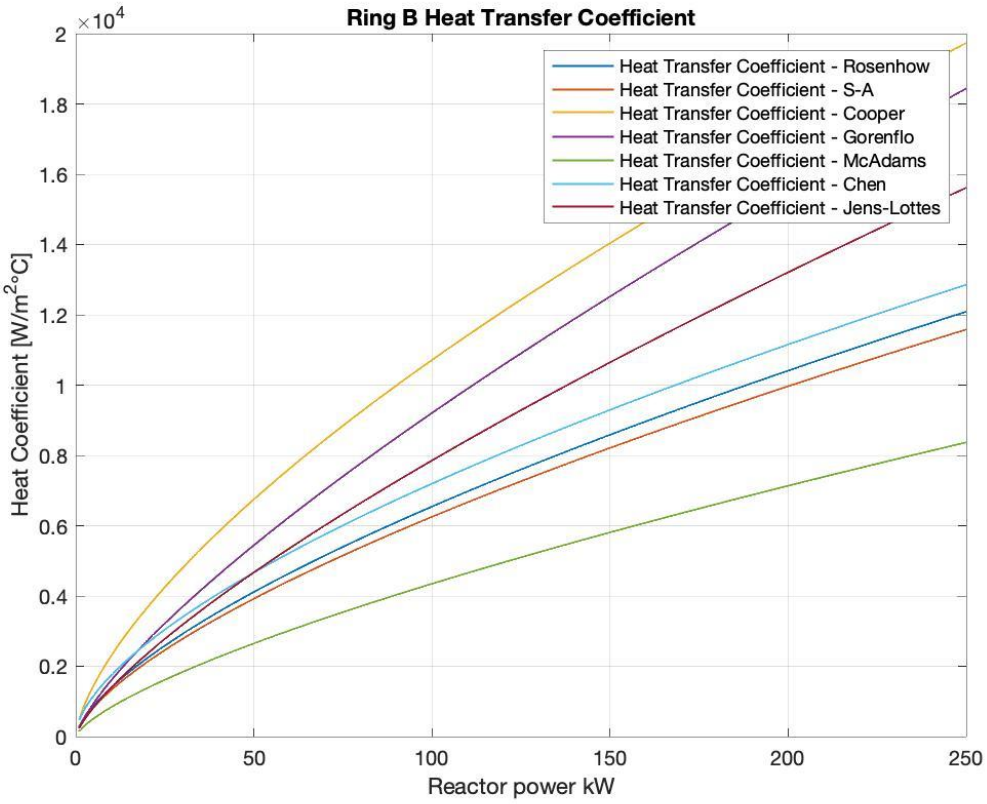

Figure 6.11: Ring B coefficents

the validity conditions. An exception must be done for McAdams that severely underestimates h. In particular, the Stephan-Abdelsalam represents an average of the obtained results, and thus it is expected to be one of the best one for the prediction of h.

In addition, the Rohsenow and Chen are probably the best to predict h, since are in the middle of other values; an exception for ring C when considering channel 1, where the higher D_h causes a decrease of h.

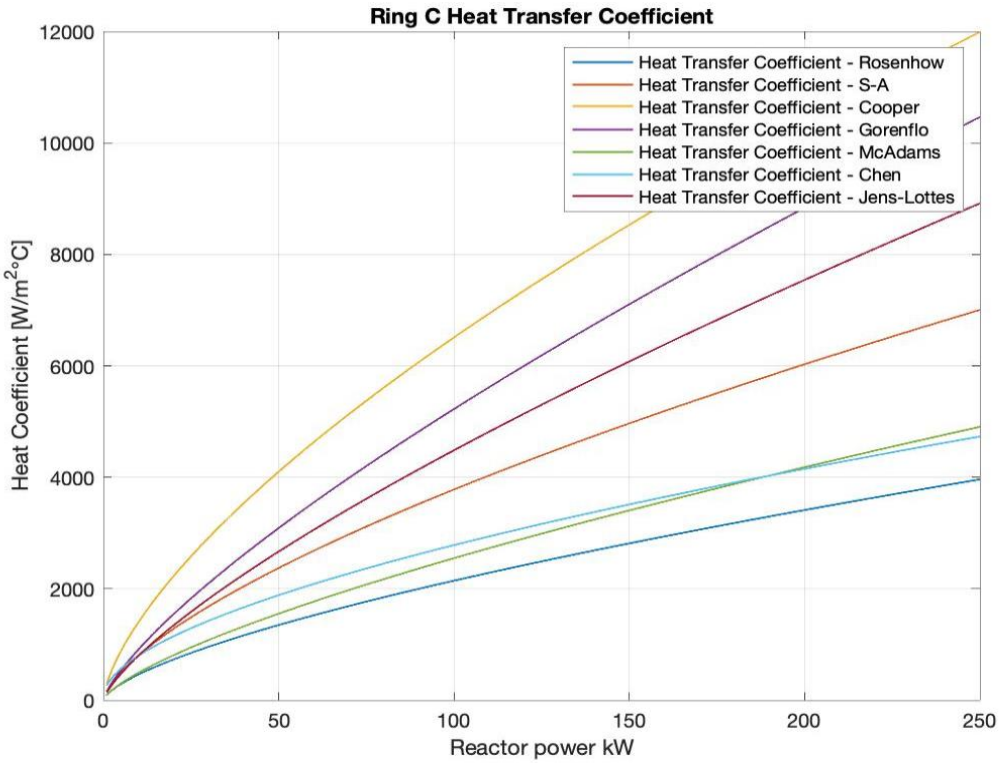

Figure 6.12: Ring C coeffcients

Now, all these correlations refer to constant heat flux along the surface, and they predict the global heat exchange factor. For the considered case, the heat flux depends on the axial coordinate. As such, the variation of h alongside z is now plotted, considering as an example only channel 0 and an element of ring B at 250 kW, where subcooled boiling is expected to happen along all the length of the channel.

In other words, these correlations have been considered local-type and not global one.

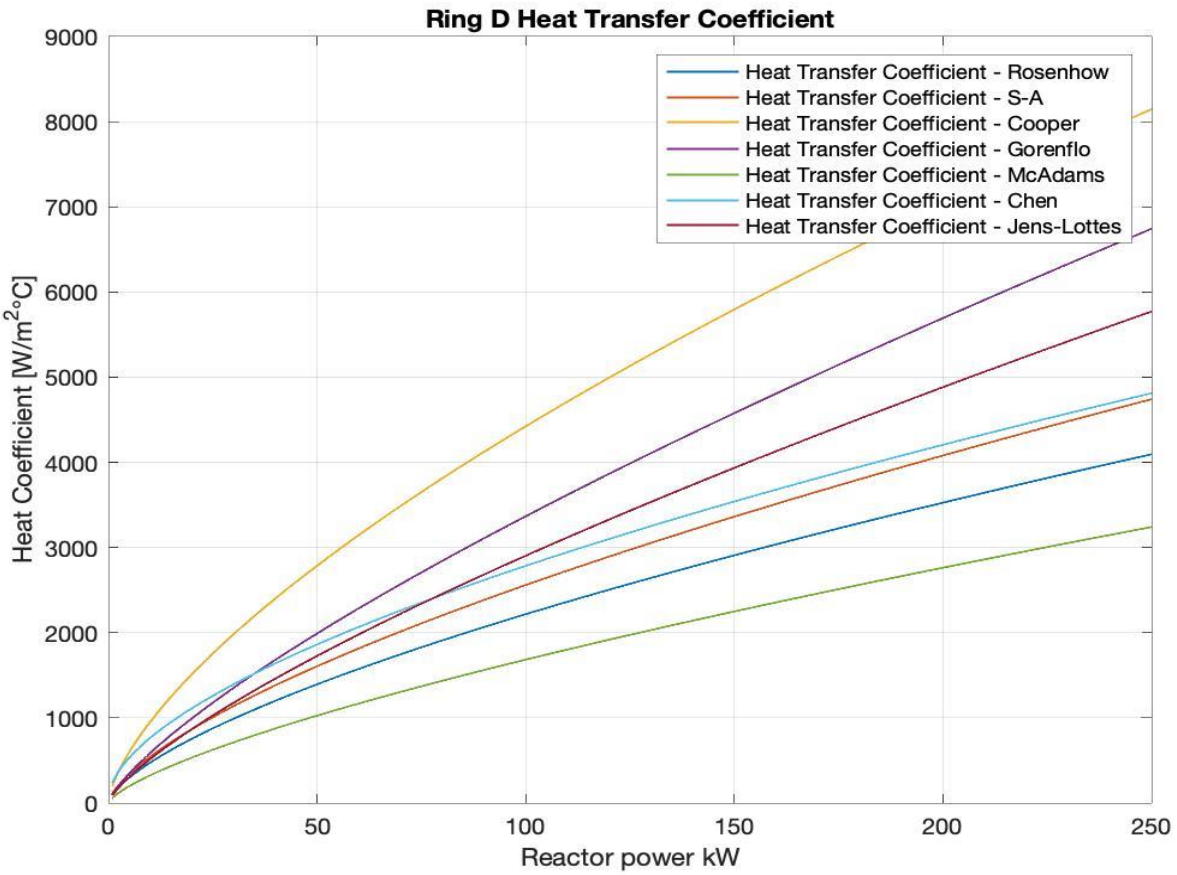

Figure 6.13: Ring D coefficients

This is not completely correct, but however for completeness in fig 6.13 is shown how heat exchange coefficient must behave with variable power generation.

The same order of power variation of various correlation is found, as expected. This graph is only a try to evaluate the local exchange coefficient, but probably it isn't completely correct, since bubbles generated more in depth probably affect those above, going to interfere with the h profile in a way that the 1D approach cannot accurately predict.

In particular the first part of the graph could be correct but the last would not, axially speaking.

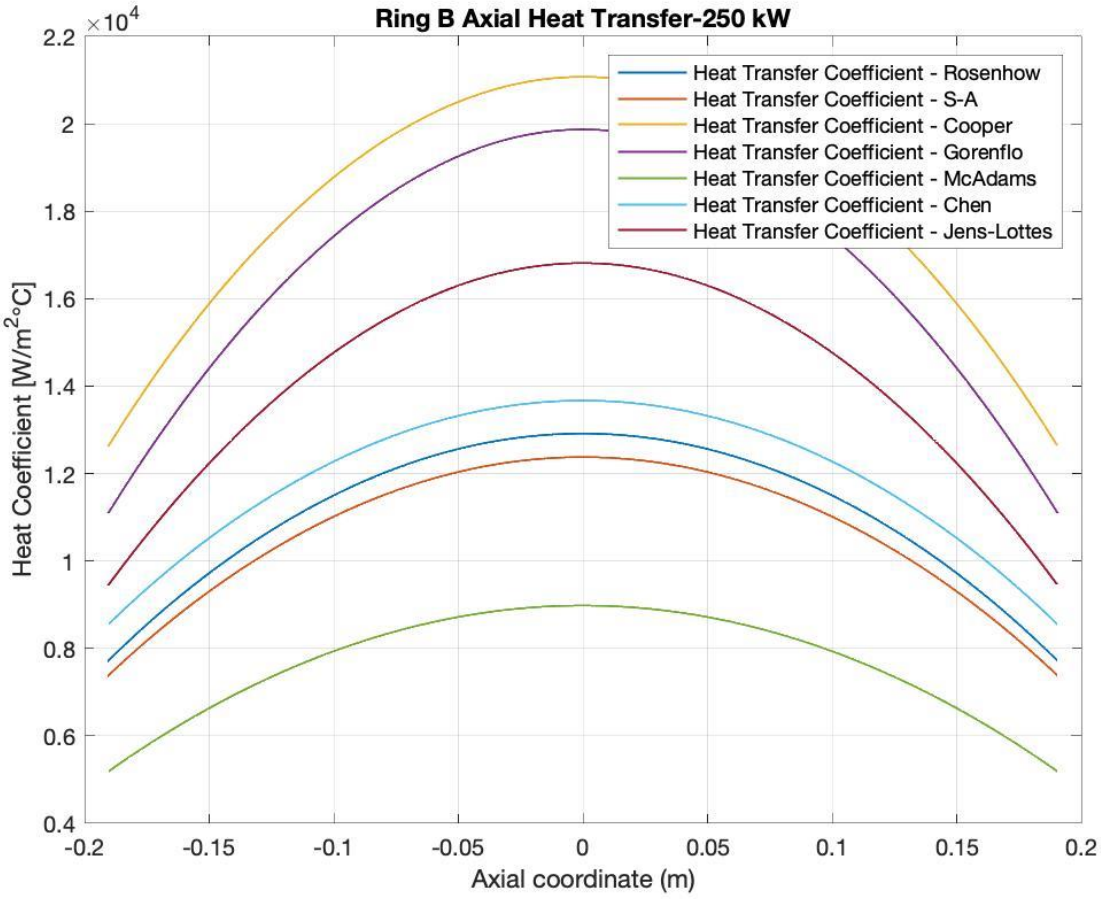

Figure 6.14: axial variation of heat exchange coefficient

Chapter 7 Temperature profiles

In this chapter is developd, using previous data found with 1D approach, a simple model that tries to reproduce temperature profile in the reactor. In order to check the validity of the accuracy of the model we refer to temperature data registered during the last academy year on Pavia's TRIGA Mark II, on LENA laboratories.

The most important data are temperatures, because they are the most meaningful data to evaluate other quantities, like mass flow, and are the simplest data to be obtained, since are obtained from thermocouples inside the core; they are also critical parameters to safety and correct operability of the reactor.

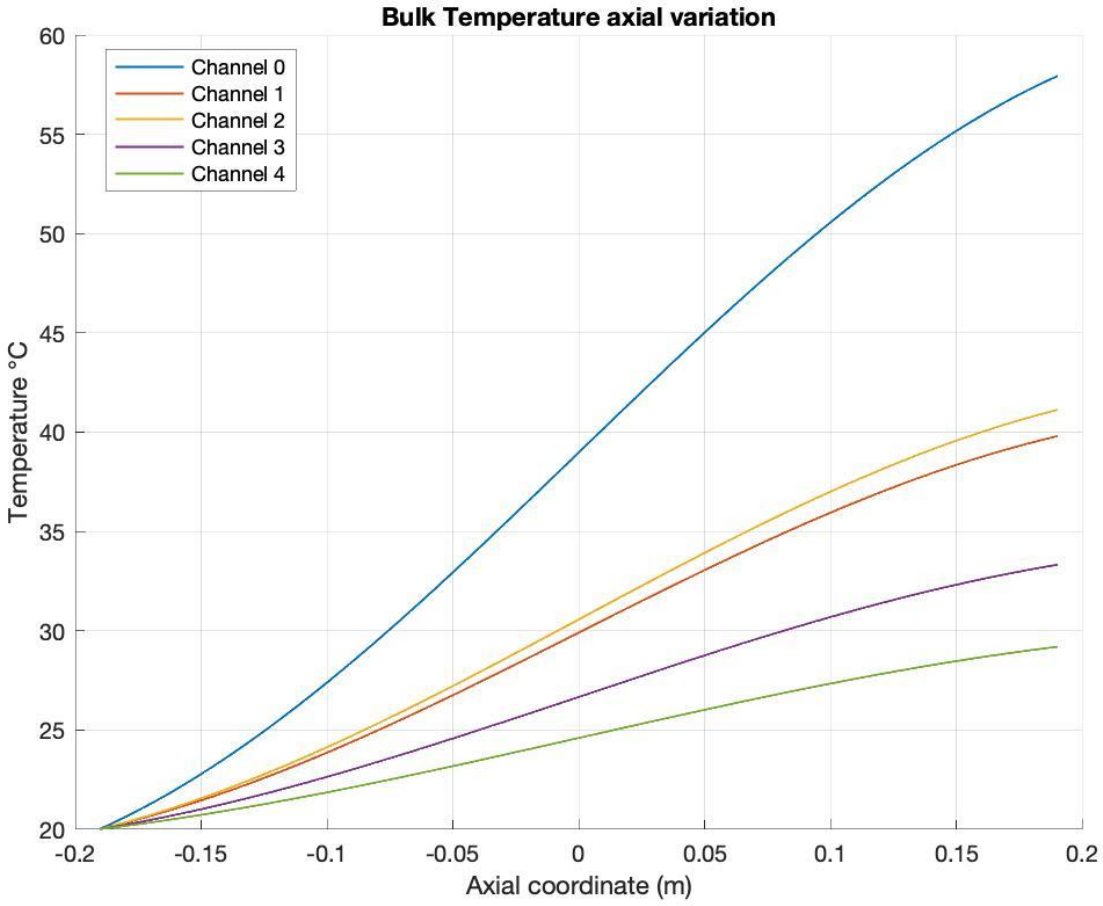

Figure 7.1: Bulk axial temperature variation at 250 kW

7.1 Bulk temperature profile

The first temperature evaluated is the bulk temperature in steady state conditions for each channel (Fig 7.1). It is important expecially to validate the mass flow found, since in stationary conditions, the power generates is transferred completely to coolant, without heat exchange factor dependence so, if temperature difference between inlet and outlet is correct, means that the model with Colebrook-White and characteristic dimensions used is correct, predicting the correct mass flow, that receives the correct power and reaches temperature differences close to experimental ones.

Most relevant data are taken on a 250-kW regime, so compared to the experimental one at this power. Moreover, all inlet temperatures are considered 20°C, neglecting some pool reheating or coolant recirculations due to spacers.

From the experiment of measuring the alpha ready coefficient, an essential parameter in evaluating the reactor response to the rapid thermal excursion, a series of data on the thermocouples that we can compare, being the experiment carried out at maximum power for a sufficient period of time.

In table 7.1 results are listed.

Table 7.1: bulk temperatures, at 250 kW (°C)

Channel number	Experimental approximative temperature difference	Temperature difference found	CFD temperature difference
0	-	37.8	37.85
1	20	19.8	19.14
2	24	21.1	21.95
3	14	13.3	14.03
4	8	9.1	9.28

From table 7.1 a good agreement with experimental data is observable, considering the use a 1D model. CFD data are taken from article of Cammi et al. [15] that tries to reproduce data with CFD 3D calculations. Another thing to note is that outlet temperature of channel 1 is lower that one of channel 2: this is due to higher mass flow rate. In fact, the ratio between power per channel and mass flow of channel 2 is higher than the 1.

All temperature profiles have been evaluated with the correct use of channel mass flows and linear power of single element, weighted by its angle exposure in channel. For example, channel 1, referring to figure 3.2:

$$T_{bulk1}(z) = T_{in} + \frac{2}{3}\frac{H_{e0}}{\pi}\frac{q_0'(z)}{\dot{m}_0 Cp} + \frac{5}{6}\frac{H_{e1}}{\pi}\frac{q_1'(z)}{\dot{m}_1 Cp} \tag{7.1}$$

Where pedix are referred to channel number. With the same coefficients explained in chapter 3 (eq 3.13), all axial tempreature profiles of other channels are reproduced.

7.2 Single phase temperatures

Is useful to plot some temperature profiles considering only single-phase behavior. Obviously, are expected higher temperatures than in reality are, since double phase coefficient are an order of magnitude higher. The most relevant discordance with reality can be seen in ring B elements at full power, where centerline temperatures is found about 600°C, despite knowing from experimental data and construption parameters that it doesn't exceed 320°C. Thermal resistances are the same descripted in single phase chapter (eqs from 5.10 to 5.13).

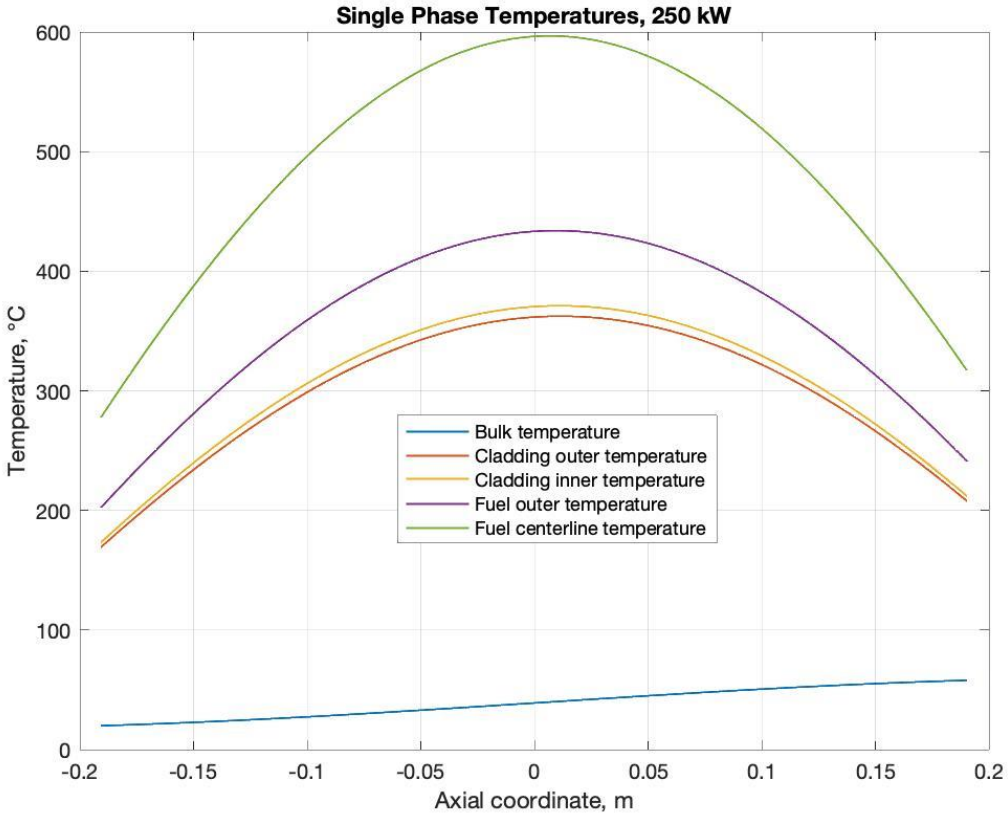

Figure 7.2: element of ring B in channel 0 temperature profile considering single phase.

Temperature profiles like these could be reached considering a not-boiling coolant, that is what happens in metal-cooled reactor; these types of coolant haven't boiling capacity to lower temperature, but they don't suffer thermal crisis.

If temperature would be so high, element failure will occur, since cladding is not designed to substain these temperatures, generating decomposition in Uranium, Zircoinium and hydrogen if exposed at temperatures above 400°C.

Fortunately, this model cannot be taken into consideration in the event of exceeding the onset temperature, therefore it will be discarded in favor of the one that uses two-phase coefficients.

7.3 Double phase temperature profiles

The evaluation of temperature profiles in mixed situation is a fundamantal part of this work, here the combination of single-phase behavior with double phase one is used, as it happens in reality. Single-phase h coefficents are used for points where water temperature doesn't reach the saturation conditions, and onset temperature if it does.

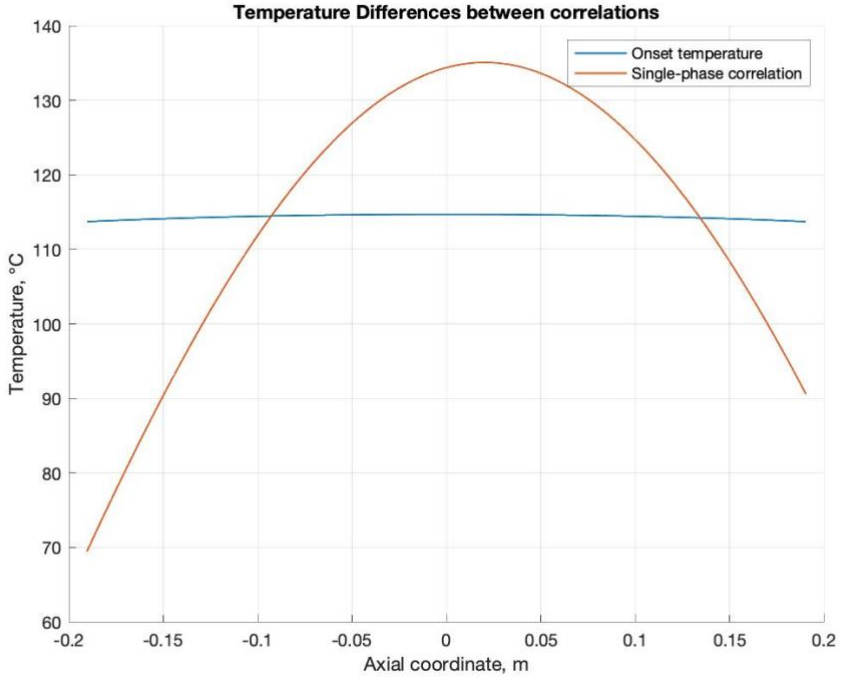

Figure 7.3: differences in cladding temperature in ring D

In other words, if temperature reaches in a point the saturation temperature, a "truncation" of the cladding temperature rises with the onset one.

This difference can be visible in fig 7.3. Single phase coefficient considered is the one calculated with Dittus-Boelter, since it is the most reliable one, and the onset temperature because it is a very good in wall temperature predictions for low pressures.

Where the two lines in fig 7.3 intersect, boiling starts, preventing a further rise in temperature, as would happen if this phenomenon did not occur. In ring B fig 7.4, we can see a more pronunced effect of subcooled boiling, since it happens in all the active length of element, stopping the temperature hundreds of degrees lower.

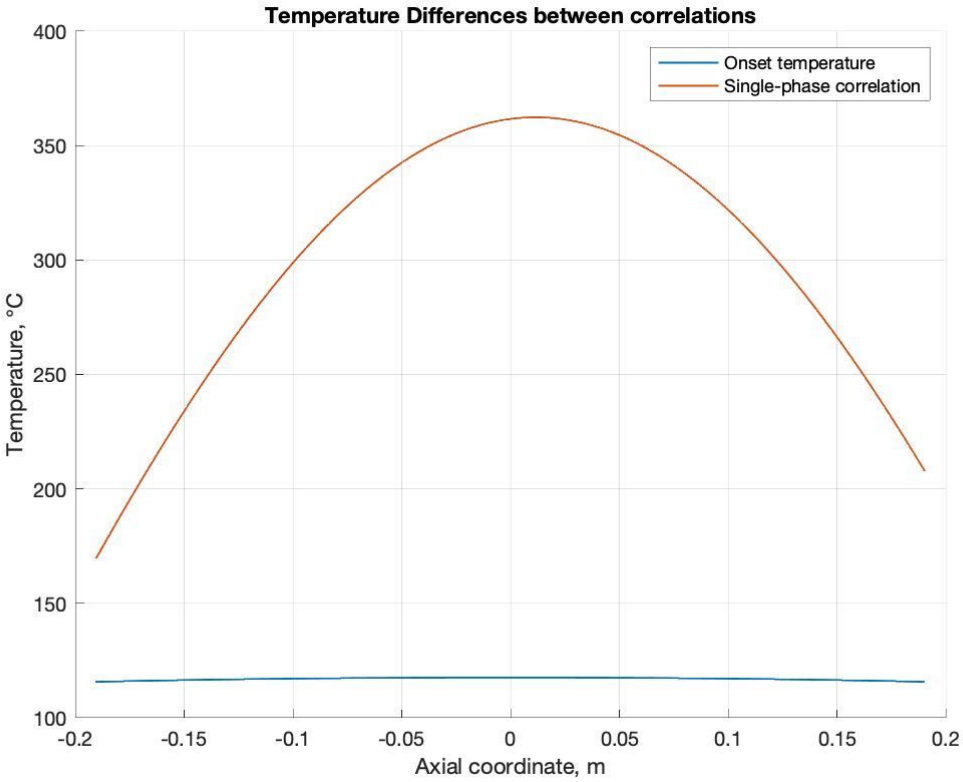

Figure 7.4: differences in cladding temperature of ring B

Temperatures are evaluated using the linear power in this way:

$$T_{cl,out}(z) = T_b(z) + \frac{q'(z)}{2\pi R h} \tag{7.2-7.5}$$

$$T_{cl,in}(z) = T_{cl,out}(z) + \frac{q'(z)\ln\left({R}/{R_{cli}}\right)}{2\pi K_{cl}}$$

$$T_{f,out}(z) = T_{cl,in}(z) + \frac{q'(z)}{2\pi R_{cli} h_{gap}}$$

$$T_{f,centre}(z) = T_{f,out}(z) + \frac{q'(z)}{4\pi K_f}$$

Like in fig 7.5, the temperature profile of fuel centerline where maximum is reached, is about 350°C, a little higher that one admitted, 320°C but, for this case, without considering gap thermal conductivity varying with temperature and 1D model it can be considered a good result. In this channel and ring, there is subcooled boiling in all active length of the section, since power fluxes are so high to improve saturation temperature near all the layers close to all surface length.

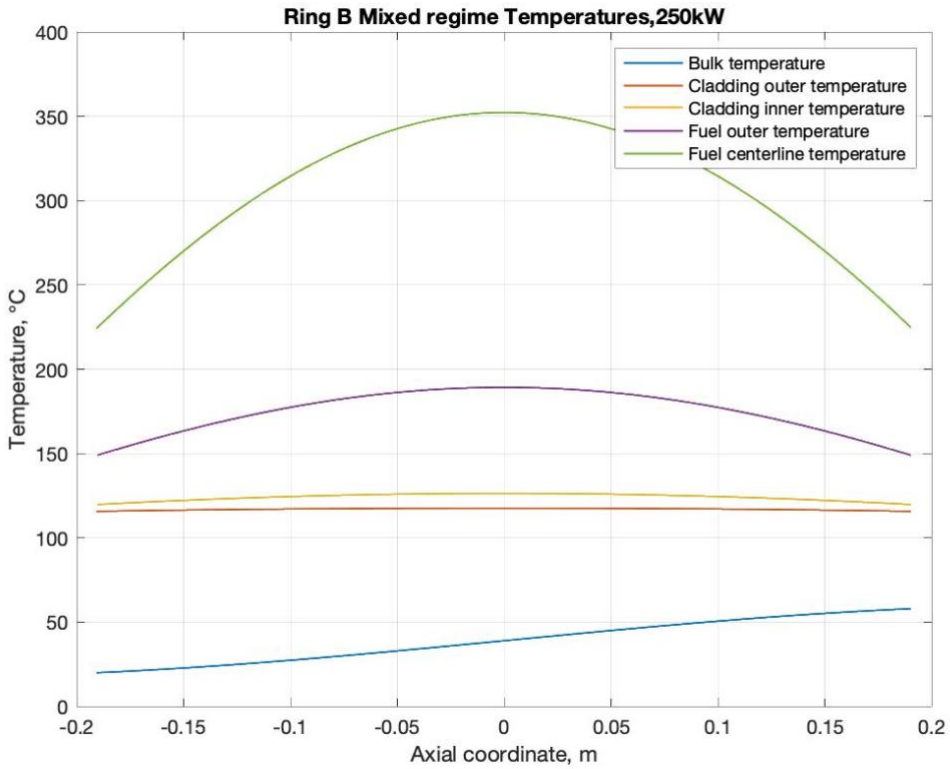

Figure 7.5: temperature profiles on ring B

Another profile has been calculated for ring B, using the same parameters for water-cladding exchange, but another averaged thermal condictivity for overall fuel element, considered homogeneous. From some other, more detailed calculations, [3] it has been calculated a weighted thermal resistance that considers all layers of elements and their dimension and temperature dependance, resulting in:

$$K_{el} = 16.8 \frac{W}{m°C}$$

From this the centerline temperature immediately comes over, from knowing the wall one, like in fig 7.6.

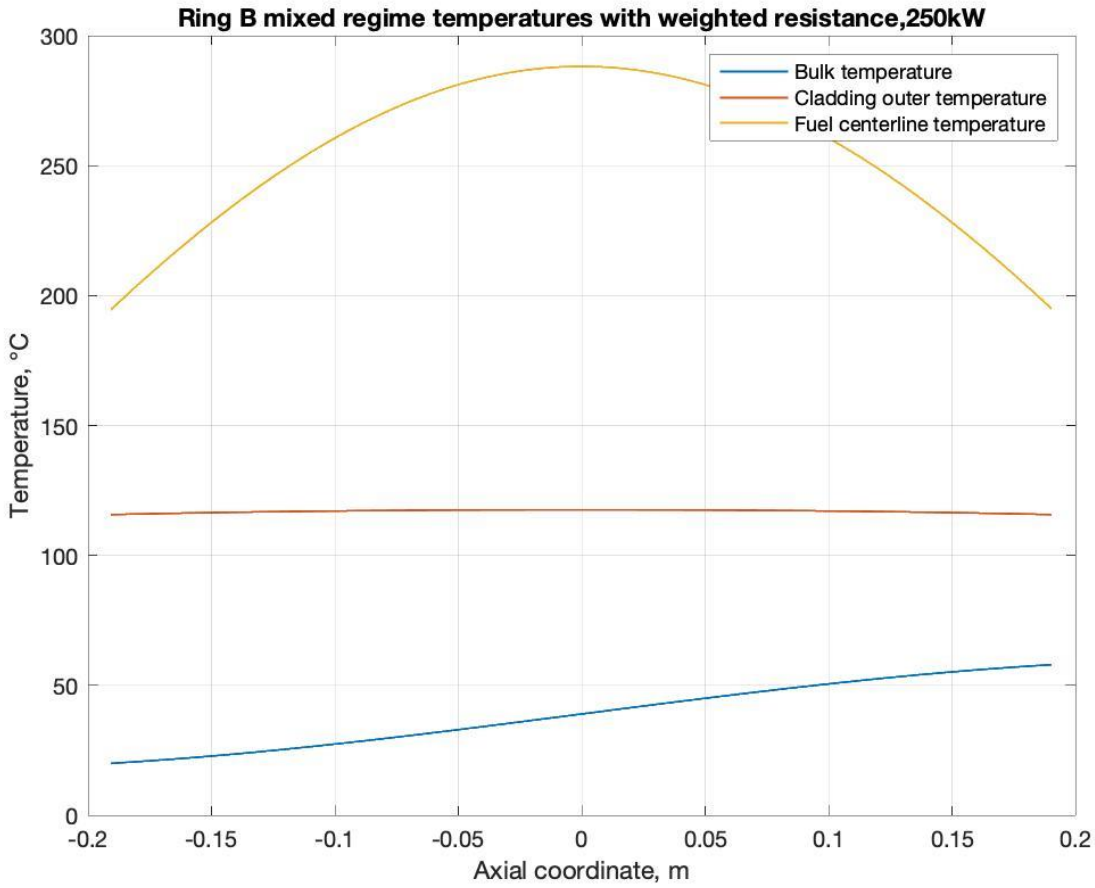

Figure 7.6: ring B temperature profiles with weighted thermal resistance

These temperatures result more realistic in function of centerline temperature, since is 280°C in hottest section. This weighted conductivity is a result of probably gap conductance varying, since gases inside conduct more at higher temperatures.

Higher the temperature difference, higher must be the thermal power exchanged, reducing the global temperatures.

In fig 7.7 can be seen ring C, exposed to channel 1 temperature profiles, where subcooled boiling occurs in the most of active height, excluding the lower part. The maximum canterline temperature found is about 226°C, and recorded data from prompt alfa misurations experiments says that maximum centerline temperature for this ring is 231°C. A very good reprodution of the experimental data for 1D model.

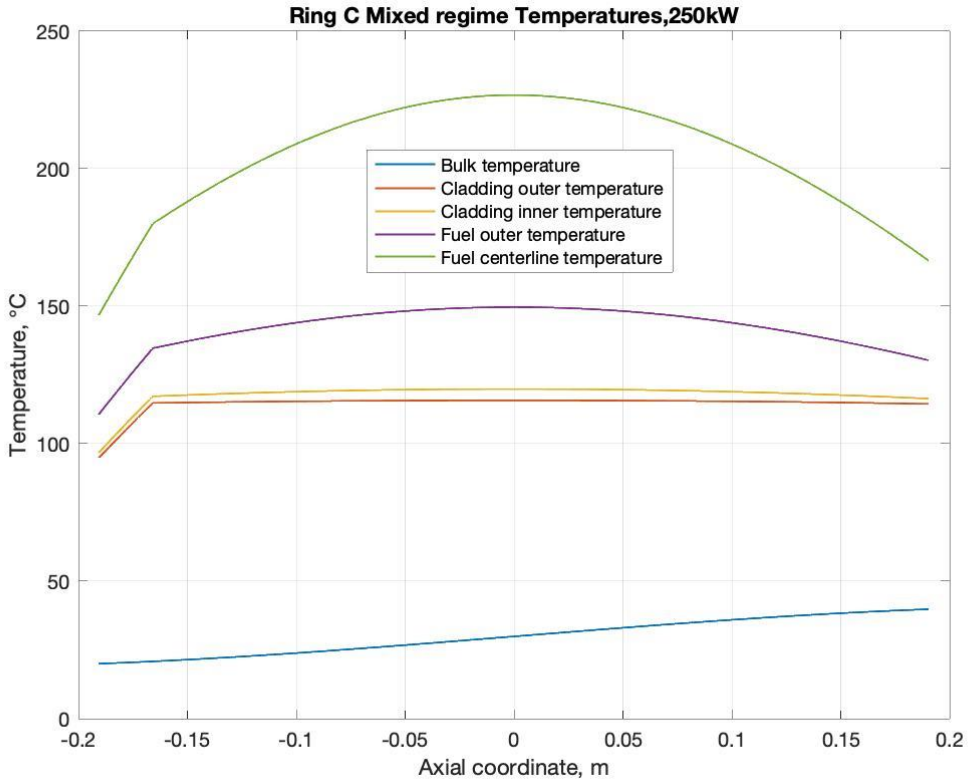

Figure 7.7: Ring C temperatures

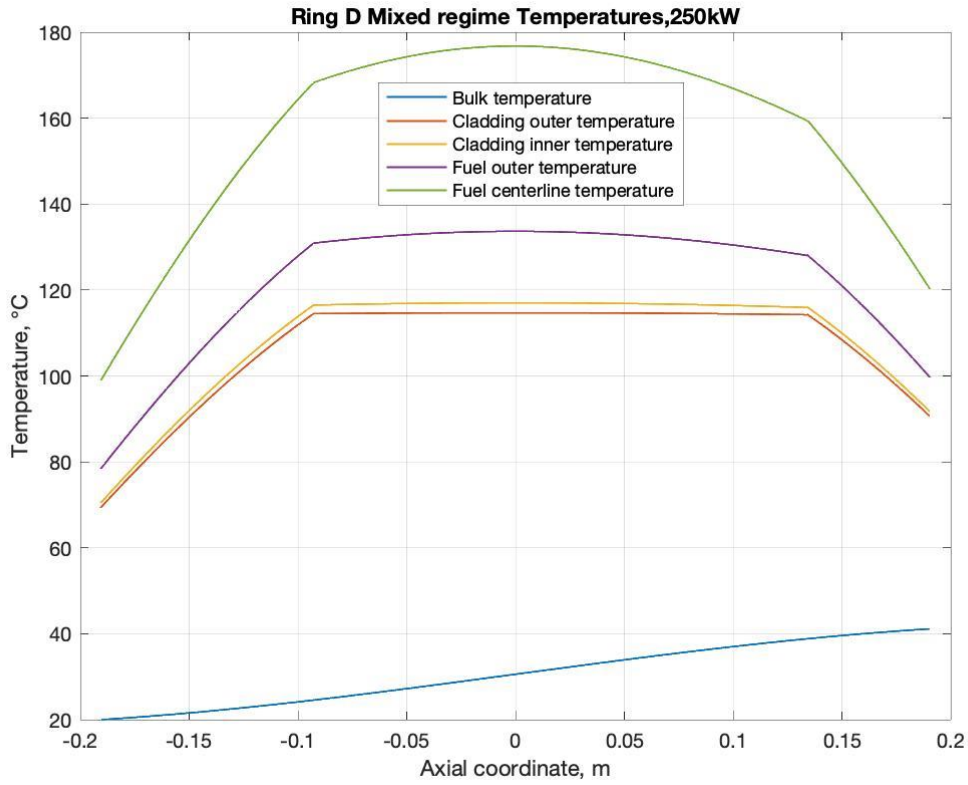

Figure 7.8: Ring D temperatures

In fig 7.8 are exposed ring D profiles; here the subcooled boiling occurs only in central part.

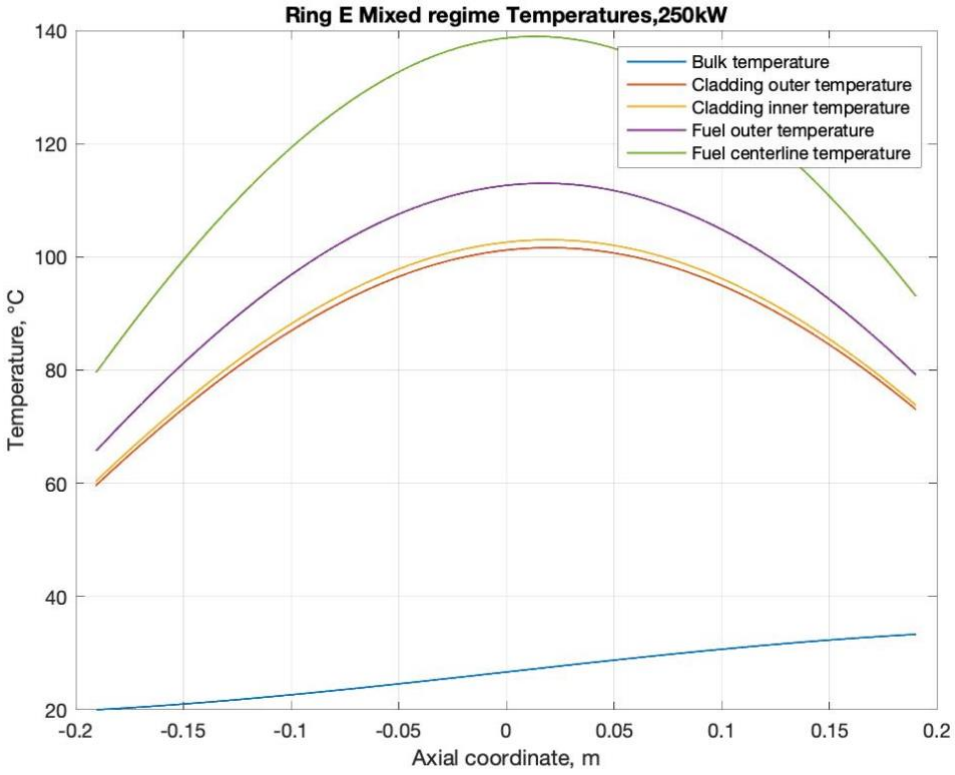

Figure 7.9: Ring E temperatures

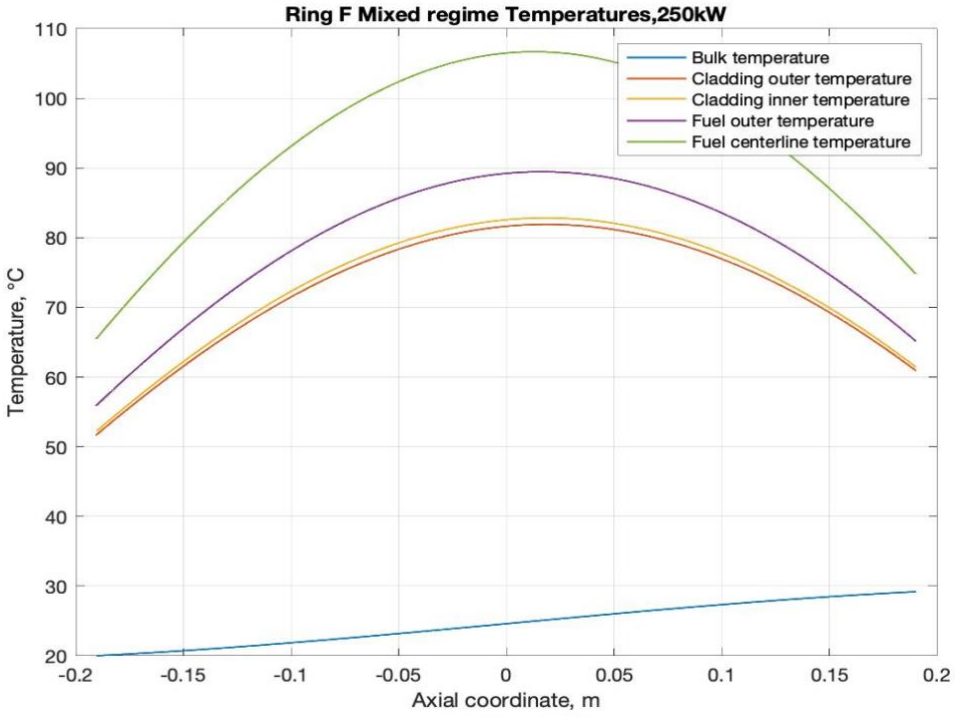

Figure 7.10: Ring F temperatures

Like shown figs 7.9 and 7.10, there isn't subcooled boiling in the last two rings, referred to adjacent channels 3 and 4 respectively, since heat flux is not enough to bring to saturation temperature the water. In fact, the graph should be identical to the one considering only the single-phase behavior.

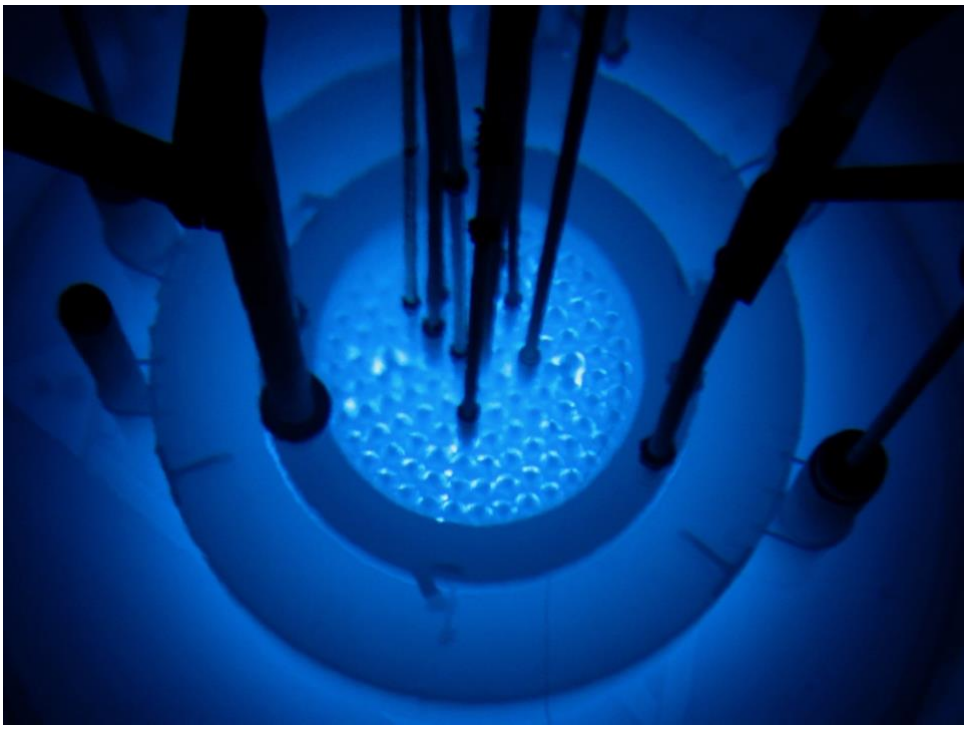

Figure 7.11: full power operation reactor, Brazilian TRIGA.

In fig 7.11 is shown the view of the reactor in operation, where microscopic bubbles come only from the innermost channels, while outside they are not seen. The fig 7.11 shows that in the internal part of the reactor the image is more blurred, unlike the external one, which is sharper, due to the presence of microscopic bubbles carried by the natural circulation.

Moreover, CFD calculations confirm that subcooled boiling is verified in the first three channels, where in number 2 only in the central part of element.

By varying the reactor power, however, it is possible to find the steady-state power for which it is possible to observe the start of subcooled boiling in each channel.

Table 7.2: power reactor where we can see subcooled boiling

	Channel 0, Ring B	Channel 1, Ring C	Channel 2, Ring D	Channel 3, Ring E	Channel 4, Ring F
Power (kW)	39	107	188	-	-

7.3.1 Double phase temperature profiles with natural convection coefficients

Considering natural convection heat transfer coefficient instead the one determined using Dittus-Boelter correlation, similar results are found, since the values are in the same order of magnitude, but finding extended subcooled region, being the natural coefficient a little lower.

Infact it is observed the same behavior in channel 0, in channel 1 boiling is extended to all region, and also boiling for most of ring D; a small region of subcooled boiling in ring E is observed, that is in contrast with previous parameters.

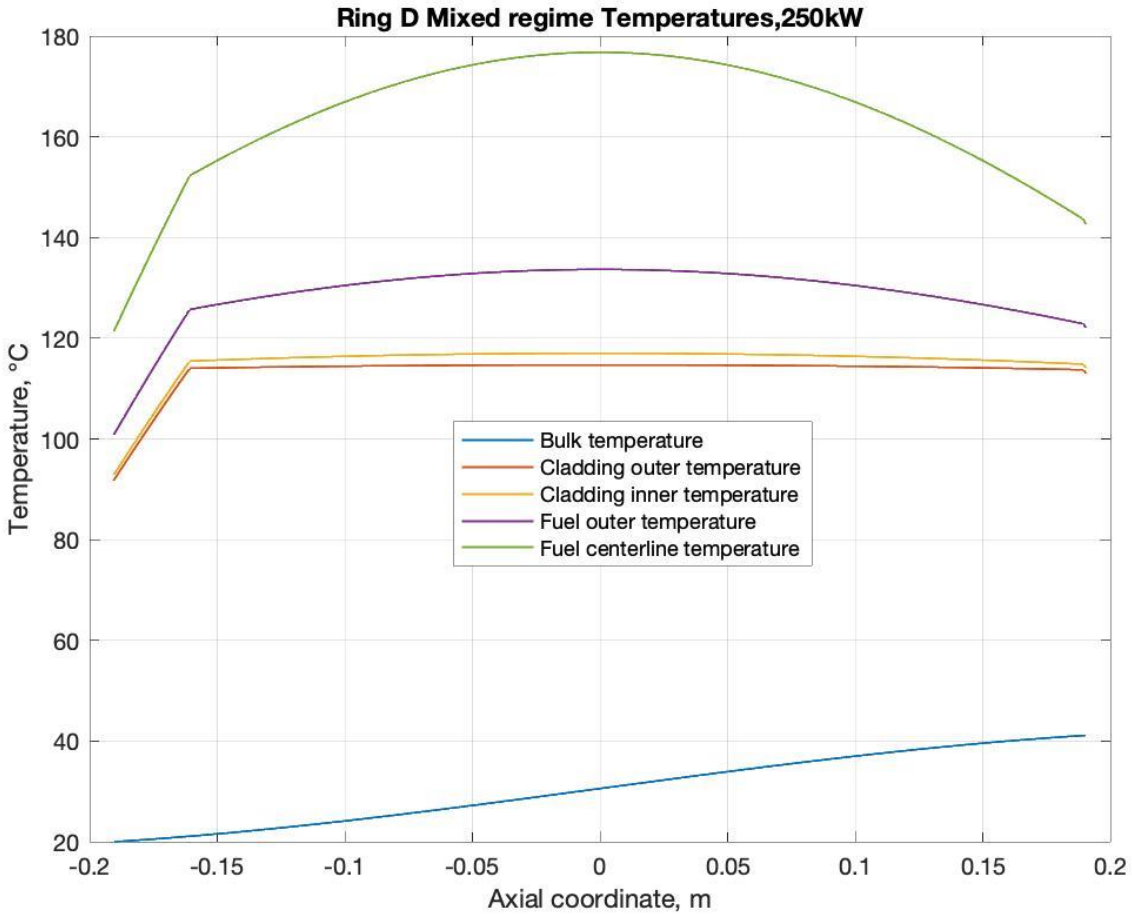

Figure 7.12: extended boiling region of ring D due to natural convection

If natural convection is considered, from table 7.3 we see the estimation of the powers at which subcooled boiling should begin to occur

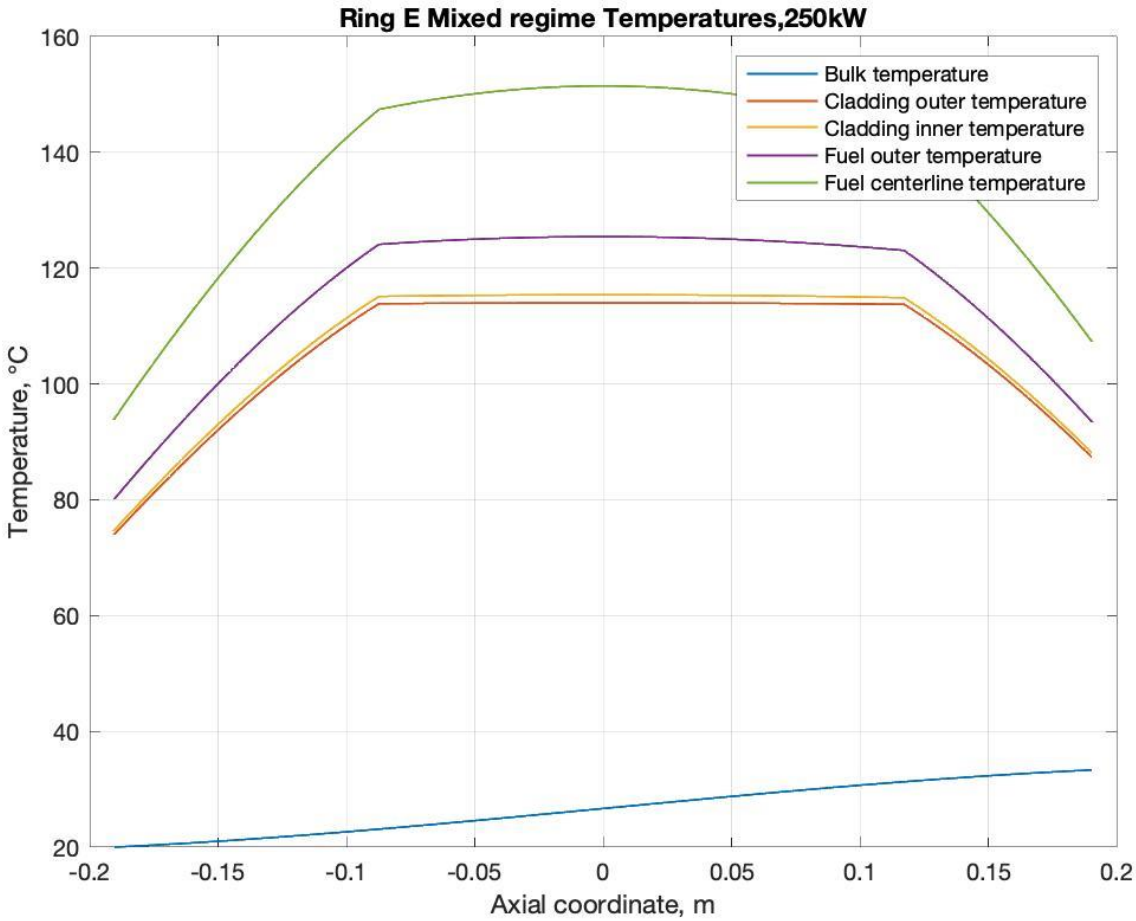

Figure 7.13: ring E profile with considering natural convection heat exchange factor

Table 7.3: power to have subcooled boiling per ring, in case of natural coefficient

	Channel 0, Ring B	Channel 1, Ring C	Channel 2, Ring D	Channel 3, Ring E	Channel 4, Ring F
Power (kW)	27	73	125	208	-

In the last channel and ring F is not seen anyway subcooled boiling.

7.4 Other channel analysis

Another analysis must be done for the reactor, and other two channels must be speedly analyzed in order to evaluate temperature and if boiling occur.

This wasn't done before because it has been chosen to express other 5 channel results in a logical way, to be compared in a "decreasing power way" philosophy.

The channels analyzed are the one which has the number 13 and 14 in the fig 3.2. They are triangular-type channels, and having a lower hydraulic area, they could present a non regular behavior, not following the before adopted "decreasing power way" philosophy. All quantities have been calculated with the same method used before for other channels, starting from dimensions, natural convection coefficients, single and double one and finally temperatures, shown in this chapter.

We refer to them as channel 13 and 14. The hydraulic areas are calculated from:

$$A_{h13} = \frac{\sqrt{3}(6X\cos(80°))^2}{4} - \frac{\pi}{2}R^2 \tag{7.6-7.7}$$

$$A_{h14} = 6X^2\cos(80°)\left(1 - \frac{3\sqrt{3}}{2}\cos(80°)\right) - \frac{\pi}{2}R^2$$

Wetted perimeter is easily calculated like triangular channel 0 for the two channels:

$$p_{wet} = \pi R \tag{7.8}$$

Power distribution of channel is calculated using linear power of ring combinated like geometry of these channels expects:

$$q'_{13} = {}^1\!/_6\ q'_C + {}^1\!/_3\ q'_D \tag{7.9-7.10}$$

$$q'_{14} = {}^{1}/_{3}\ q'_{D} + {}^{1}/_{6}\ q'_{E}$$

So, using the same procedures used before, temperature profiles are immediately plotted.

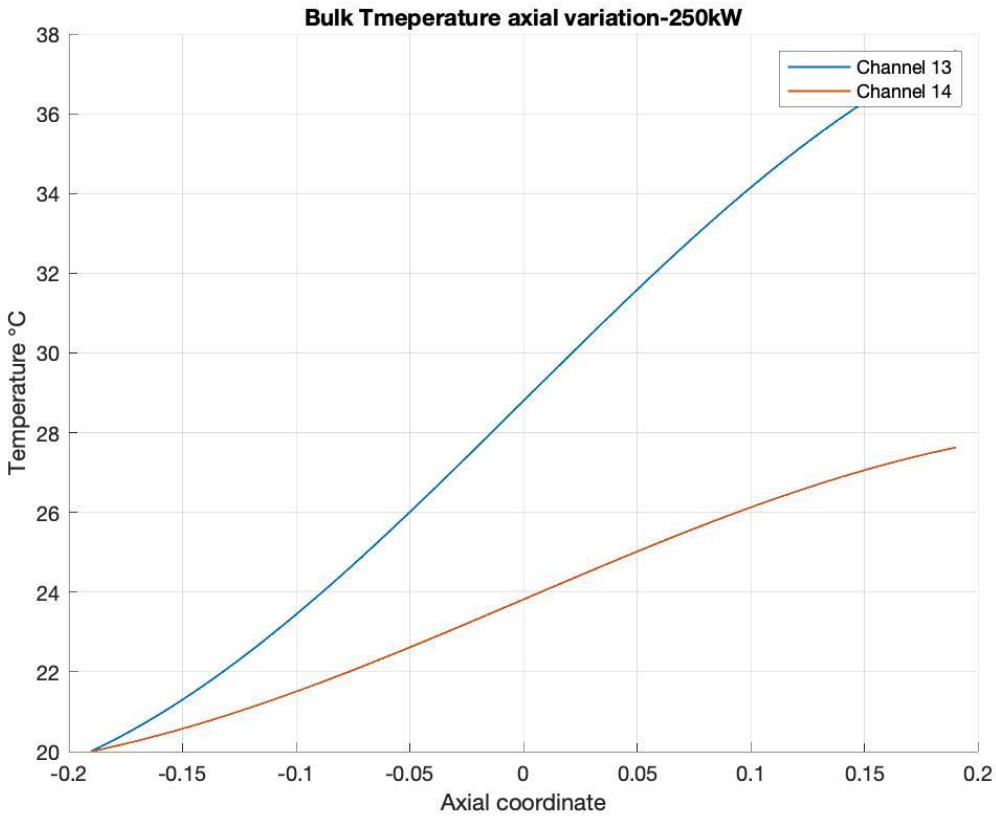

Figure 7.14: channel 13 and 14 bulk temperature

And temperature profiles, considering single-phase coefficients, fig 7.15 and 7.16.

Table 7.4: bulk temperatures, at 250 kW (°C)

Channel number	Experimental approximative temperature difference	Temperature difference found	CFD temperature difference
13	18	17.94	21.41
14	10	7.90	9.24

As we can see, the channels don't present subcooled boiling, although more restricted geometry.

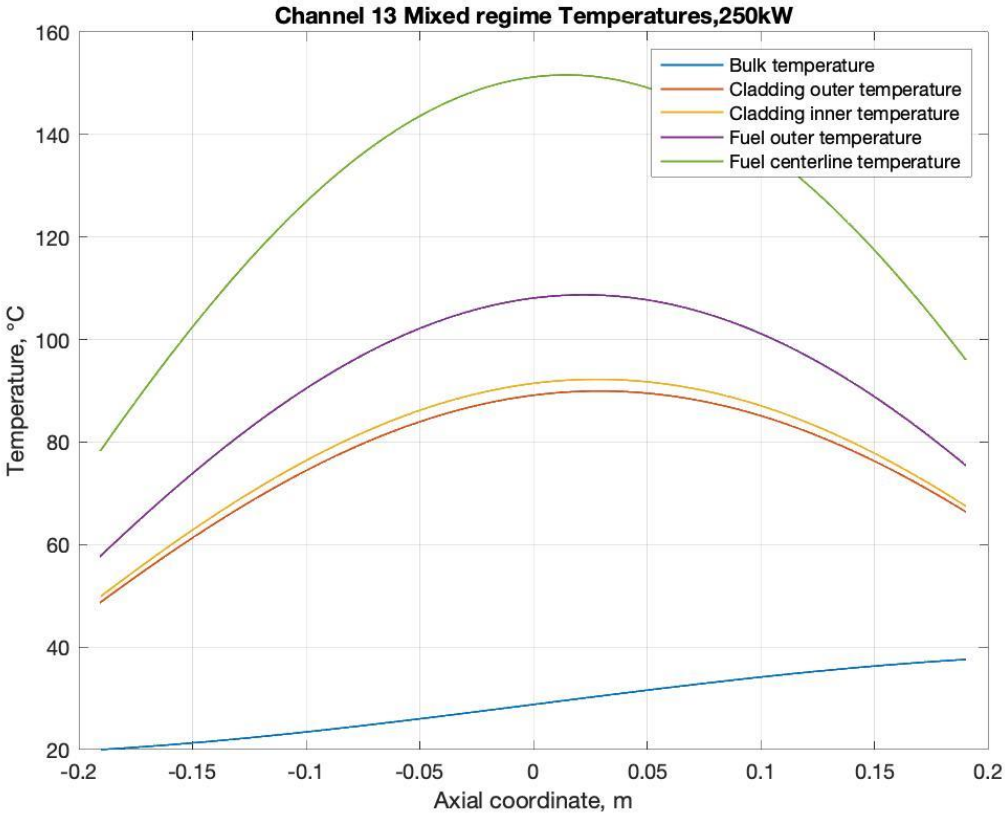

Figure 7.15: channel 13 temperature profiles

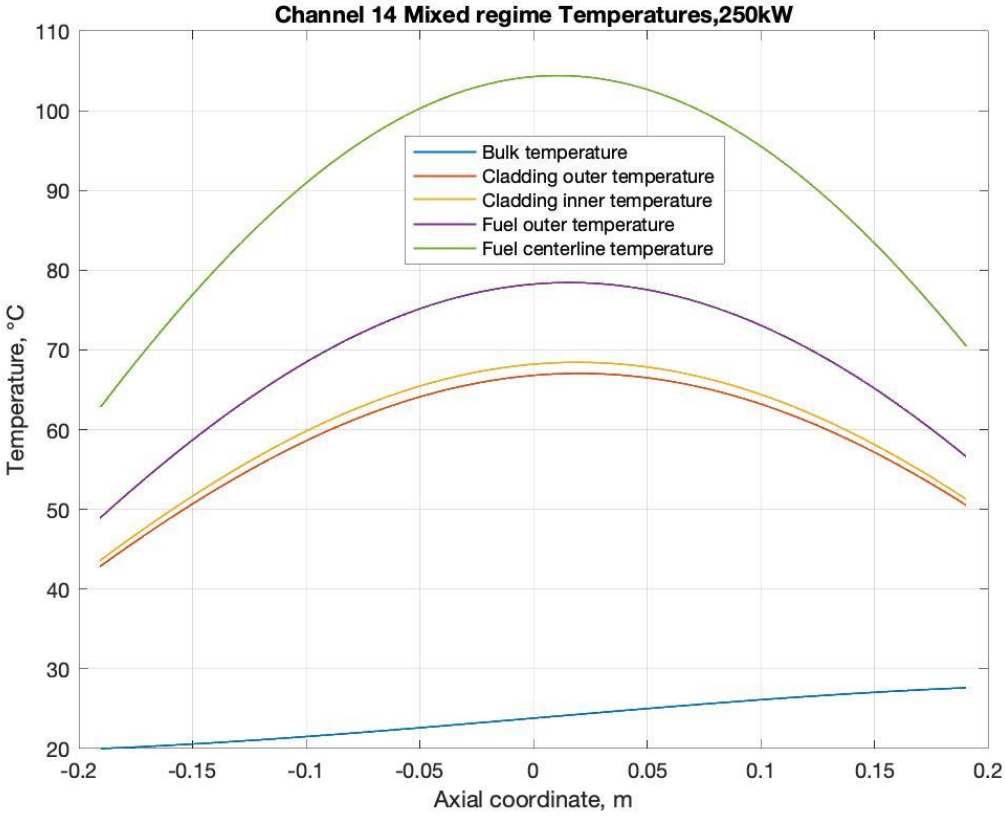

Figure 7.16: channel 14 temperature profiles

Chapter 8 DNB ratio and critical heat flux

In this chapter a detailery explanation of the departure frome nucleate boiling and the importance of critical heat flux will be done. Further some correlations will be used to estimate the DNBr, a fundamental parameter for safety.

8.1 Departure from nucleate boiling

In figure 8.1 there is a summarization of heat coefficient dependence on heat flux

Once the boiling starts, when ONB temperature is reached, boils are forming attatched to the heating wall (point A), growing up to a size sufficient to overcome adhesion due to surface tension through buoyancy, as said before.

When bubble detaches from surface it condenses giving latent heat to water, generating turbulence that guarantees ever “fresh” water close to surface, enhancing heat exchange coefficient (point B).

However, if the flow is so high as to generate too many bubbles, these interfere to each other, hindering this mixing of bubbles and subcooled water, resulting in a reduction in the efficiency of this process in increasing the exchange coefficient (point P).

This phenomenon is called departure from nucleate boiling, and it is present until the known critical flow is reached (point C). At this point, the boil is so developed, that creates a steam film attached to the surface that which causes the heat exchange coefficient to collapse, causing the wall temperatures to skyrocket, leading to the problems described above.

After this descent of the h coefficient, a minimum h is reached, that is called Leidenfrost point (D) and then it rises again, due to the fact that the difference in temperature between the liquid and the wall begins to be felt, making the irradiation the preferential method of heat exchange. The law of irradiation is:

$$\dot{Q}_{irr} = \varepsilon k(T_w{}^4 - T_l{}^4) \tag{8.1}$$

In the above equation ε is the absorbance of materials, considered as 1 for geometry and materials, and k is the Stephan-Boltzmann constant; temperatures are in kelvin.

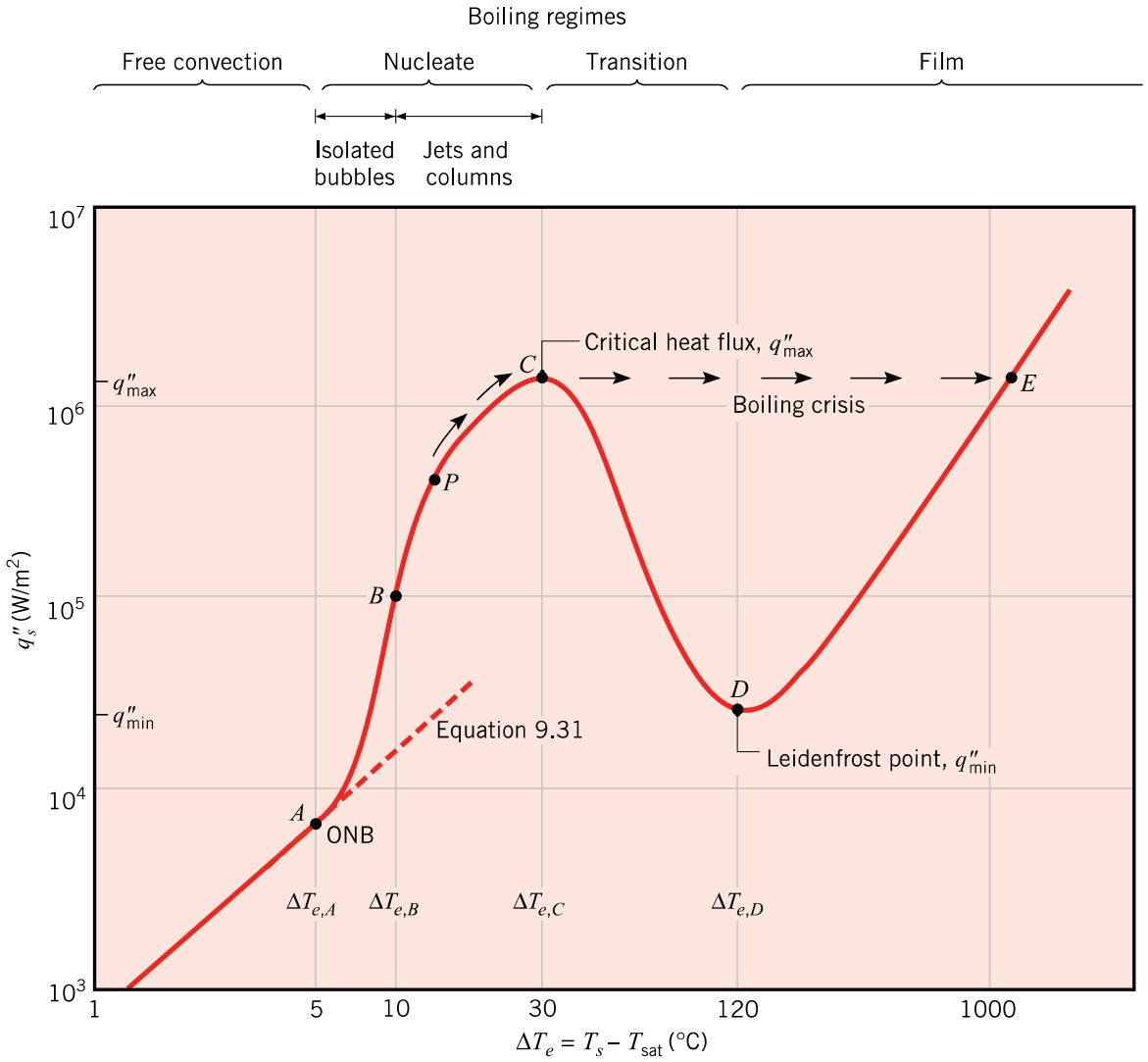

Figure 8.1: departure from nucelate boiling phases [8].

It's important to evaluate how far the reactor is from critical flux, and its related quantity called DNBr, Departure from Nucleate Boiling ratio.

This is substantially a local ratio between local critical heat flux, and local heat flux generated by the wall.

$$DNBr(z) = \frac{q''_{critic}(z)}{q''(z)} \tag{8.2}$$

Since critical heat flux is function of bulk temperature, because is required less heat to bring water to onset temperature, considering constant along z the heat flux, the most critical section normally is the upper, due to higher temperature reached.

In nuclear case is not so simple becausee we have variable flux along z and the most critical section is where higher flux is produced, near midplane, where temperatures, especially in channel 0 are higher than inlet one. Let's start to present the most suitable correlation to fine DNBr.

8.2 Bernath correlation

This correlation has been developd in imperial units, since comes from American studies on nuclear reactors.

$$v = \frac{Re\,\mu_{in}}{\rho_{in}} \tag{8.2}$$

$$T_{critic} = 57\ln(P) - \left(\frac{54\,P}{15+P}\right) - \frac{v}{4} \tag{8.3}$$

$$h_{critic} = 10890\frac{D_h}{D_{heat}+D_h} + 48\frac{v}{{D_h}^{0.6}} \tag{8.4}$$

$$q''_{critic}(z) = h_{critic}(T_{critic} - T_b(z)) \tag{8.5}$$

Where v is the parameter called specific velocity in ft/s, P is pool pressure measured in psia, D_{heat} is the heated diameter, that comes from heated perimeter, defined in the geometry chapter , and is equal to hydraulic one, except for channel 0:

$$D_{heat} = \frac{4A_h}{p_{heat}} \tag{8.6}$$

With hydraulic diameter is expressed in ft, h_{critic} is the critical heat coefficient, expressed in pcu/h ft2 °C, and q''_{critic} is the critical heat flux, expressed in pcu/h ft2. The unit pcu is the acronym of power centigrade unit and is equal to 1.8 BTU.

This correlation is very useful also for pressure used in TRIGA.

8.3 Bowring correlation

This is a purely empirical correlation (local-conditions type) for water, originally developed for the prediction of CHF in rod bundles during blowdown transients.

$$\chi_{eq} = \frac{Cp(T_{sat} - T_{in})}{\Delta h_{sat}} \tag{8.7}$$

Where is a ratio between sensible and latent heat, a simple way to describe the average title of steam in water. This correlation is based on modified pressure, defined as:

$$P_m = 0.145\ P \tag{8.8}$$

Where pressure is in MPa. Considering modified pressure less than 1 MPa, there are some correction factors that will be used later.

$$F_1 = \left\{ {P_m}^{18.942} e^{[20.89(1-P_m)]} + 0.917 \right\} \Big/ 1.917 \qquad (8.9\text{-}8.12)$$

$$F_2 = \frac{1.309\, F_1}{\left\{ {P_m}^{1.316} e^{[2.444(1-P_m)]} + 0.309 \right\}}$$

$$F_3 = \left\{ {P_m}^{17.023} e^{[16.658(1-P_m)]} + 0.667 \right\} \Big/ 1.667$$

$$F_4 = F_3 {P_m}^{1.649}$$

To calculate the critical heat flux, we need other parameters based on phisical conditions:

$$A_b = \frac{2.317\, F_1 \Delta h_{sat} D_h G}{4\left[1 + 0.0143 F_2 \sqrt{D_h} G\right]} \qquad (8.13\text{-}8.15)$$

$$C_b = \frac{0.077 F_3 D_h G}{1 + 0.347 F_4 \left(\frac{G}{1356}\right)^n}$$

$$n = 2 - 0.5 P_m$$

Where all units, except pressure are measured in S.I. units, and G, is the mass flow per area, obtained dividing the massflow per the hydraulic area, and it's expressed in kg/m2s.

$$G = \frac{\dot{m}}{A_h} \qquad (8.16)$$

Finally, the critical heat flux has the form:

$$q''_{critic} = \frac{A_b - {D_h G \Delta h_{sat} \chi_{eq}}/{4}}{C_b} \tag{8.17}$$

This correlation is valid in the conditions

$$2 < P < 190\ bar$$

$$136 \leq G \leq 18\,600\ kg/m^2 s,$$

$$2 < D_h < 45\ mm$$

$$0.15 < H_a < 3.7\ m$$

All conditions are respected, except the pressure, that is a little lower, but this is not so low to consider it unreliable, and the order of magnitude of G, that is between 200 and 15, so out for some channels, but most interesting conditions are when heat flux, and so mass flow, is high enough to permit to use this correlation.

8.4 Tong correlation

This correlation was developed for cooling channels in which a highly subcooled liquid flows upward in a vertical channel. It is based on steam average title and the area mass flow.

$$C_T = 1.76 - 7.433\chi_{eq} + 12.222{\chi_{eq}}^2 \tag{8.18}$$

$$q''_{critic} = \frac{\Delta h_{sat} C_T {G^{0.4}} {\mu_{in}}^{0.6}}{{D_h}^{0.6}} \tag{8.19}$$

The ranges of validity are out of range, since this correlation has been developd by Tong for PWRs, but could be interesting to see the results.

8.5 Results and comment

Results of DNB ratio are summarized in fig 8.2, for channel 0, which is the most critical part of reactor in terms of departure form nucleare boiling.

The DNBr has been plotted il fig 8.2 starting from 50 kW, since before there is no point of interest. As can be seen, the most critical point is at full power, obviously, and the ratio varies from 6 to 9, with various correlations at 250 kW.

In commercial PWR the minimum local value of DNBr reachable by the plant in full power must be higher than 1.3 to be licensed, so, once again, a demonstration of how safe is the TRIGA reactor is done also from this point of view.

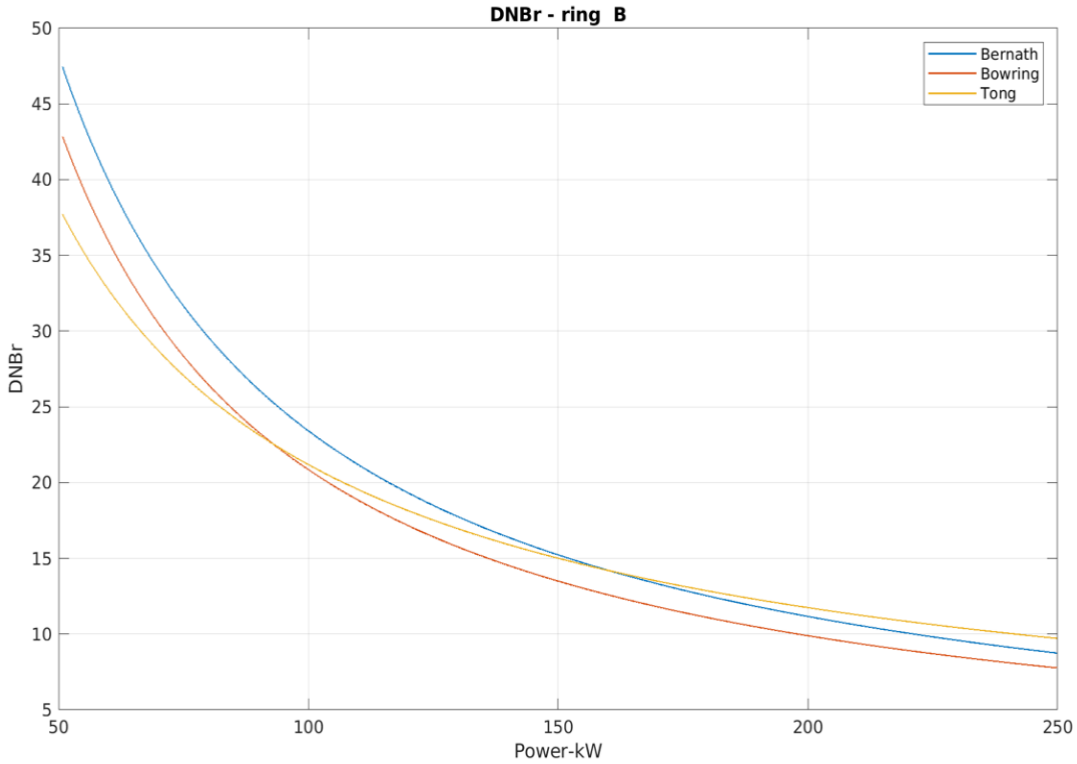

Figure 8.2: DNBr with all correlations ad different powers, channel 0, ring B

Other rings have higher value of DNBr, since it depends prevalently by heat flux, that in other rings is lower than ring B; an example can be seen in fig 8.3, where in fact there is a negligible probability to reach critical flux.

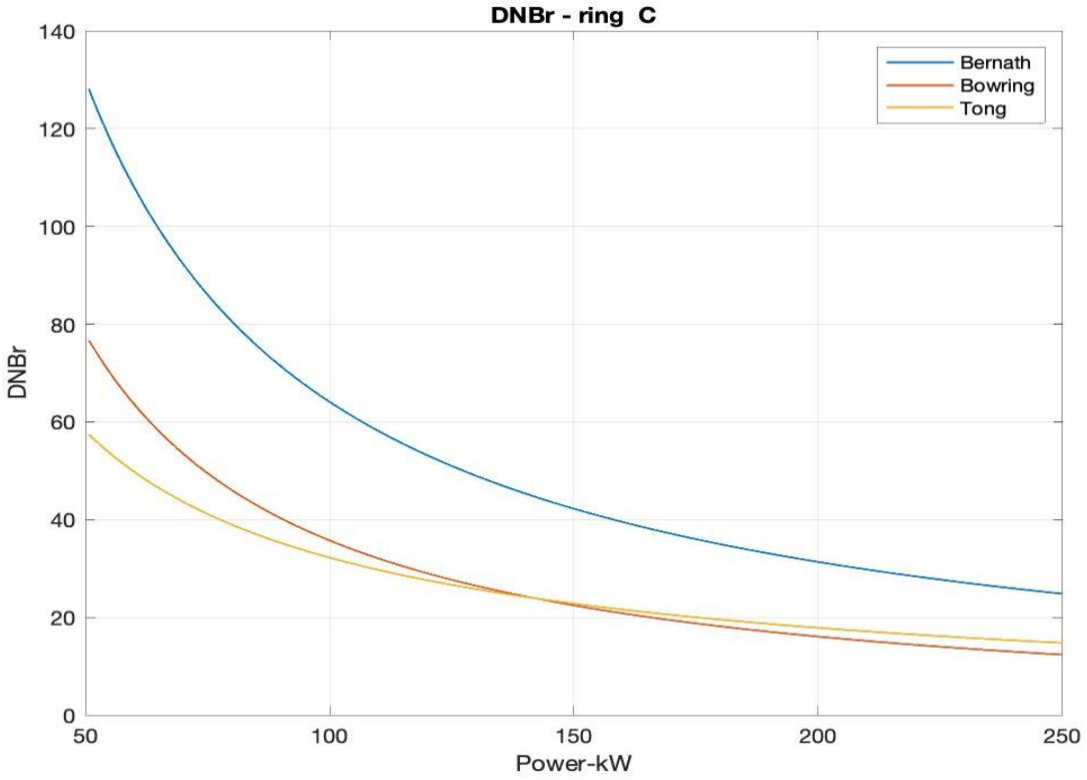

Figure 8.3: ring C channel 1 DNBr

Chapter 9 Relap results

In this chapter the main objective is to reproduce the behavior and numbers obtained before with a software used for the nuclear transient simulations. This software is Relap5, that is a software developd in USA for the simulations, licensing and design of nuclear plants or thermal-hydraulic components.

This software uses its own programming code, constituted by many numbers called cards, each one with its meaning in terms of options and parameters. A sequential combination of these one tells the program to simulate a particular condition on a particular geometry.

In this program there are some simple components that can be combined to build a plant or a small structure of the components that interact with each other, simulating each type of transient or steady state condition. For the simulation of a TRIGA channel, a simple pipe is used, considering that this geometry is a perfect compromise between most important geometry features and computation simplicity.

9.1 Relap model

The model that this program uses comes from some evaluations starting from the known equations of balance of mass, momentum and energy.

The RELAP5 thermal-hydraulic model solves eight field equations for eight primary dependent variables. The primary dependent variables are pressure (P), phasic specific internal energies (U_v, U_f), vapor volume fraction (void fraction) (α), phasic velocities (v_g, v_f), noncondensable quality (X_n), and boron density (ρ_b). The independent variables are time (t) and distance (x).

The first equation solved is the mass continuity equation:

$$\frac{\partial(\alpha_i \rho_i)}{\partial t} + \frac{1}{A_h}\frac{\partial(A_h \alpha_i \rho_i v_i)}{\partial x} = \dot{m}_\iota \tag{9.1}$$

Where i is the index for every phase, liquid or gas. Normally, no sink or source of mass are considered. The second one is the momentum equation, that consider also non-linear terms:

$$\begin{aligned} \alpha_i \rho_i A_h \frac{\partial v_i}{\partial t} + \frac{1}{2}\alpha_i \rho_i A_h \frac{\partial {v_i}^2}{\partial x} & \\ = -\alpha_i A_h \frac{\partial P}{\partial x} - \alpha_i \rho_i A_h FW_i(v_i) - \alpha_i \rho_i A_h FI_i(v_i - v_j) & \\ - \dot{m}_J A_h (v_{iI} - v_i) - C\alpha_i \alpha_j \rho A_h \left[\frac{\partial v_i - v_j}{\partial t} + v_j \frac{\partial v_i}{\partial x} - v_i \frac{\partial v_j}{\partial x}\right] & \end{aligned} \tag{9.2}$$

Where FW_i and FI_i are relative velocity correction coefficents, and index i and j are aever relative to the two phases.

The last three terms represent the momentum exchange between the two phases and the summation on the two equations for two phases must be zero.

The energy conservation is the last equation to be solved:

$$\frac{\partial(\alpha_i \rho_i U_i)}{\partial t} + \frac{1}{A_h}\frac{\partial(A_h \alpha_i \rho_i v_i U_i)}{\partial x} = -P\frac{\partial \alpha_i}{\partial t} - \frac{P}{A_h}\frac{\partial(\alpha_i v_i A_h)}{\partial t} + \dot{Q}_i + S_i \tag{9.3}$$

Where U_i is the internal energy of phase, $\dot{Q}$ is the power immitted and S_i is the sink term.

All these equations are not solved in this form, but with help of some algorithms are simplified in function of the case analyzed and after solved.

These equations are also solved in terms of void fraction, in order to verify if the system is or not in an ebullition condition.

From void fraction and phase regimes the software provides some maps in function of the component, regime and conditions to simulate.

Relap5 uses a lot of correlations to predict all behaviors that can be simulated. All correlations are contained in a software map that chooses the better one for the condition presenting. Pipe simulated it is part of the vertical volume flow regime map.

This map is composed by some conditions that can happen in the pipe component, in function of void fraction, velocity of phase and heat flux. For each case some quantities are evaluated in order to identify the correct regime of flow.

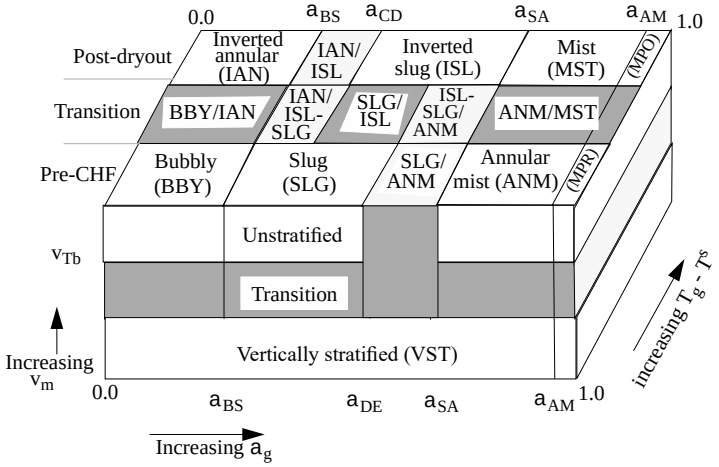

Figure 9.1: vertical flow regime map [9]

Obviously, we choose regimes of low void fractions and pre-CHF heat flux. Once determined the correct regime the program uses the correlations of Dittus-Boelter if boiling is not found and Chen correlation if it does. These correlations are represented by equations 5.2 and 6.19.

9.2 Pipe simulation results

A pipe volume of 20 sub-volumes has been built, in order to simulate the power distribution that there is in the chosen channel. The power is given to the water coolant from the wall of pipe. The total length of the pipe is equal to the active length of channel, obviously, and the diameter equal to hydraulic one of channel simulated.

The choice of this tool is to verify if the previous model and found data are close to one determined by the program, in order to have another confirm of our model.

The plotted quantities can only be plotted in function of time so, since this program was born to simulate transient, all quantities are visible after a transient. To reach steady-state values, a long-time transient simulation has been implemented with time longer enough to see the stabilization of quantities.

About quantities the most relevant ones are, like before, bulk temperature and heat exchange coefficient. In transient simulaton a primary part of single phase can be visible and after the starting of the subcooled boiling that enhances the h coefficient. Bulk temperatures are the first to be analyzed. Channel 0 is the first, fig 9.2.

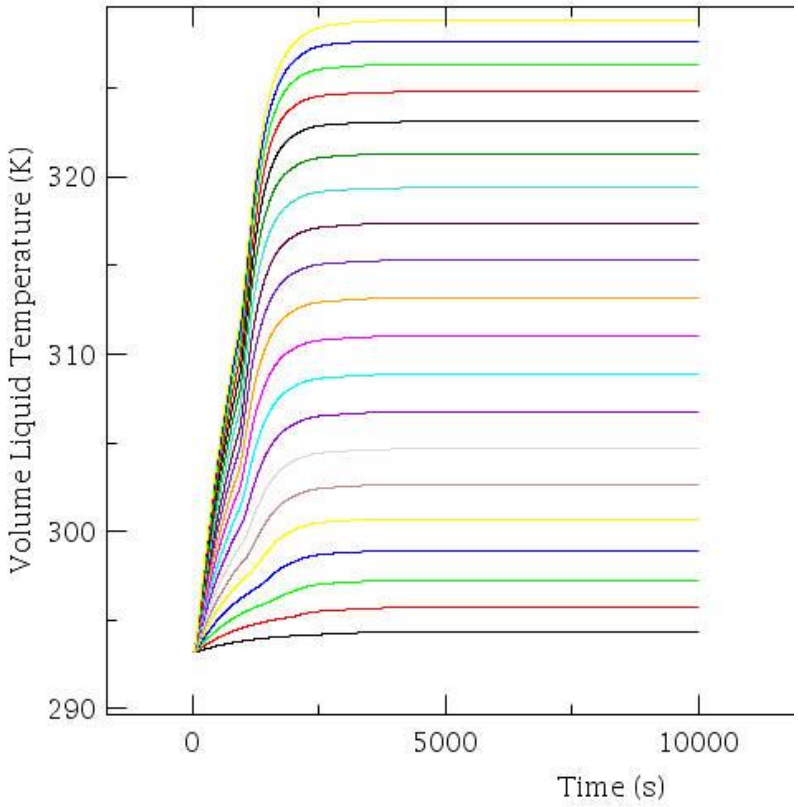

Figure 9.2: time evolving channel 0 temperatures, of all 20 sections

Each line represents a volume water bulk temperature starting from bottom to top, reaching a temperature difference between inlet and outlet of about 35.89°C.

Now, about h, channel 0 plot has been divided in two parts, since h is higher in central part, in order to see better the difference between different magnitude at different heights of this quantity. In first graph is plotting the first ten parts from bottom (fig 9.3), and in the other the remaining ten (fig 9.4).

After a time, as visible in fig 9.3, we see a rapid increase of heat exchange coefficient, since saturation temperature is reached and boiling starts. Obviously, higher the flux, higher is h, for reasons said before. This quantity doesn't increase more, since steady state conditions is reached.

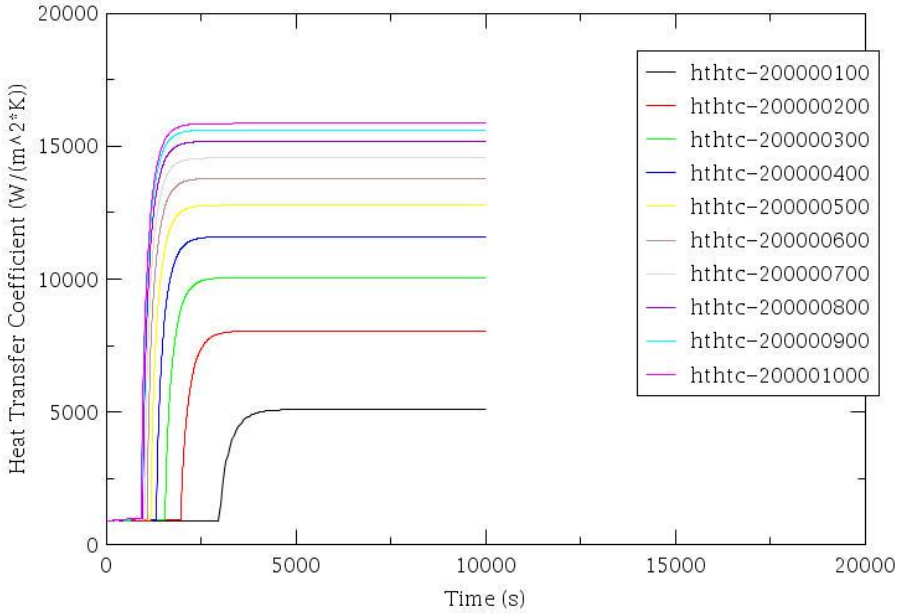

Figure 9.3: first part of channel 0 heat transport coeffient

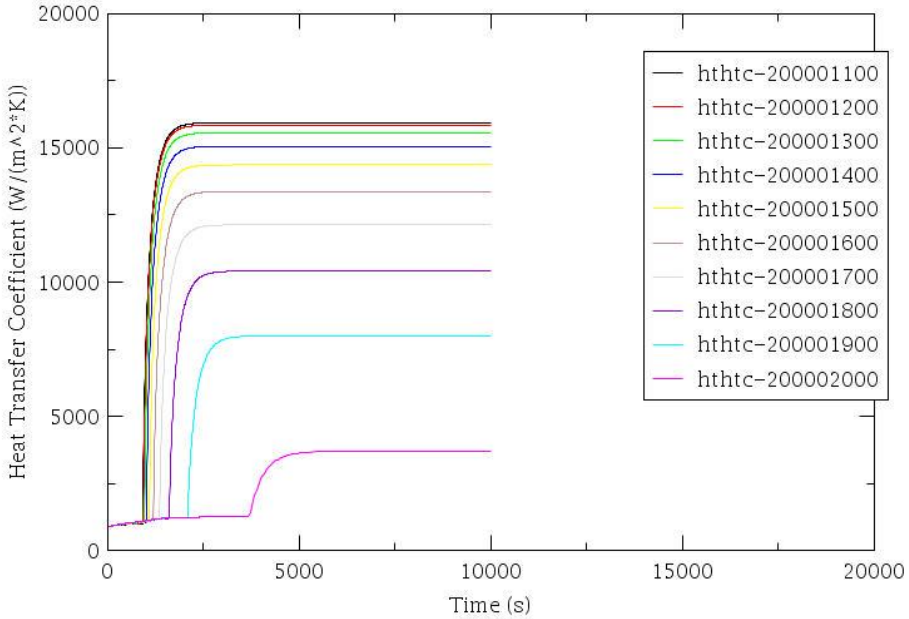

Figure 9.4: second part of channel 0 heat transport coeffient

In fig 9.4 are represented the values for second part of channel, from center to top. In the legend the two last numbers 11, 12 etc represent the section considered. Subcooled boiling is confirmed in all the channel, like in 1D model, and also the form of axial variation of heat exchange coefficient described in the last part of chapter 6 of double phase correlations. Reagarding the correlation that close represent these results for channel 0 can be the Jens-Lottes or Chen one, since more or less catch the same values of heat exchange coefficents.

Another quantity that is relevant is the wall temperature, that can be visible in fig 9.5.

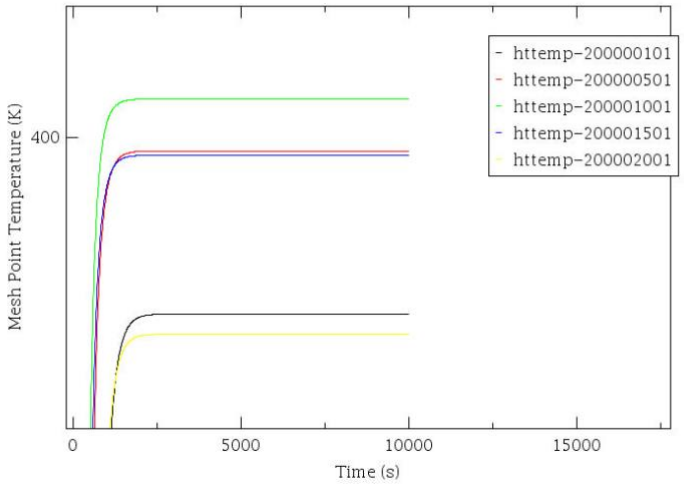

Figure 9.5: wall temperature of most important sections of channel 0

As visible, few degrees over the saturation temperature are reached, with the maximum in the central sections, as predicted before.

For channel 0 is also plotted the critical heat flux, being the hottest and so the most critical channel, fig 9.6. It can be visible an order of some MW/m2, which is and order higher than the highest heat flux reached in channel 0, that is calculated as 0.32 MW/m2. So, the values of DNBr calculated in previous chapter are close to these one.

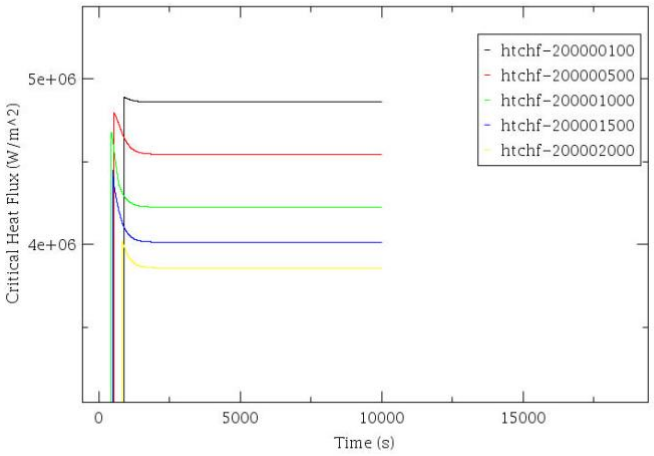

Figure 9.6: critical heat flux in various sections

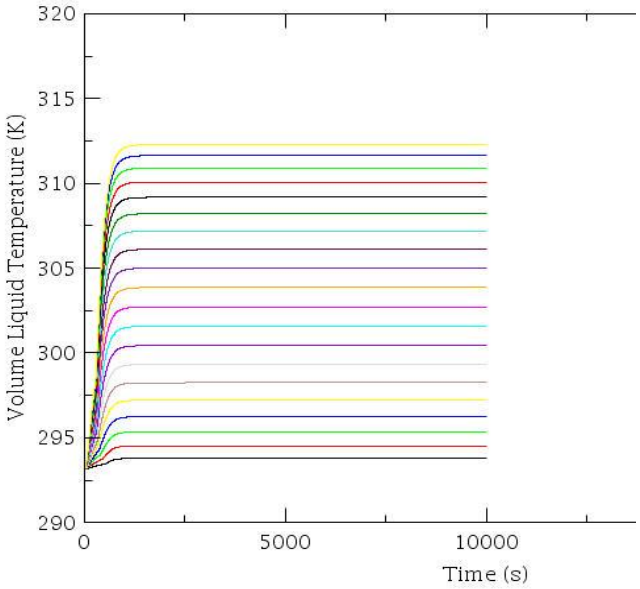

Figure 9.7: channel 1 bulk temperatures

As viewable in fig 9.7 bulk exit temperatures of channel 1 are closer to one calculated in previous analyisis, reaching a temperature difference of 19.06°C. In the same way of channel 0, in fig 9.8 and 9.9 are plotted h coefficents, and subcooled boiling is visible in all the channel.

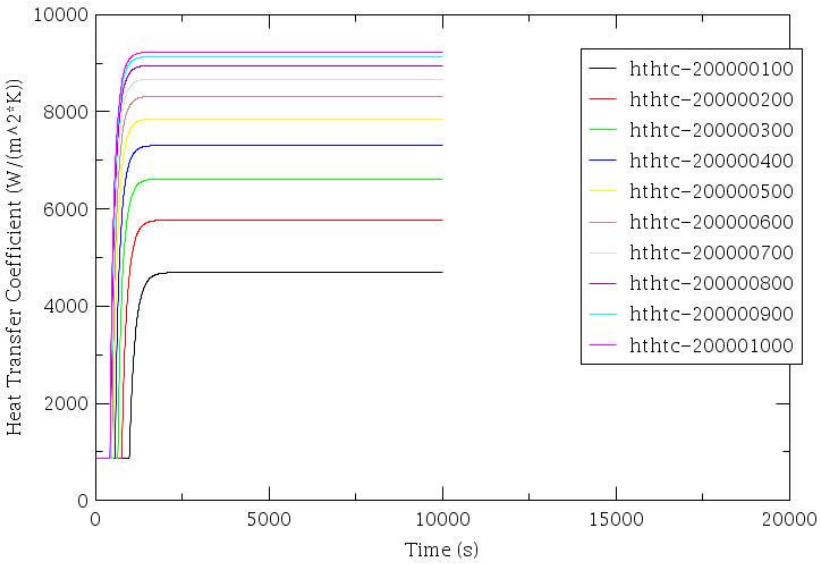

Figure 9.8: lower part channel 1 coefficents

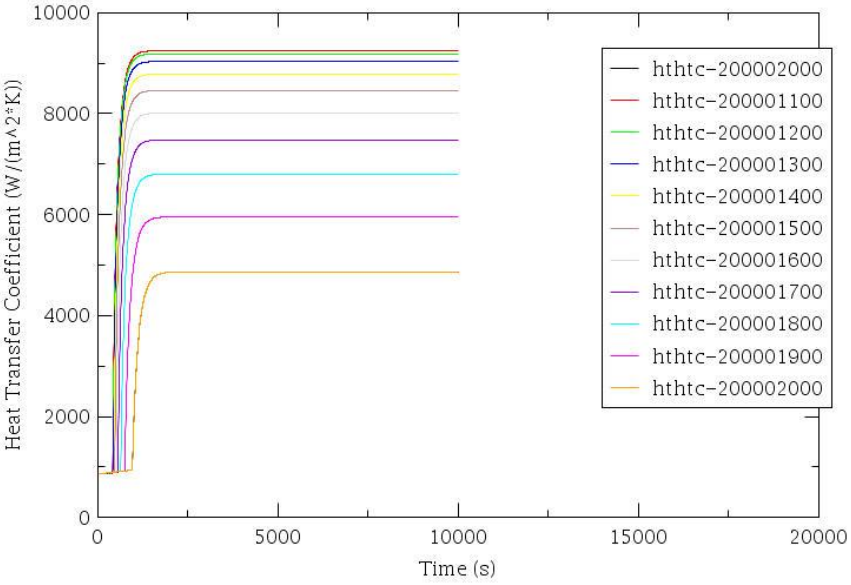

Figure 9.9: upper part channel 1 coefficents

Considering wall temperatures for channel 1 (fig 9.10):

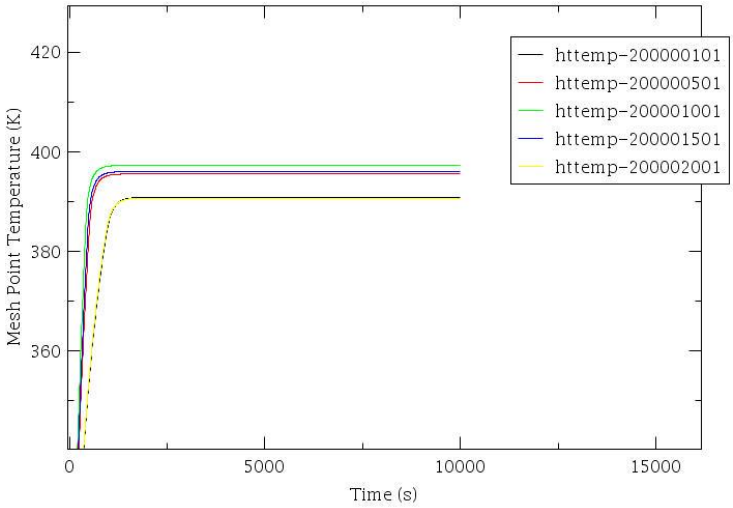

Figure 9.10: channel 1 wall temperatures

it is visible that temperature are also some degrees above saturation temperature, but lower than channel 0.

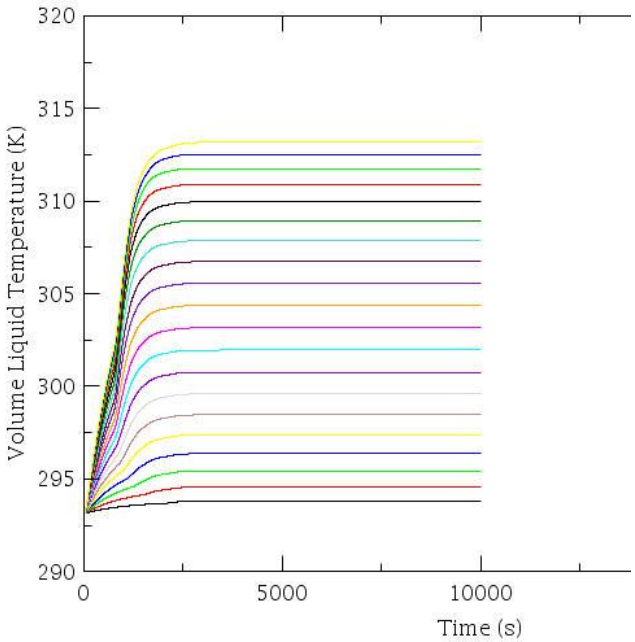

Figure 9.11: channel 2 bulk temperatures

Also for channel 2 bulk temperatures are similar to one predicted before, with temperature difference of 19.9°C (fig 9.11). In this channel, the subcooled boiling is found most part of the channel, except the upper and lower two sections. Differenlty form other two approaches here in fig 9.12 are plotted most relevant sections, in order to appreciate the differences

between the two behaviors. The highest and lowest sections present a single-phase behavior, since onset temperature is not reached, but all the other sections boils.

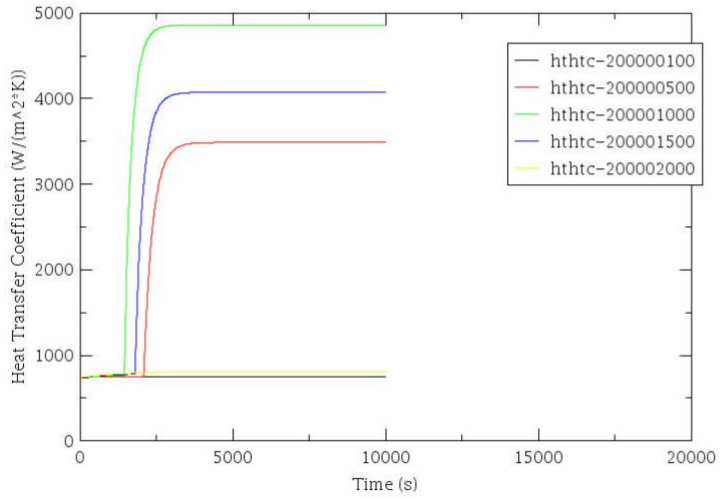

Figure 9.12: channel 2 h in most relevant sections

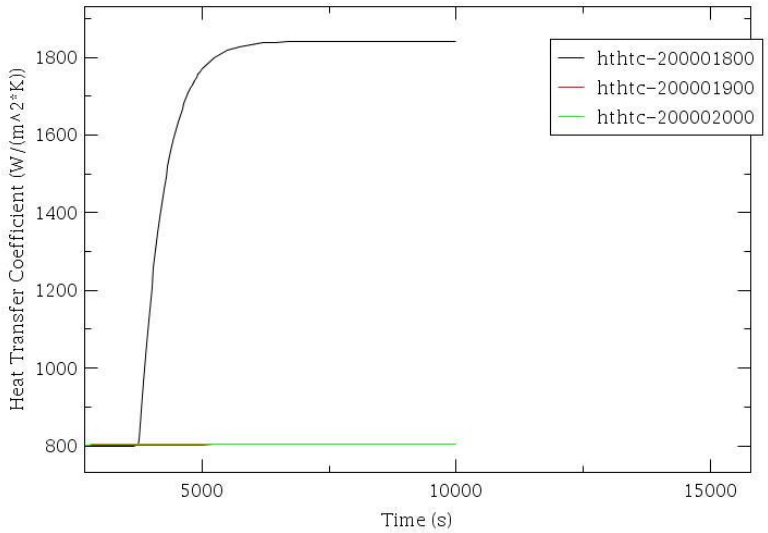

Figure 9.13: upper sections behavior of channel 2

In fig 9.13 are more evident the different behavior of last two sections, where heat exchange coefficient is similar and is found using Dittus-Boelter correlation, and the number 18, where boiling starts, changing correlation to Chen and enhancing h. It can be noted that in transient

simulations like this, also for all boiling sections there is a time interval within the boiling doesn't occur, since water needs to be reheated until saturation temperature.

Other confirmation of this behavior could be seen in fig 9.14, where wall temperatures of highest, non boiling sections are compared with the one in central section.

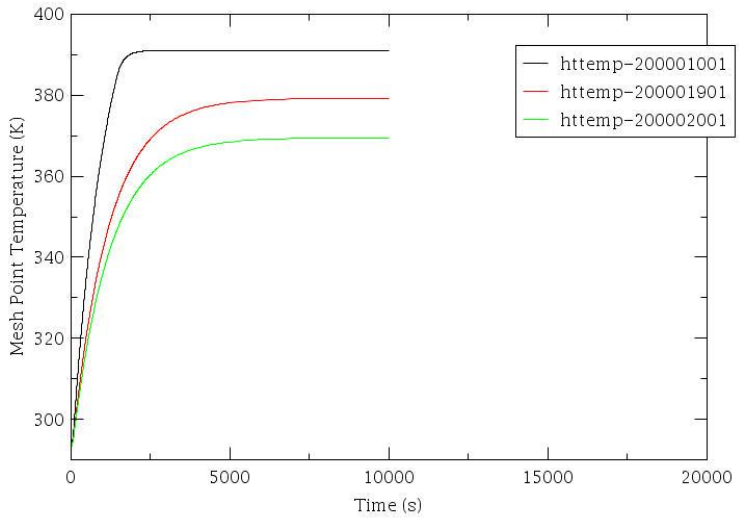

Figure 9.14: some wall temperatures of channel 2

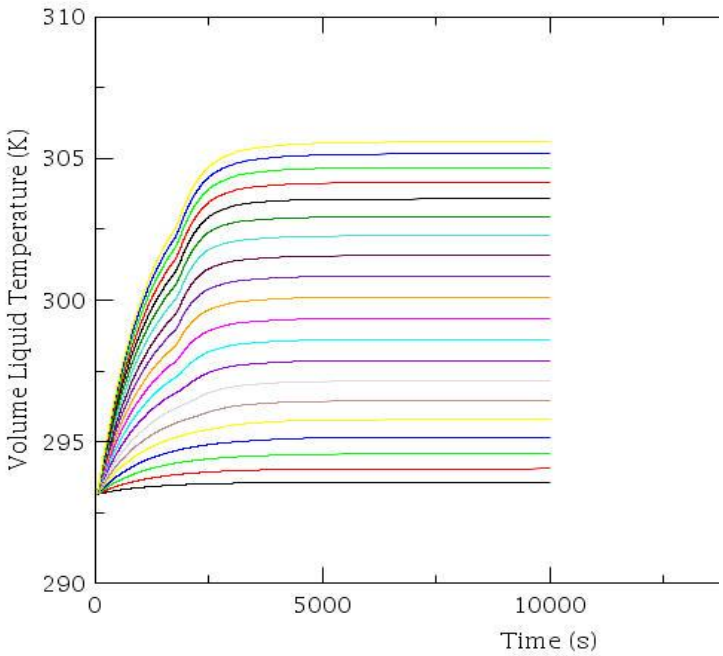

Figure 9.15: bulk temperatures for channel 3

There is a different shape in reaching steady state temperature: in central sections it is reached in a sharp way, but in other two the temperature increase is smooth, meaning that boiling stops the temperature at a precise level.

Channel 3 is the first where subcooled boiling is not observed, as predicted with correlations. As before, bulk temperature difference is very similar to one found in previous part of the work.

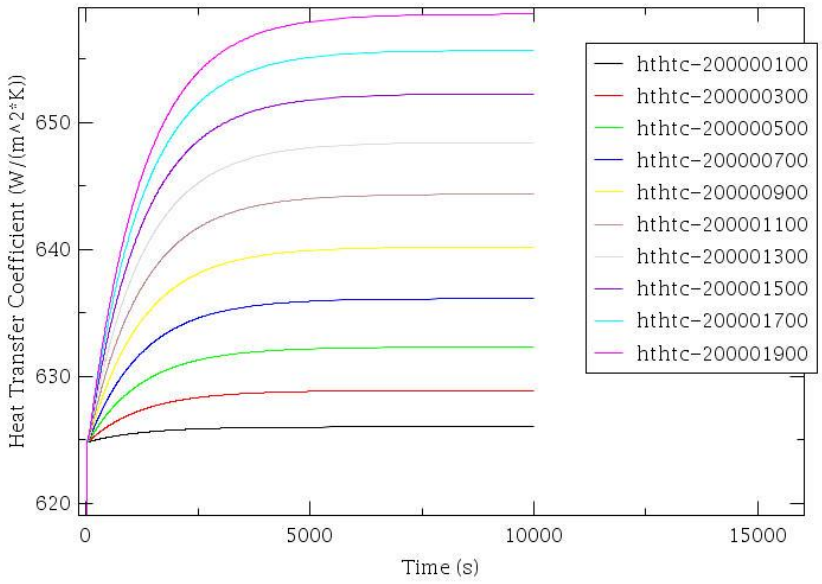

Figure 9.16: single phase coefficients of channel 3

In fig 9.16 it can be seen the heat exchange coefficients of 10 sections of the channel, from bottom to top; the values are very close to one found in single phase correlation and no "jump" of h is seen, meaning that boiling doesn't occur.

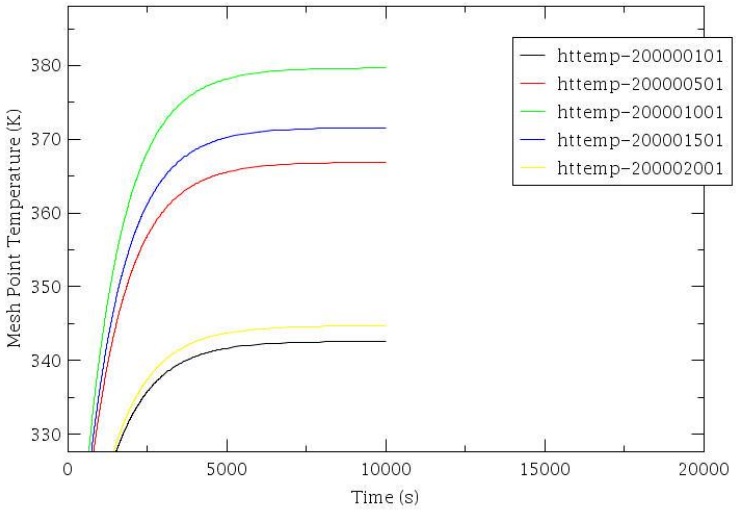

Figure 9.17: wall temperatures of channel 3

In fact, as seen in fig 9.17 in no section temperature reaches the saturation temperature that in kelvin is about 383 K.

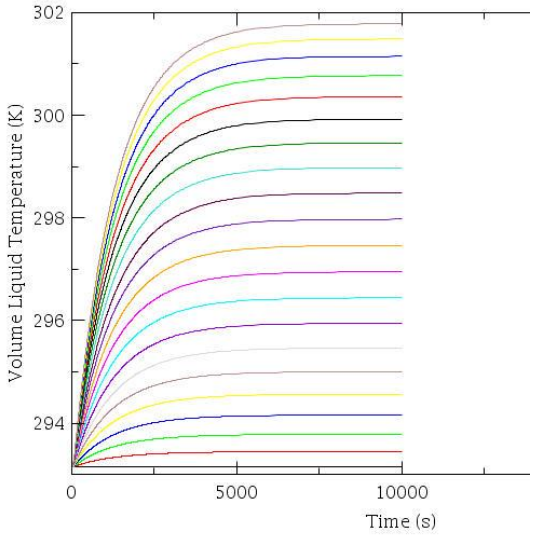

Figure 9.18: channel 4 temperature profiles

Also in channel 4 is confirmed the behavior found in previous chapter, that no boiling is observed.

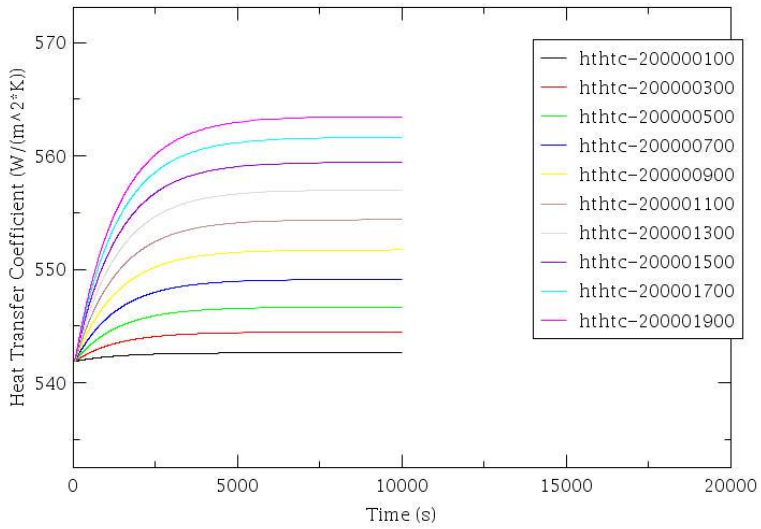

Figure 9.19: channel 4 heat exchange coefficients

Like channel 3, this is confirmed by wall temperature in fig 9.20.

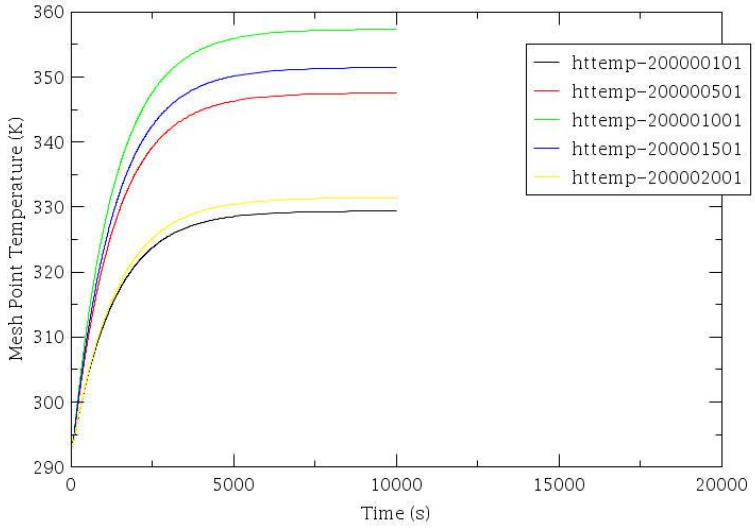

Figure 9.20: wall temperatures of channel 4

And ever like channel 3, the exchange coefficients are close to those caculated with the Dittus-Boelter.

Table 9.1 summaryzes the bulk temperature difference with ones calculated with correlations.

Table 9.1: relap bulk temperature results compared with 1D approach

Channel number	Experimental approximative temperature difference	Temperature difference found with 1D approach	Temperature difference found by Relap
0	-	37.8	35.9
1	20	19.8	19.1
2	24	21.1	19.9
3	14	13.3	12.5
4	8	9.1	8.61

Chapter 10 Conclusions

The work has provided excellent results, since all models predicts very well the basic known experimental data. Once again, after calculation it can be viewed the intrinsic safety of this type of reactor with regard to the thermal crisis, having verified with calculations its distance from reaching critical flow conditions.

From correlation of single phase and onset temperature one, subcooled boiling occurs in all channel 0, in most part of channel 1 and half channel 2. In other channels is observable continuity in temperature profiles due to not intervent of subcooled boiling that lowers it.

Using natural coeffients instead, is visible the extension of subcooled boiling to all regions of channel 0 and 1, a great extension of channel 2 and subcooled boiling occurs in half of channel 3, where with previous correlations isn't observed.

Relap, calculates heat exchange coefficients similar to these calculated in chapter 6 determined with double phase correlations, while single-phase coefficients are very close on 1D approach. It predicts boiling on all channel 0,1 and part of channel 2. No subcooled boiling is observed in channel 3 and 4. These results predict results similar to those obtained from the calculation with the single-phase heat exchange coefficients. Also, bulk temperatures are in agree with 1D model.

10.1 Channel 0 comparison

It can be useful to see how well 1D and relap results are close one to each other. For simplicity we choose channel 0 at 250 kW since is the most meaningful condition, but this could be extended to every condition and channel of reactor.

Obviously the first comparation should be between bulk temperature profiles.

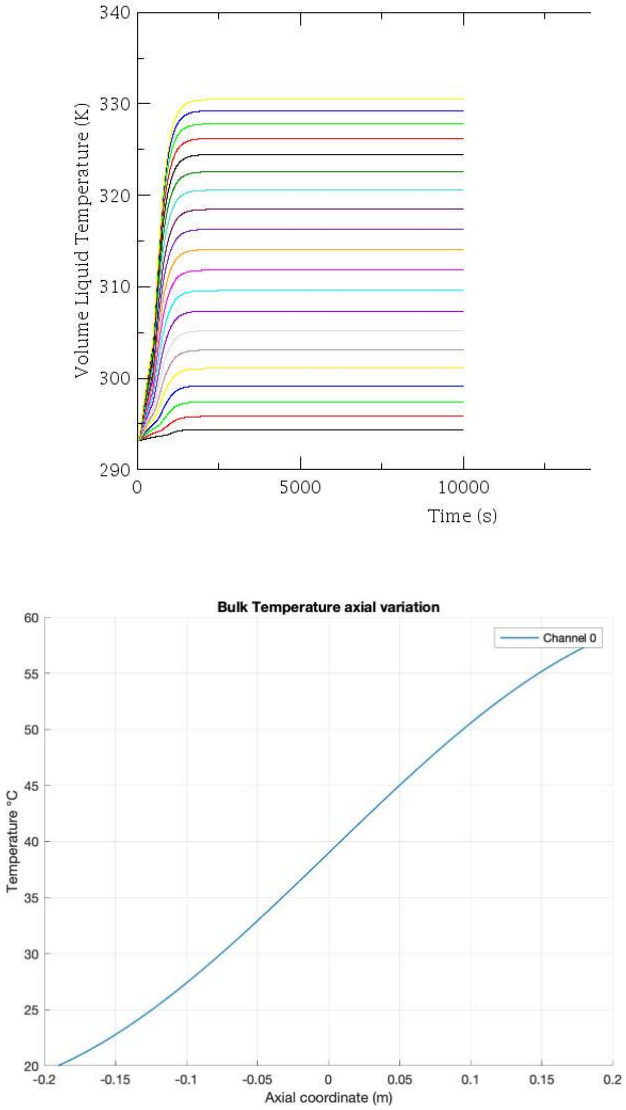

Figure 10.1-2: bulk temperatures profile of Relap and first approach, respectively

We see an agreement in figs 10.1 and 10.2 since temperature start from 20°C and rise 57.8 and 57.9 °C respectively.

Considering instead the heat exchange coefficients (figs 10.3 and 10.4) we have tried to plot the local correlation of Chen for 1D approach and the coefficients found by Relap:

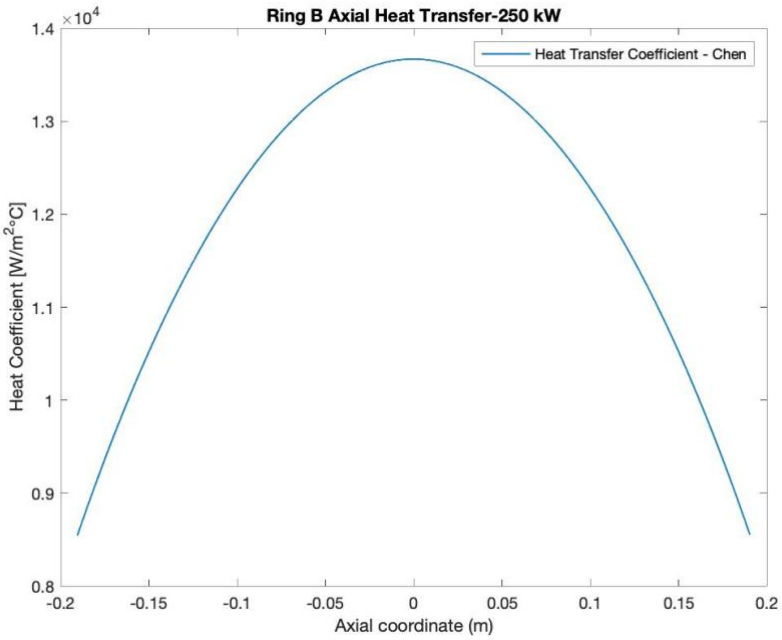

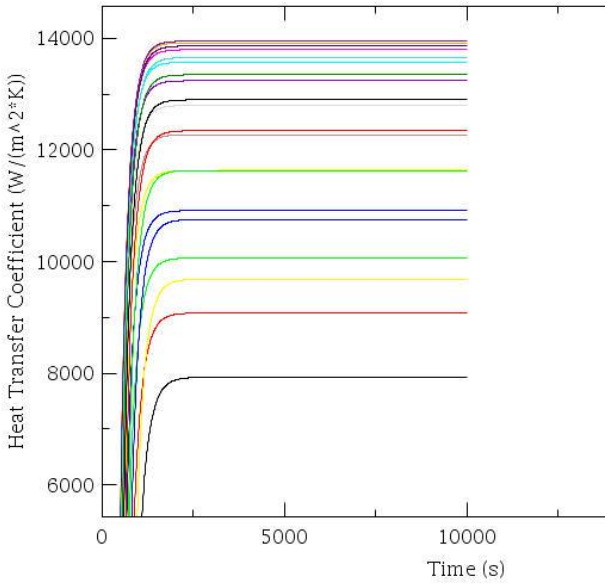

Figure 10.3-4: h coefficient for 1D corrlelation and Relap

As we can see the coefficient interval along z is nearly the same, being the one of Relap a little bigger.

Wall temperature could be another parameter to take into account:

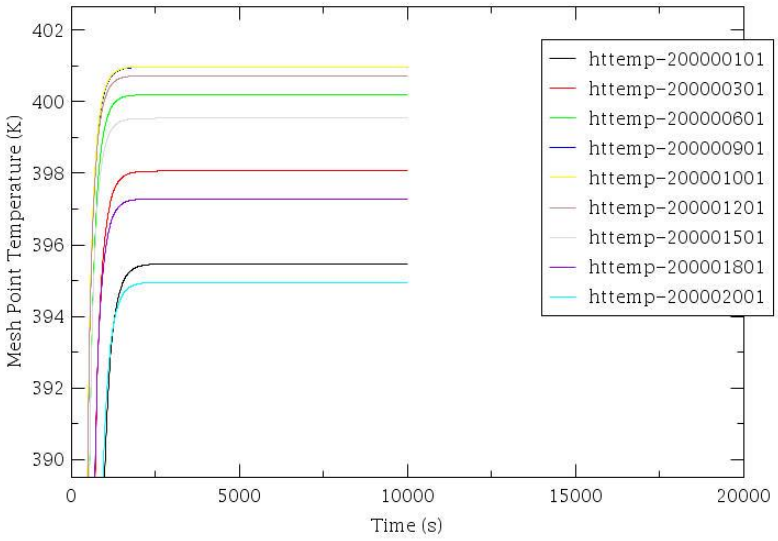

Figure 10.5: Relap wall temperature

Wall temperatures in fig 10.5 rise from 122 in lower section to 128°C in the upper one, while in fig 10.6 from 115.7 to 117.6°C. This difference is not completely negligible and derived from the fact that in first case Relap uses the coefficient of exchange to calculate this temperature, while instead in 1D approach is considered a correlation that find the onset temperature, that is the minimum that must have the wall to see boiling, so probably the temperature would be a little higher that one found using 1D approach.

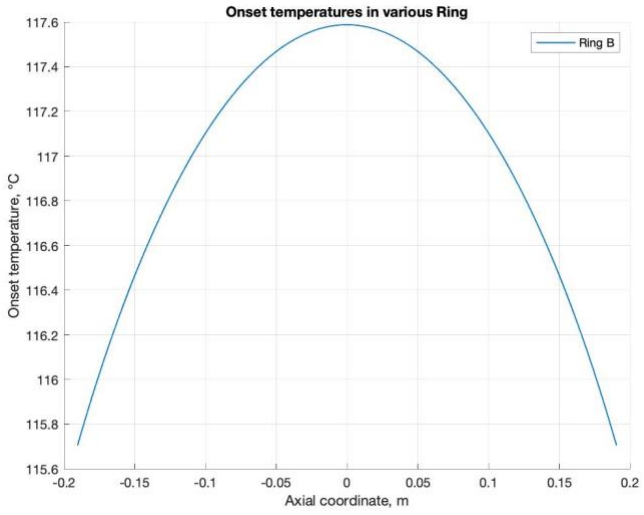

Figure 10.6: onset temperature from 1D correlations

The last comparison done is between critical heat fluxes calculated. For 1D approach Bernath correlation was chosen, because it is the only one variable with z, in order to see differences.

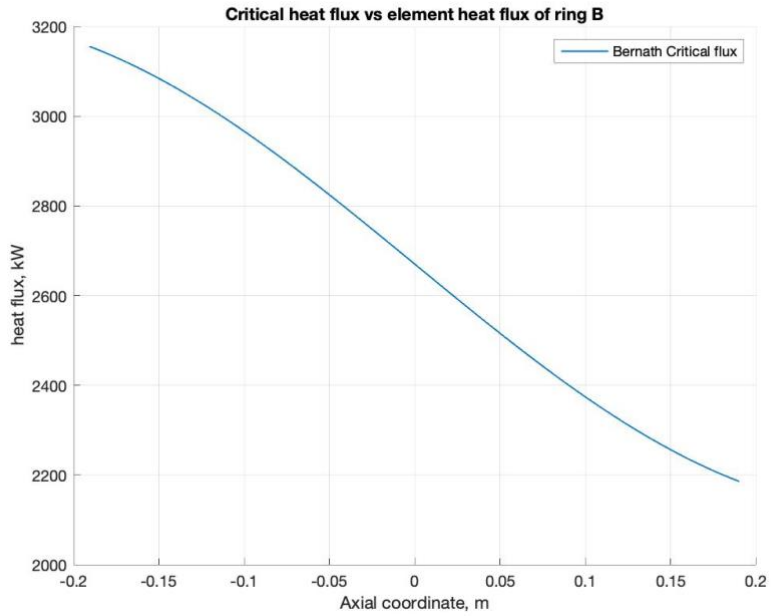

Figure 10.7: CHF from Bernath

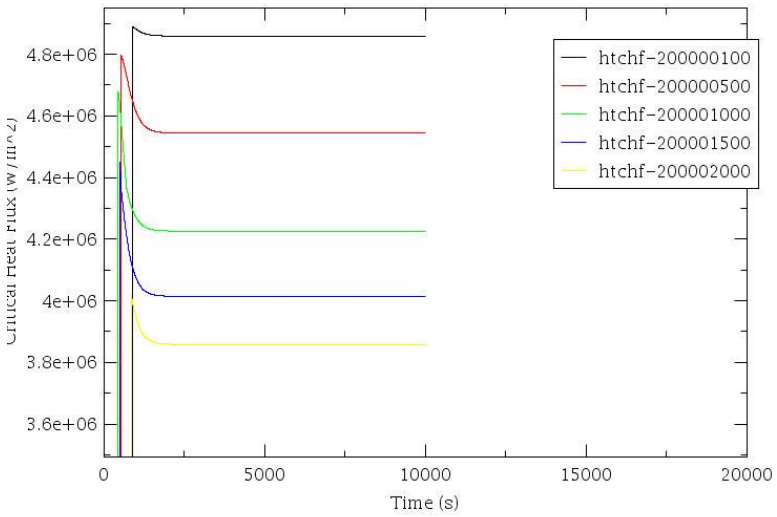

Figure 10.8: critical heat flux determined from Relap

The critical heat flux determined with Relap is higher than one determined with Bernath correlation, probably because Relap uses different correlation coming from flow regime map

respect to the one chosen for 1D. The behavior, however, is more or less the same, with critical heat flux that diminished in function of z, because bulk temperature is higher.

10.2 Extension of this work

These results come from the simplest analysis that could be done for every heat structure, but although this has brought excellent results in terms of distances from the most important experimental data.

This work could be extended introducing localized charge losses provided by grid and spacers and using a 3D approach considering all discontinuities of the reactor in its complexity.

Other works are taking place in this field, like the CFD work that tries to simulate better the conditions of this reactor. Obviously, this analysis would be a first try to reproduce experimental data, and if more complex and precise approaches woud be done, better resolutions of data will be reached.

Acronyms

Acronym	Meaning
TRIGA	Training, Research, Isotopes, General, Atomics
DNB	Departure from Nucleate Boiling
DNBr	Departure from Nucleate Boiling ratio
TRANS	Transient control rod
SHIM	Shim control rod
REG	Reg control rod
CFD	Calculation of Fluid Dynamics

Variables

Variable	Name	Measure unit
φ	Weisman first correction factor	-
σ	Surface tension of fluid	N/m
ν	Cinematic diffusivity	m_2/s
μ	Viscosity of fluid	Pa s
θ	Disposition angle per ring	°
ε	Absorbance coefficient	-
$\Delta\rho$	Inlet-outlet density difference	kg/m_3
ΔT	Temperature fluid density difference between two points	°C
ΔP_{ρ}	Pressure loss due to density change	bar
γ	Tension angle between water and steel	°
β	Expansion coefficient	1/°C
α	Thermal diffusivity	m_2/s
X	Reactor pitch	m
v	Velocity of fluid	m/s
U	Overall heat exchange coefficient	W/m°C
TR	Generic linear thermal resistance	m°C/W
S	Chen second correction factor	-
Rgh	Roughness parameter	µm
Re	Reynolds number	-
Ra	Raileigh number	-
R	Fuel element radius	m
Pr	Prandtl number	-
P	Pool pressure at reactor level	bar
Nu	Nusselt number	-
n	Various correlation exponents	-
k	Stephan-Boltzmann constant	$W/ m_2°C_4$
H	Total channel length	m
h	Heat exchange coefficient	$W/ m_2°C$
Gr	Grashof number	-

g	Gravity acceleration	m2/s
G	Mass flow per unit area	kg/s m2
F	Chen correction first correction factor	-
Cp	Specific heat of fluid (water)	kJ/kg°C
C	Weisman second correction factor	-
χ_{ring}	Power fraction produced per ring	-
χ_{eq}	Equivalent vapor title	-
ρ_{in}	Inlet density	kg/m3
μ_w	Fluid viscosity at wall temperature	Pa s
μ_{in}	Fluid viscosity at inlet temperature	Pa s
$\Delta\rho_{sat}$	Density difference between liquid and vapor saturated fluid	kg/m3
ΔT_w	Wemperature difference between wall and saturation	°C
ΔT_s	Temperature difference between bulk and surface	°C
ΔP_l	Pressure loss due to friction	bar
Δh_{sat}	Latent heat of fluid	kJ/kg
v_a	Average bubble velocity	m/s
T_{w}	Wall temperature	K
T_{sat}	Saturation temperature	°C
T_s	Wall surface temperature	°C
T_{ons}	Onset temperature	°C
T_{l}	Liquid temperature	K
$T_{f,out}$	Fuel outer temperature	°C
$T_{f,centre}$	Fuel centerline temperature	°C
T_{critic}	Critical temperature for Bernath correlation	°C
$T_{cl,out}$	Cladding out temperature	°C
$T_{cl,in}$	Cladding inner temperature	°C
T_b	Bulk temperature	°C
t_b	Average bubble formation time	s
$RW_{convection}$	Thermal resistance weight for conduction	-
R_{cli}	Cladding inner radius	m
q_{el}''	Heat flux produced of fule element	kW/ m2
q_{el}'	Linear power produced of fuel element	kW/m
q_{ch}''	Channel heat flux	kW/ m2
q_0''	Standard conditions Gorenflo correlation heat flux	kW/ m2
q_0'	Linear power produced at midplane	kW/m
q'	Linear power produced	kW/m
p_w	Wetted perimeter	m

P_m	Modified pressure for Bowring correlation	bar
p_{heat}	Heated perimeter	m
P_{cr}	Critical pressure	bar
Nu_c	Petrukov correlation corrected Nusselt number	-
N_{el}	Number of elements per ring	-
$\dot{m}$	Mass flow rate	kg/s
M_w	Water molecular weight	g/mol
K_w	Water thermal conductivity	W/m°C
K_f	Fuel thermal conductivity	W/m°C
K_{cl}	Cladding thermal conductivity	W/m°C
h_{gap}	Gap heat exchange coefficient	W/ m_2°C
H_e	Extrapolated length	m
h_{critic}	Critical heat exchange factor for Bernath correlation	W/ m_2°C
H_a	Active length	m
h_0	Standard condition Gorenflo heat exchange coefficient	W/ m_2°C
f_m	Moody friction factor	-
F_g	Gorenflo correction factor	-
f_d	Darcy friction factor	-
F_{1-4}	Bowring correlation correction factors	-
D_L	Laplace length scale	m
D_{heat}	Heated diameter	m
D_h	Hydraulic diameter	m
D_c	Characteristic dimension	m
D_b	Bubble average diameter	m
C_T	Tong correlation coefficient	-
$C_{surface}$	Surface correction factor for Rohsenow correlation	-
C_b	Bowring second factor	-
A_h	Hydraulic area	m_2
A_b	Bowring First factor	-
$\dot{Q}_{ring}$	Power produced per ring	kW
$\dot{Q}_{irr}$	Irradiation exchanged power	W
$\dot{Q}_{el}$	Power produced per element	kW
$\dot{Q}_{ch}$	Power transferred to channel	kW

Bibliography

1. D.Alloni, A. Borio di Tigliole, A. Cammi, 'Final characterization of the first critical configuration for the TRIGA Mark II reactor of the University of Pavia using the MonteCarlo code MCNP', Progress in Nuclear Energy 74
2. S. Mostafa Ghiaasiaan, 'Two-Phase Flow Boiling and Condensation in Conventional and Miniature Systems', Cambridge University Press
3. A. Cammi, R. Ponciroli, A. Borio di Tigliole, 'A zero-dimensional mode for simulation of TRIGA Mark II dynamic response', Progress in Nuclear Energy 68
4. A. Borio di Tigliole, A. Cammi, M. Clemenza, 'Benchmark evaluation of reactor critical parameters and neutron fluxes distributions at zero power for the TRIGA Mark II reactor of the University of Pavia using the MonteCarlo code MCNP', Progress in Nuclear Energy 52
5. M.Q. Ruda, M. Rahman, 'Thermo-hydrodynamic design and safety parameter studies of the TRIGA Mark II research reactor', Annals of Nuclear Energy 31
6. A. Z. Mesquita, 'Experimental Heat Transfer Analysis of the IPR-R1 Reactor'
7. W. Rohsenow, J. Hartnett, Y. Cho, 'Handbook of Heat Transfer', McGraw Hill
8. Incropera, DeWitt, 'Fundamentals of Heat and Mass Transfer'
9. Relap manuals V1-V5, RELAP5 Code Development Team
10. B.M Lekakh, M.S. Kazimi and J.E.Meyer, 'Boiling Heat Transfer For High Velocity Flow of Higly Subcooled Water', MITNE-315
11. Kaichiro MISHIMA, Futoshi TANAKA, Takashi HIBIKI, Yasushi SAITO & Tomoaki TAKEDA, 'Heat Transfer Study for Thermal-Hydraulic Design of the Solid-Target of Spallation Neutron Source'
12. S. Boarin, A. Cammi, M.E. Ricotti, D. Chiesa, 'Setting-up a control-oriented model for simulation of TRIGA Mark II dynamic response'
13. Antonio Cammi, Matteo Zanetti, Davide Chiesa, 'Characterization of the TRIGA Mark II reactor full-power steady state'
14. N.E Todreas, M.S. Kazimi, 'Nuclear Systems I: Thermal Hydraulics Fundamentals', Chapter 8
15. C. Introini, A. Cammi, 'A complete CFD study on natural convection in the TRIGA Mark II reactor', submitted to Progress on Nuclear Energy, 2020.